


3-2-2016

Enhancement of Supercapacitor Energy Storage by Leakage Reduction and Electrode Modification

Tete Tevi

Follow this and additional works at: <http://scholarcommons.usf.edu/etd>

 Part of the [Electrical and Computer Engineering Commons](#), and the [Organic Chemistry Commons](#)

Scholar Commons Citation

Tevi, Tete, "Enhancement of Supercapacitor Energy Storage by Leakage Reduction and Electrode Modification" (2016). *Graduate Theses and Dissertations*.

<http://scholarcommons.usf.edu/etd/6148>

This Dissertation is brought to you for free and open access by the Graduate School at Scholar Commons. It has been accepted for inclusion in Graduate Theses and Dissertations by an authorized administrator of Scholar Commons. For more information, please contact scholarcommons@usf.edu.

Enhancement of Supercapacitor Energy Storage by Leakage Reduction and Electrode
Modification

by

Tete Tevi

A dissertation submitted in partial fulfillment
of the requirements for the degree of
Doctor of Philosophy
Department of Electrical Engineering
College of Engineering
University of South Florida

Major Professor: Arash Takshi, Ph.D.
E. Lee Stefanakos, Ph.D.
Jing Wang, Ph.D.
Sylvia W. Thomas, Ph.D.
Manoj Ram, Ph.D.
Shengqian Ma, Ph.D.

Date of Approval:
February 15, 2016

Keywords: Electrochemical Capacitors, Self Discharge,
Conducting Polymers, Modeling, Simulation

Copyright © 2016, Tete Tevi

DEDICATION

To my family and to the memory of my father whose dream has become a reality.

ACKNOWLEDGMENTS

I would like to express my sincere thanks to my advisor Dr. Arash Takshi for his mentorship, support, advice, selflessness, and kindness throughout my graduate career. I am greatly honored to be one of his first graduate students and very grateful for the guidance he has provided me in my research.

I would like to thank Dr. Elias (Lee) Stefanakos for giving me the opportunity to join the University of South Florida, College of Engineering and for supporting me at the beginning of my program.

I would like to thank Dr. Jing Wang, Dr. Sylvia W. Thomas, and Paula C. Algarin-Amaris for their much appreciated contributions on some of the research projects and for allowing us to use many facilities in their laboratories.

I would also like to thank Dr. Manoj Ram and Dr. Shengqian Ma for their time, insights, and helpful advices. I would like to thank Dr. Rasim Guldiken of the Department of Mechanical Engineering for being the chairperson for my Ph.D. defense.

I would like to thank all my organic electronic laboratory colleagues (Anand kumar Santhanakrishna, Houman Yaghoubi, Shantonio W. Saint Birch, Sara Bakhshi, Hadi Ebrahimi, Fatemeh Rahimi, and Riaz Ahmed Liyakath) for the collaboration and friendship we had in the lab.

Finally and not the least, I would like to express my deepest gratitude to my lovely wife Cikavi, to my daughters, and to my mother for their love, encouragement, and support of all kinds.

TABLE OF CONTENTS

LIST OF TABLES	iv
LIST OF FIGURES	v
ABSTRACT.....	viii
CHAPTER 1: INTRODUCTION.....	1
1.1 Energy Crisis.....	1
1.2 Supercapacitors	2
1.3 Motivation of this Work.....	4
1.4 Scope of Dissertation	5
CHAPTER 2: BACKGROUND.....	6
2.1 Historical Overview	6
2.2 Electrochemical Reaction	6
2.2.1 Redox Reaction.....	6
2.2.2 Nernst Equation	7
2.2.3 Electrons Tunneling in Quantum Mechanics.....	8
2.3 Different Types of Electrochemical Capacitors.....	10
2.3.1 Electrical Double Layer Capacitors (EDLCs)	10
2.3.1.1 Helmholtz Model	12
2.3.1.2 Gouy and Chapman Model	12
2.3.1.3 Stern and Graham Model	13
2.3.1.4 Bockris, Devanathan, and Muller Model (BDM)	14
2.3.2 Pseudocapacitors.....	15
2.3.3 Hybrid Capacitors	17
CHAPTER 3: ELECTROCHEMICAL PARAMETERS, TEST TECHNIQUES, TOOLS, AND INSTRUMENTS USED	19
3.1 Introduction.....	19
3.2 Supercapacitors Electrochemical Parameters	19
3.2.1 Capacitance	19
3.2.2 Energy	20
3.2.3 Power	20
3.3 Electrochemical Analysis Techniques	21
3.3.1 Cyclic Voltammetry Technique.....	21
3.3.2 Galvanostatic Technique.....	22
3.3.3 Impedance Technique	23
3.3.4 Open Circuit Measurements	23

3.4 Tools and Instruments Used.....	24
3.4.1 Electrochemical Instrument	24
3.4.2 Solar Simulator	24
3.4.3 Scanning Electrons Microscope (SEM) and Atomic Force Microscope (AFM)	25
3.4.4 Conductivity Measurements	25
3.4.5 Test Equipment Developed.....	25
3.4.6 Other Tools and Instruments Used	27
3.5 Conclusion	28
CHAPTER 4: APPLICATION OF POLY (P-PHENYLENE OXIDE) AS BLOCKING LAYER TO REDUCE SELF-DISCHARGE IN SUPERCAPACITORS	29
4.1 Introduction.....	29
4.2 Experimental.....	34
4.2.1 PPO Electrodeposition	34
4.2.2 Atomic Force Microscopy (AFM).....	35
4.2.3 Electrochemical Impedance Spectroscopy (EIS).....	35
4.2.4 Device Fabrication and Characterization.....	35
4.3 Results and Discussion	36
4.3.1 PPO Deposition and Characterization	36
4.3.2 Supercapacitor Characterization	40
4.3.2.1 Specific Capacitance Measurement Using Cyclic Voltammetry...41	
4.3.2.2 Leakage Current Estimation Using Self-Discharge Profile	42
4.3.2.3 R_s Measurement Using Galvanic Pulses	44
4.4 Discussion.....	45
4.5 Conclusions.....	47
CHAPTER 5: MODELING AND SIMULATION STUDY OF THE SELF-DISCHARGE IN SUPERCAPACITORS IN PRESENCE OF A BLOCKING LAYER.....	48
5.1 Introduction.....	48
5.2 Modeling.....	50
5.3 Results and Discussion	55
5.3.1 Parameter Extraction and Estimation of $k(V, d)$ from Experimental Results.....	55
5.3.2 Simulation Results for PPO as the Blocking Layer	57
5.3.3 Simulation Results for Devices with Various Thickness of the PPO Layer	58
5.3.3.1 Constant Initial Voltage	58
5.3.3.2 Constant Initial Energy Density.....	60
5.4 Conclusion	62

CHAPTER 6: EFFECT OF TRITON X-100 ON THE DOUBLE LAYER CAPACITANCE AND CONDUCTIVITY OF POLY(3,4- ETHYLENEDIOXYTHIOPHENE):POLY(STYRENESULFONATE) (PEDOT:PSS) FILMS	63
6.1 Introduction.....	63
6.2 Experimental.....	66
6.2.1 Electrode Fabrication.....	66
6.2.2 Cell Fabrication and Characterization	67
6.3 Results and Discussion	69
6.3.1 Specific Capacitance Measurements Using Cyclic Voltammetry	69
6.3.2 Fast Galvanic Pulse Measurements	70
6.3.3 Electrochemical Impedance Spectroscopy	73
6.3.4 Stability Study.....	76
6.3.5 Surface Morphology	77
6.4 Conclusion	77
 CHAPTER 7: PHOTOACTIVE SUPERCAPACITORS FOR SOLAR ENERGY HARVESTING AND STORAGE.....	 79
7.1 Introduction.....	79
7.2 Experimental.....	81
7.2.1 Materials and Equipment.....	81
7.2.2 Electrode Fabrication.....	82
7.3 Results and Discussion	82
7.4 Conclusions.....	92
7.5 Acknowledgements.....	92
 CHAPTER 8: CONCLUSIONS AND FUTURE WORKS	 93
 REFERENCES	 96
 APPENDIX A: COPYRIGHT PERMISSIONS.....	 112
 APPENDIX B: SUPPLEMENTARY MATERIAL FOR CHAPTER 4	 116
 APPENDIX C: SUPPLEMENTARY MATERIAL FOR CHAPTER 5	 119
 APPENDIX D: SUPPLEMENTARY MATERIAL FOR CHAPTER 7	 121
 APPENDIX E: MATLAB CODE FOR THE POTENTIOSTAT IN CHAPTER 3.....	 123
 APPENDIX F: MATLAB CODE FOR CHAPTER 5.....	 134

LIST OF TABLES

Table 1 Hybrid supercapacitors with the electrode material, the capacitance per mass, and the energy/power density.	17
Table 2 Simulated values for C_{eq} , R_p , and R_s in the glassy carbon electrode with and without the PPO coating	39
Table 3 The characteristics of the supercapacitors without and with the blocking layer.	44
Table 4 Simulated characteristics of the supercapacitors for different thicknesses of the blocking layer (PPO) with the same initial voltage.	60
Table 5 Simulated characteristics of the supercapacitors for different thicknesses of the blocking layer (PPO) at different charging voltages and same initial specific energy	60
Table 6 Simulated values for CPE, R_p , and R_s in the of 0.0, 3.0, and 5.0 wt% Triton-X 100 electrode.	75
Table 7 Comparison between impedance parameters in the dark and light.	89

LIST OF FIGURES

Figure 1 Ragone plot showing the energy density versus power density of supercapacitors compared to other energy storage devices	2
Figure 2 Schematic of a supercapacitor	3
Figure 3 Schematic of electron tunneling in quantum physics	9
Figure 4 Schematic of the double layer formed by two planes (IHP=Inner Helmholtz plane and OHP=Outer Helmholtz plane) where ions are adsorbed to the electrode-electrolyte interface.).....	11
Figure 5 Schematic of the double layer models.....	14
Figure 6 Simple electrical model of the double layer	15
Figure 7 Schematic of different types of pseudocapacitors	16
Figure 8 (a) Developed Potentiostat device, with (b) the graphical user interface, and (c) a sample of real time data obtained with the device.....	26
Figure 9 Equipment used	27
Figure 10 A cross section view and a simplified model for a supercapacitor.	30
Figure 11 Schematics of the electrode–electrolyte interface (double layer charges) in supercapacitors.....	31
Figure 12 Phenol monomer and PPO polymer.	33
Figure 13 A picture of the fabricated supercapacitor.....	36
Figure 14 Electrodeposition of PPO on a glassy carbon electrode using CV method (scan rate 50 mV.s ⁻¹); the decrease in the current with subsequent scans indicates the growth of the insulating layer.	37
Figure 15 AFM topographic and phase images of: (a) and (c) uncoated glassy carbon surface and (b) and (d) electro-polymerized PPO on a glassy carbon electrode surface.....	38

Figure 16 (a) Magnitude and (b) phase of the measured and simulated impedance for the glassy carbon electrodes with and without the PPO layer	39
Figure 17 Cyclic voltammograms for two supercapacitors: with and without the PPO blocking layer.....	42
Figure 18 Self-discharge profile in two supercapacitors with and without the blocking layer.....	43
Figure 19 Galvanic pulses for measuring series resistance in supercapacitors with and without PPO layer.	45
Figure 20 Schematics of the electrode–electrolyte double layer interface in supercapacitors.....	49
Figure 21 Reaction rates versus voltage in devices (a) without and (b) with the blocking layer.....	56
Figure 22 Simulated and experimental self-discharge profiles with 1.5 nm thick PPO as the blocking layer.....	57
Figure 23 Simulated self-discharge profiles with PPO as the blocking layer for different thicknesses.....	58
Figure 24 Simulated specific energy profiles with PPO as the blocking layer for different thicknesses.....	59
Figure 25 (a) Self discharge voltage and (b) specific energy profiles in devices with various thickness of the blocking layer.....	61
Figure 26 Treated PEDOT–PSS film on ITO substrate.....	67
Figure 27 Cyclic voltammetry curves for different values of Triton X-100 percentage.	69
Figure 28 Specific capacitance as a function of Triton X-100 percentage.	70
Figure 29 Galvanic pulses for PEDOT–PSS electrodes with 3.0 wt% Triton X-100.....	71
Figure 30 Series resistances for different values of Triton-X 100 percentage.	72
Figure 31 Film conductivity as a function of Triton-X 100 percentage.	72
Figure 32 Nyquist plots of electrodes made with PEDOT:PSS with different percentages of Triton X-100	73
Figure 33 (a) Magnitude and (b) phase of impedance from the electrode made of PEDOT:PSS containing 3.0 wt% of Triton X-100	74

Figure 34 Cyclic voltammetry curves before and after 3000 cycles of charging and discharging a symmetrical cell with polymer electrodes containing 3.0 wt% Triton X-100.	76
Figure 35 SEM images of PEDOT-PSS on ITO electrodes with (a) and (b) 0.0 wt%; (c) and (d) 3.0 wt%; and (e) and (f) 5.0 wt% Triton X-100.	78
Figure 36 (a) Schematic of an electrochemical device with a composite of a conducting polymer and a dye as the photosensitive anode electrode (– terminal).	80
Figure 37 Photovoltaic and energy storage effect in the cell with PEDOT:PSS-porphyrin dye composite electrode	84
Figure 38 (a) CV results from devices with only CP, only dye, and 1:1, 1:2, 2:1 CP-dye composite electrodes.	86
Figure 39 Optical absorption of the films of only CP and only dye on two ITO electrodes.....	86
Figure 40 The change in the open circuit voltage in different cells under illumination and after cessation of light.	87
Figure 41 Photoelectric study of the cell with 2:1 CP-dye composite electrode (a) CVs in dark and light with slow scan rate (2 mV s^{-1}).....	89
Figure 42 Open circuit voltage of a cell with CP and N749 dye composite electrode in light and dark.....	90
Figure 43 Energy diagram of the photoactive supercapacitor	92

ABSTRACT

Supercapacitors have emerged in recent years as a promising energy storage technology. The main mechanism of energy storage is based on electrostatic separation of charges in a region at the electrode-electrolyte interface called double layer. Various electrode materials including carbon and conducting polymers have been used in supercapacitors. Also, supercapacitors offer high life cycle and high power density among electrochemical energy storage devices. Despite their interesting features, supercapacitors present some disadvantages that limit their competitiveness with other storage devices in some applications. One of those drawbacks is high self-discharge or leakage. The leakage occurs when electrons cross the double layer to be involved in electrochemical reactions in the supercapacitor's electrolyte. In this work, the first research project demonstrates that the addition of a very thin blocking layer to a supercapacitor electrode, can improve the energy storage capability of the device by reducing the leakage. However, the downside of adding a blocking layer is the reduction of the capacitance. A second project developed a mathematical model to study how the thickness of the blocking layer affects the capacitance and the energy density. The model combines electrochemical and quantum mechanical effects on the electrons transfer responsible of the leakage. Based on the model, a computational code is developed to simulate and study the self-discharge and the energy loss in hypothetical devices with different thicknesses of the blocking layer. The third research project identified the optimal amount of a surfactant (Triton-X 100) that had a significant effect on the double layer capacitance and conductivity of a spin-coated PEDOT:PSS (poly(3,4-

ethylenedioxythiophene): poly(styrenesulfonate)) electrode. The effect of the concentration of the surfactant was investigated by measuring the electrochemical properties and the conductivity of different electrodes. The electrodes were fabricated with different concentrations of the surfactant. Scanning electron microscopy characterizations confirmed the structural change in the PEDOT:PSS that contributed to the capacitance and conductivity enhancement. A final research project proposed an approach on how to utilize the modified PEDOT:PSS added to different photoactive dyes to design a photoactive supercapacitor. The new approach showed the possibility of using a supercapacitor device as an energy harvesting as well as a storage device.

CHAPTER 1: INTRODUCTION

1.1 Energy Crisis

Due to the depletion and shortage of non renewable fossil fuels based energy sources, a serious challenge in the current century is the energy crisis [1]. Also, the emissions of non-renewable energies (oil, gas, coal) have increased negative impacts on the environment, humans, and human activities. Those emissions known as greenhouse-gas emissions are in form of carbon dioxide (CO₂) (~82%), methane (CH₄) (~9%), Nitrous oxide (N₂O) (~6%), and fluorinated gases (hydrofluorocarbons, perfluorocarbons, and sulfur hexafluoride) (~3%) according to the United States Environmental Protection Agency (EPA) [2]. The greenhouse-gas emissions have exacerbated climate change effects [3]. Those effects have increased research efforts towards the development of renewable energy sources.

Research interests towards renewable sources of energy have increased to address the energy crisis caused by the shortage fossil fuels energy sources such as natural gas and oil coupled with their greenhouse-gas emissions. The new forms of energy are now applied in different sectors including transportation for hybrid vehicles and in applications such as wireless sensors [4], [5]. Using renewable sources such as photovoltaic panels or windfarms for energy harvesting, requires energy storage devices since the captured form of energy (e.g. wind or solar energy) is not available all the time.

1.2 Supercapacitors

For electrical and electronic applications, the available types of energy storage devices include fuel cells, batteries, electrolytic capacitors, and supercapacitors also known as ultracapacitors, or electrochemical capacitors. The mechanism of charge storage in both fuel cells and batteries is based on chemical reactions at the electrodes [6], [7]. In contrast, the main mechanism of charge storage in supercapacitors is the electrostatic force between charges. Batteries and fuel cells have a relatively high energy density compared to supercapacitors, however their power density is low [8], [9]. On the other hand, supercapacitors provide better energy density compared to electrolytic capacitors and offer a good alternative for batteries in applications where high power density (fast charging/discharging capability) is needed [10]. Figure 1, known as Ragone plot, shows a comparison of power density and energy density of different energy storage devices.

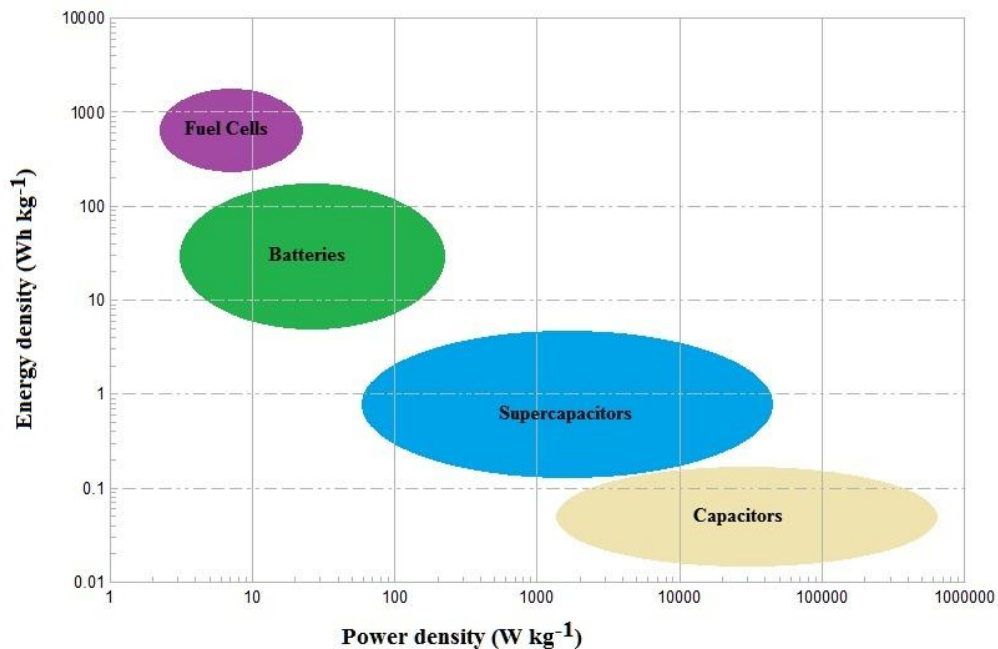


Figure 1 Ragone plot showing the energy density versus power density of supercapacitors compared to other energy storage devices

In addition to high power density, supercapacitors have large lifetime cycle ($\sim 10^6$), are environmentally friendly, and can be operated at low temperature [11].

In a simplistic form, a supercapacitor is made with two porous electrodes separated by an electrolyte containing positive and negative ions (Figure 2). The energy storage can be achieved by an electrostatic double layer formed at the electrode-electrolyte interface, or by electrochemical charge-transfer reactions. The mechanism behind the charge storage determines the type of supercapacitor. There are 3 types of supercapacitors including the Electric Double Layer Capacitor (EDLC), the electrochemical pseudocapacitor, and the hybrid capacitor (a combination of EDLC and pseudocapacitor)[12]. The scope of this work is mainly focused on EDLCs. The device structure and the mechanisms of charge storage are explained in the next chapter.

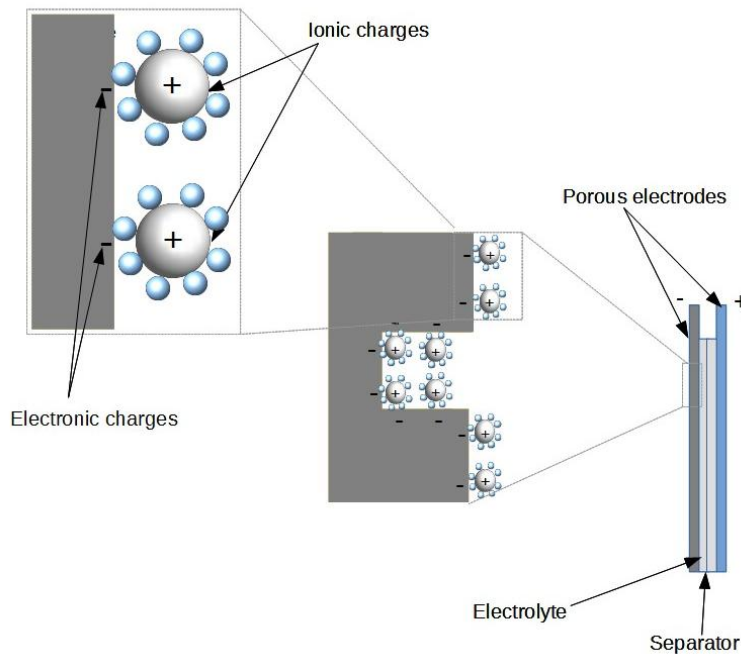


Figure 2 Schematic of a supercapacitor

1.3 Motivation of this Work

Supercapacitor applications have been increasing and diversifying, since its early utilization as computer backup power supply in 1978 [13]. Today, supercapacitors are used in some consumer electronics, power tools, wireless sensors, and transportation [14]. With increasing commercial applications, supercapacitor market is projected to attract 3.5 billion USD in revenue by 2020 [15]. At the same time, the supercapacitor global market is also expected to grow at a Compound Annual Growth Rate (CAGR) of 26.93% [16].

The increasing supercapacitor research interests and technology advancement by many research groups and companies have been motivated by this growth. The research efforts are aimed at finding new solutions to supercapacitors challenges, paving ways to their usage in new or existing applications. A serious disadvantage of supercapacitors, which limits their implementation in some practical applications, is their high self discharge. Despite their high power density, supercapacitors have high leakage current [17]. In electrical double layer capacitors (EDLCs), Faradaic electrochemical reactions can be induced by charge transfer across the electrode-electrolyte interface resulting in leakage [18].

Additionally, among materials used for supercapacitor electrodes, conducting polymers have been researched as composite elements with other materials to increase their capacitance [19]–[22]. Those materials are developed with synthesis techniques of different levels of complexity that could be a serious disadvantage for their industrial production. Conducting polymers have the advantages to have low environmental impact, high storage capacity, and low fabrication costs [20]. Despite their easy industrial processing and fabrication using techniques such as spin coating or inkjet printing [23], [24], conducting polymers such as poly(3,4-ethylenedioxythiophene): poly(styrenesulfonate) (PEDOT:PSS) when used as main electrode

material have low double layer capacitance and power due to their low conductivity and compact structure [25]. The objective of this research was to improve supercapacitor storage capabilities by providing a practical solution to reduce the leakage current and enhancing the capacitance in conducting polymer films to be utilized as composite material for photoelectrochemical supercapacitors.

1.4 Scope of Dissertation

In this dissertation, different research projects are presented. They pertain to the reduction of electric double layer capacitors' self-discharge and the improvement of the double layer capacitance of PEDOT: PSS. The basics and theories of supercapacitors used in the research projects are briefly reviewed in chapter 2. Chapter 3 presents the techniques used to characterize the capacitors developed in different research projects. Chapter 4 discusses the experimental results about reducing the self-discharge via application of a blocking layer. The effect of the blocking layer has also been studied by developing a theoretical analytical equation and a simulation tool in Matlab environment (Chapter 5). In Chapter 6, the effect of adding a surfactant (Triton X-100) to PEDOT: PSS has been presented which indicates the capacitance enhancement by increasing the polymer porosity. Chapter 7 applies the results of the previous chapter combined with a different approach to solar energy generation and storage to develop a novel photoactive supercapacitor. Chapter 8 concludes this work and presents its future possibilities.

CHAPTER 2: BACKGROUND

2.1 Historical Overview

Supercapacitive electrochemical energy storage was known since 1850's [26] with the theoretical investigation of the Electric Double layer by German Physicist Hermann L. F. von Helmholtz [27]. Since their accidental discovery in General Electric laboratories in 1950's and their first commercial applications in the 1970's, real interest for supercapacitors have started to increase from the 1990's due to their ability to provide a high burst of power needed for acceleration in hybrid vehicles [28]. In 1957, Howard I. Becker designed an electrochemical capacitor using porous carbon [29] which he mistakenly called electrolytic capacitor. Almost a decade later (1966), engineers and scientists at Standard Oil of Ohio (SOHIO) developed another similar electrochemical capacitor. SOHIO sold the technology to NEC (Nippon Electric Company, Japan) who introduced its first commercial application as backup power for computer memory in 1971 [26]. NEC coined the electrochemical capacitor "Supercapacitor" because of the high capacitance exhibited [30]. Since supercapacitors are essentially electrochemical cells, the basic of electrochemistry is reviewed in this chapter as the background for the research work presented in the following chapters.

2.2 Electrochemical Reaction

2.2.1 Redox Reaction

A redox reaction is an electrochemical reaction that generally involves electrons transfer [31]. It combines two half reactions including an oxidation and a reduction that may occur

simultaneously [32], [31]. The reaction in which a material loses electron is called oxidation and when the material gains electrons, it is called reduction. Essentially, the oxidation state of the material changes in a redox reaction [33].

A redox potential (or reduction potential) is a quantification method used to measure a chemical element affinity to electrons. It can therefore be used to determine the redox behavior of a chemical substance or reaction. The redox potential of a redox reaction is a potential at which the redox reaction can occur and it is a combination of both reduction and oxidation half reaction potentials. In standard (or equilibrium) conditions [31], [32] the reduction potential E_o across a cell between the anode and the cathode is given by:

$$E_o = E_{o\ ox} - E_{o\ red} \quad (1)$$

where $E_{o\ ox}$ is the oxidation half reaction potential at the anode and $E_{o\ red}$ the reduction half reaction potential at the cathode.

2.2.2 Nernst Equation

Let's assume a chemical system governed by the electrochemical reaction $Ox + e \rightarrow Red$ where Ox is the oxidized and Red the reduced species. The reaction quotient Qr is given by [32]–[34]:

$$Qr = \frac{\{Red\}}{\{Ox\}} \quad (2)$$

where $\{Red\}$ and $\{Ox\}$ are the respective concentrations of species Red and Ox.

The redox potential of the system E is given by the Nernst equation [31], [34], [35] in this form:

$$E = E_o - \frac{RT}{nF} \ln Q_r \quad (3)$$

where R is the gas constant ($8.314 \text{ J mol}^{-1} \text{ K}^{-1}$), T the temperature ($^{\circ}\text{K}$), Q_r the reaction quotient, n the number of electrons, and F the Faraday constant (96500 C).

At equilibrium concentrations, $E=0$ which gives:

$$E_o = \frac{RT}{nF} \ln Q_r \quad (4)$$

2.2.3 Electrons Tunneling in Quantum Mechanics

In redox reactions, electron transfers are involved between electrochemical species. When electrons face a potential barrier, their transfer rate is affected. Let's consider an electron with an energy U facing a potential barrier, V . According to classical mechanics, the electron can only "go over" the potential barrier if $U > V$ [36]. In quantum mechanics, however, the electron, due to its dual property to behave as a particle as well as a wave (called wave-particle duality [37], [38]), has a certain probability to tunnel through the potential barrier [39] (Figure 3). The probability of the tunneling is related to the electron wavefunction ψ (i.e. the function that describes the quantum property of the electron) along x direction that can be found by solving the Schrodinger equation at the barrier in this form [40]:

$$\frac{\partial^2 \psi(x)}{\partial x^2} + \frac{2m}{\hbar^2} (U - V) \psi(x) = 0 \quad (5)$$

where m is the mass of the electron and \hbar is the reduced Planck constant.

The solution to Equation (5) when $V > U$ is given by:

$$\psi(x) = Ae^{-\alpha x} \quad (6)$$

where

$$\alpha = \sqrt{\frac{2m(V-U)}{\hbar^2}} \quad (7)$$

The solution of the wave function at the potential barrier shows an exponential decay along x which suggests exponential drop of the tunneling rate for a redox reaction in presence of an energy barrier layer.

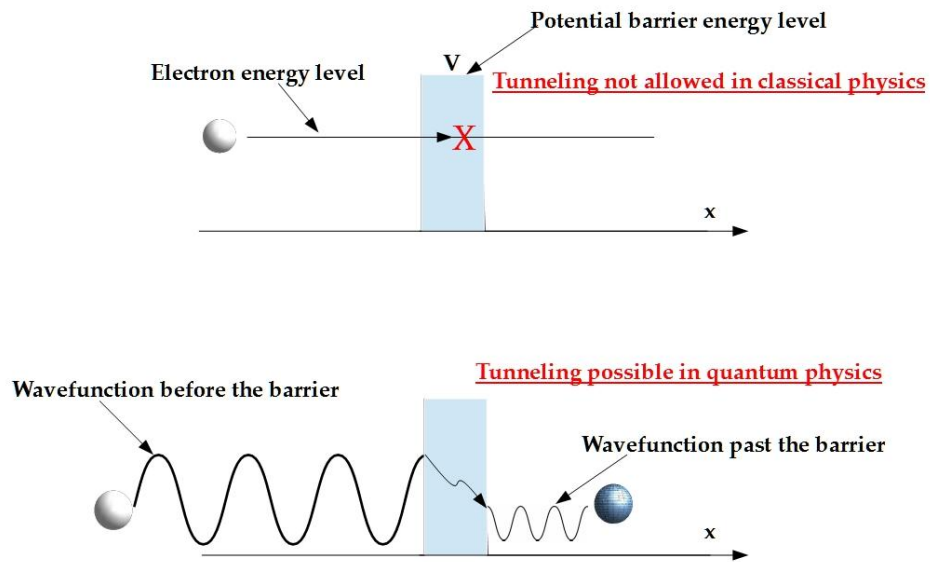


Figure 3 Schematic of electron tunneling in quantum physics

2.3 Different Types of Electrochemical Capacitors

Supercapacitors can be classified into three types: Electrical Double Layer Capacitors (EDLCs), pseudo capacitors, and hybrid capacitors. EDLCs have generally carbon based electrodes and store energy by electrostatic adsorption of charges at the interface of the electrodes and electrolyte. Ionic charges adsorb in the electrolyte while electronic charges accumulate in the electrode forming what is called the electric double layer. Pseudo capacitors achieve their energy storage by electrochemical reactions at the interface. Hybrid capacitors combine the double layer and the Faradic reactions to store energy [41]–[44].

2.3.1 Electrical Double Layer Capacitors (EDLCs)

Most of the commercially available EDLCs are composed with two highly porous carbon electrodes in an electrolyte separated by an insulator (Figure 2). The mechanism of energy storage is based on electrostatic adsorption of charges at the interface of the electrode and electrolyte [45]. During charging of the capacitor, positive and negative ionic charges in the electrolyte are separated and adsorb respectively to the negative and positive electrodes. Figure 4 shows a simplified view of the layers of charges (electric double layer) that form at the interface of one electrode.

Due to their energy storage mechanism that relies on the formation of the double layer at the interface of the electrode and electrolyte, EDLCs can be well understood by analogy with a simple parallel plate capacitor. Consequently, the capacitance of an EDLC taken from one electrode can be given by:

$$C = \epsilon \epsilon_0 \frac{A}{d} \quad (8)$$

where C is the capacitance, ϵ the dielectric constant of the double layer, ϵ_0 the dielectric constant of vacuum ($8.85 \times 10^{-12} \text{ F.m}^{-1}$), A the actual surface of the electrode, and d the double layer thickness.

Different theories have been proposed to explain the double layer that forms when two charged conductors are in close proximity. They include the Helmholtz model, the Gouy-Chapman model, the Stern and Graham models, and the Bockris, Devanathan, and Muller (BDM) model.

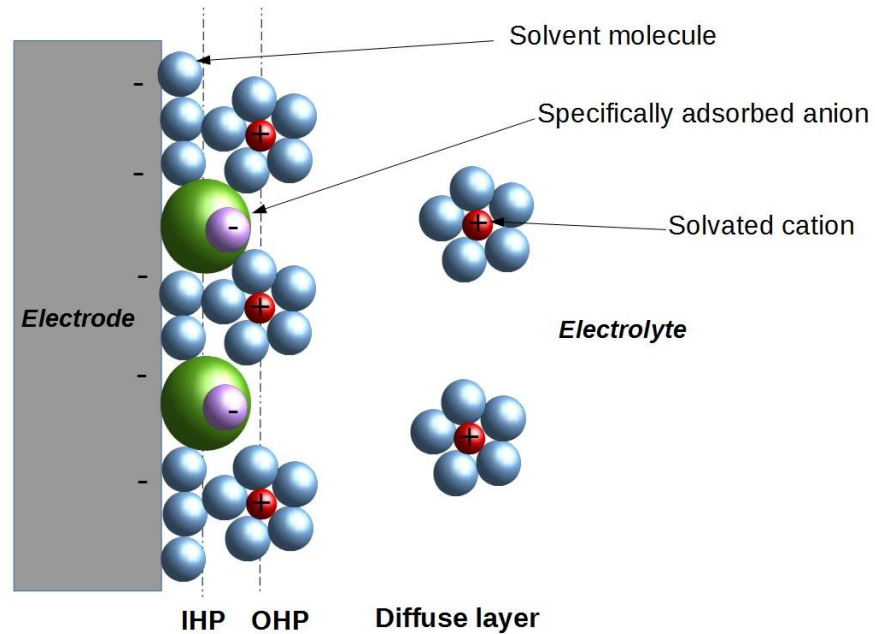


Figure 4 Schematic of the double layer formed by two planes (IHP=Inner Helmholtz plane and OHP=Outer Helmholtz plane) where ions are adsorbed to the electrode-electrolyte interface. (Adapted from [31])

2.3.1.1 Helmholtz Model

The idea of an electrical double layer was first introduced by Helmholtz in 1853. When a charged conductor (electronic charges) is in contact with an electrolyte (ionic charges), an electrostatic charge separation between two layers of opposite charges occurs at the electrode-electrolyte interface. The two layers are apart by only the thickness of one molecule. In this case, there is no electron transfer between the layers [46], [47]. Hence, the capacitance of a Helmholtz double layer can be found from Equation (8).

Although the model developed by Helmholtz does not consider the effect of ions behind the first layer of directly adsorbed ions at the interface, it is widely used due to its simple image which explains the capacitance of an EDLC.

It should be noted that the Helmholtz model works better in electrolytes with high ion concentration. This is mostly the case for EDLCs.

2.3.1.2 Gouy and Chapman Model

Gouy (1910) and Chapman (1913) developed the model separately to describe the dynamics of ions close but not adsorbed to the interface (the diffuse layer) and considered the thermal motion of ions in the electrolyte (see Figure 5).

The model known as the diffuse double layer showed that different parameters such as the applied potential, the concentration of ions in the electrolyte, and their thermal motion affect the capacitance of the double layer [48]. To find the total amount of the charge in the diffuse layer and the ion distribution in space, Poisson equation (9) and Boltzmann equation at both positive and negative electrodes (10, 11) must be solved [49]:

$$\frac{d^2\Phi}{dx^2} = \frac{-4\pi\rho}{\varepsilon} \quad (9)$$

$$N_+ = N_{+0} \exp\left[-\frac{(n_+e\Phi)}{kT}\right] \quad (10)$$

$$N_- = N_{-0} \exp\left[-\frac{(n_-e\Phi)}{kT}\right] \quad (11)$$

where ρ is the volumetric charge density, Φ the electric potential, and ε the dielectric constant; N_+ (N_-) the concentration of ions in the diffuse layer, N_{+0} (N_{-0}) the concentration of ions in the bulk solution, n_+ (n_-) the valence of the ions, and T the absolute temperature ($e= 1.602 \times 10^{-19}$ C, $k=1.38 \times 10^{-23}$ J/K).

2.3.1.3 Stern and Graham Model

Stern developed the model in 1923 which included both Helmholtz and Gouy-Chapman models. His model separated the double layer into two regions, a uniform region of ions close to the electrode (stern layer), and a diffuse layer reaching into the bulk of the electrolyte [50] (Figure 5.c).

Graham added in 1947 the specific adsorption of ions to the Stern model. The Stern-Graham model include three layers: the inner Helmholtz plane (IHP), the outer Helmholtz plane (OHP), and the diffuse layer [51].

The capacitance of the Stern-Graham model can be found by applying the Langmuir theory [49]:

$$C_s = C_d \frac{\partial \sigma}{\partial \sigma_A} \quad (12)$$

where C_s is the capacitance of the Stern layer (obtained with Equation 8), C_d the capacitance of the Gouy-Chapman diffuse layer, σ the surface charge density on the electrode, and σ_A the surface charge density of the specifically adsorbed ions.

2.3.1.4 Bockris, Devanathan, and Muller Model (BDM)

The BDM model (1963) added to the Stern-Graham model the presence of solvents molecules. Using water as solvent, they showed that some of the water molecules were adsorbed at the interface inside the inner Helmholtz plane. The alignment of the dipole of water molecules would be different depending on their distance from the electrode. Molecules close to the electrodes would have fixed dipole alignment due to their proximity with the electronic charges in the electrode [49]. Figure 5 shows the different double layer models discussed above.

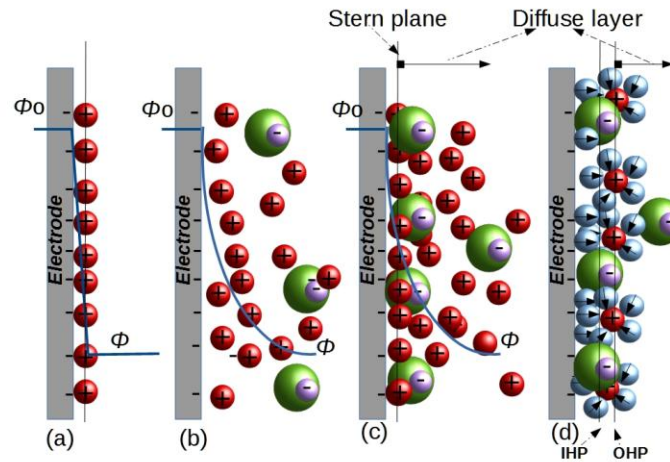


Figure 5 Schematic of the double layer models. (a) Helmholtz model, (b) Gouy-Chapman model, (c) Stern model, and (d) Bockris, Devanathan, and Muller (BDM) model (IHP=Inner Helmholtz plane and OHP=Outer Helmholtz plane). Φ_0 is the electrode surface potential and Φ is the potential at the electrode-electrolyte interface. (Adapted from [49] and [51])

To understand charge storage and discharging mechanisms of EDLCs, a simple electrical model is often used [41], [52] (Figure 6), where C is the capacitance (representing the capacity for charge storage in all the layers in a double layer structure), R_s is the equivalent series resistance and R_p is the discharge parallel resistance (the resistance through which the capacitor self discharges). In double layer capacitors, self-discharge occurs when the electronic charges on the electrode pass through the electrode-electrolyte interface to engage in electrochemical reactions in the electrolyte [52].

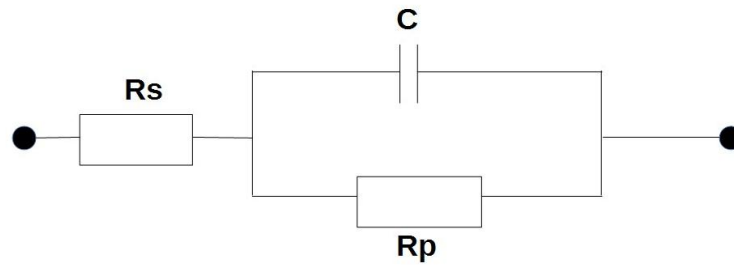


Figure 6 Simple electrical model of the double layer

2.3.2 Pseudocapacitors

Pseudocapacitors are the second type of electrochemical capacitors that rely on faradic or electrochemical reversible redox reactions to store energy. This type of storage mechanism is called Pseudocapacitance. The electrode materials are mostly made with transition metal oxides (e.g. ruthenium oxide, manganese oxide) and conducting polymers (e.g. PEDOT:PSS, Polypyrrole, Polyaniline etc). The Faradic (electrochemical) reactions occur at or close to the surface of the electrodes and can be classified into three different types [53]–[55].

The types of faradic reactions that can induce pseudo capacitance include: underpotential deposition (adsorption pseudocapacitance), redox pseudocapacitance, and intercalation pseudo capacitance [53] (Figure 7).

Underpotential deposition exists when reversible adsorption and removal of atoms occur at the surface of a metal in a two dimensional faradic reactions. Redox pseudocapacitance arises when reversible faradic redox reactions happen at the surface of the electrode. Intercalation pseudocapacitance is the type of pseudocapacitive effect where ions (lithium ions for example) are electrochemically intercalated into structured layers of redox material [56].

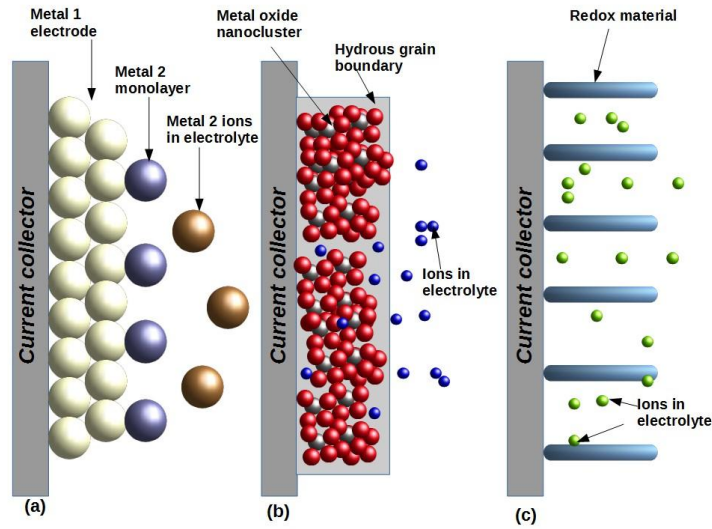


Figure 7 Schematic of different types of pseudocapacitors. (a) underpotential deposition, (b) redox pseudocapacitors, (c) intercalation pseudocapacitor. Adapted from [53]

Although the three pseudo capacitive mechanisms are physically different, they are all electrochemically governed by the Nernst equation [31], [41], [53]. When the potential E can be approximated by a linear function of $(I+Qr)/Qr$, the gravimetric capacitance C_m can be obtained by [53]:

$$C_m = \left(\frac{nF}{m}\right) \frac{(1+Qr)/Qr}{E} \quad (13)$$

where m is the molecular weight of the active material.

2.3.3 Hybrid Capacitors

Another type of supercapacitor is the hybrid capacitor. They combine the features of EDLCs and pseudocapacitors. The electrodes of these types of capacitors are made with composite materials including a double layer material (e.g. carbon or graphene) and a pseudo capacitive material (e.g. conducting polymer, transition metals etc.). Table 1 presents a summary of some of those types of capacitors found in literature [57]. They can also be asymmetric with one double layer electrode and one pseudo capacitive electrode or structured layers of double layer and pseudocapacitive electrodes [42]–[45].

There are different types of supercapacitors. They can be classified based on the electrochemical phenomena behind the storage. Despite the different types of supercapacitors, the electrochemical parameters used to evaluate their performance are the same. The next chapter presents briefly the techniques, tools, and equipment used to fabricate and assess the supercapacitors fabricated in the scope of this dissertation.

Table 1 Hybrid supercapacitors with the electrode material, the capacitance per mass, and the energy/power density. Adapted from [57].

Material	Capacitance per mass	Energy/power density
Single-walled carbon nanotubes/ Polypyrrole [58]	200 Fg ⁻¹ (Electrolyte: 1M NaPF ₆)	NA
Polyaniline –Carbon nanotube composites [59]	597.82 (Electrolyte: 1M H ₂ SO ₄)	NA
Graphene–activated carbon Composite [60]	122 Fg ⁻¹ (Electrolyte: aqueous KOH)	52.2 Wh kg ⁻¹
Graphene and carbon nanotube composite [61]	290.6 Fg ⁻¹ and 201.0 F/g (Electrolyte: 1M KCl,1M tetraethylammonium tetrafluoroborate in propylene carbonate (TEABF ₄ /PC))	62.8 Whkg ⁻¹ 58.5 kWkg ⁻¹

Table 1 (Continued)

Nanorod-Polyaniline-Graphene [60]	878.57 Fg ⁻¹ (Electrolyte: HClO ₄)	NA
Flexible Graphene/Polyaniline Nanofiber Composite [61]	210 F g ⁻¹	NA
Graphene-conducting polymer [21]	300–500 Fg ⁻¹ (Electrolyte: 1M HCl)	NA
Graphene/Polyaniline Nanofiber Composites [62]	480 Fg ⁻¹ (2M H ₂ SO ₄ aqueous)	NA
Graphene/polyaniline [63]	1126 Fg ⁻¹ (Electrolyte: 1M H ₂ SO ₄)	37.9 Whkg ⁻¹ at 141.1W/kg
Graphene-polyethylenedioxythiophene [64]	374 Fg ⁻¹ (Electrolyte 2M HCl)	NA
Graphene-Polypyrrole nanocomposite [65]	417 Fg ⁻¹ (Electrolyte: 2M H ₂ SO ₄)	94.93 W h kg ⁻¹ and 3797.2 Wkg ⁻¹
Graphene/Polypyrrole [66]	424 Fg ⁻¹ (Electrolyte: H ₂ SO ₄)	NA
Graphene/MnO ₂ [67]	256 Fg ⁻¹ (Electrolyte: 0.5M aqueous Na ₂ SO ₄)	NA
Graphene/polypyrrole nanotube/MnO ₂ [68]	469.5 Fg ⁻¹ (Electrolyte: Na ₂ SO ₄)	NA

CHAPTER 3: ELECTROCHEMICAL PARAMETERS, TEST TECHNIQUES, TOOLS, AND INSTRUMENTS USED

3.1 Introduction

Although there are different types of electrochemical capacitors, their performance can be assessed using electrochemical techniques. The electrochemical test techniques allow the measurement of the supercapacitors electrochemical characteristics such as the capacitance, the energy, and the power. The main electrochemical techniques used are the Current voltammetry (CV), the galvanic pulse, the Electrochemical Impedance Spectroscopy (EIS), and the Open Circuit Potential (OCP).

As different research activities were completed as part of this dissertation, some fabrications, measurement methods, and equipment were also designed and developed. This chapter presents briefly all the tests techniques and equipment used and developed, as well as the key electrochemical parameters of supercapacitors.

3.2 Supercapacitors Electrochemical Parameters

3.2.1 Capacitance

The capacitance, C , of an electrical system can be defined as the amount of charge ΔQ it can store at a potential difference ΔV . For an EDLC, the capacitance C is constant and given by:

$$C = \frac{\Delta Q}{\Delta V} \quad (14)$$

To compare the capacitance across different devices, materials, and technologies, the concept of specific capacitance is introduced. It is the capacitance of a device or electrode per unit mass (C_m [F/g]) or volume (C_v [F/m³]). Although C_m and C_v can demonstrate the potential of a material to be used in a device, the capacitance of a specific electrode can be presented based on the normalized capacitance to the apparent surface area of the electrode (C_s [F/m²]).

3.2.2 Energy

The energy of a supercapacitor is proportional to the capacitance and is given by:

$$Energy = \frac{1}{2} CV^2 \quad (15)$$

The specific energy is measured gravimetrically (per unit of mass), However the energy density is measured volumetrically (per unit of volume) [69].

3.2.3 Power

The power of a supercapacitor is the amount of energy delivered per unit of time. It is a very important parameter since one of the main attractions of EDLCS is the high power density compared to batteries. Similarly to the capacitance, the power can be measured gravimetrically (per unit of mass), or volumetrically (per unit of volume) [70].

The maximum power that can be delivered by an EDLC is limited by its series resistance and given by [71]:

$$P_{max} = \frac{1}{4} \frac{V^2}{R_s} \quad (16)$$

Certain electrochemical techniques can be used to evaluate supercapacitor parameters. The most commonly used techniques are: cyclic voltammetry, galvanostatic, impedance, and open circuit voltage measurements.

3.3 Electrochemical Analysis Techniques

To characterize supercapacitors, electroanalytical techniques are used. The techniques are designed to measure different electrical parameters such as potential, current, charge, or frequency of the device under test in an electrochemical environment. The cell or device under test is called an electrochemical cell which can be in two or three electrodes configuration. The two electrodes setup has a working electrode (WE, the electrode of interest) and a counter electrode (CE) which completes the circuit. In a three electrode configuration, an additional electrode called reference electrode (RE) is added to the system. The reference electrode is designed to have no current flow and a constant voltage [31], [72]. It should be noted that the three probe configuration is more useful for studying the interface between an electrode (WE) and the electrolyte. Also, it is used for supercapacitor material characterization. The two probe approach however is toward a device study.

3.3.1 Cyclic Voltammetry Technique

Voltammetry is a simple but strong method of electrochemical analysis techniques that measures the current induced by a cell under test as function of the applied voltage. Among voltammetry techniques, cyclic voltammetry (CV) is the most widely used to determine how charges behave at an electrode-electrolyte interface in a specific potential range [73].

In cyclic voltammetry, the potential of the working electrode is scanned back and forth at a constant rate ($\Delta V/\Delta t$) in a potential window for several cycles. The resulted current data, i , is

measured and plotted as a function of the voltage. CV is a very useful and simple tool to study the capacitance, particularly for EDLCs [52], [74].

The capacitance of an EDLC given by Equation (14) can be rewritten as follows (since the total charge is given by $\int i \cdot dt$) [75], [52]:

$$C = \frac{\Delta(\int i dt)}{\Delta V} = i \left(\frac{\Delta t}{\Delta V} \right) \quad (17)$$

which gives

$$C = \frac{i}{\left(\frac{\Delta V}{\Delta t} \right)} = \frac{i}{\text{Voltage scan rate}} \quad (18)$$

It can be seen that the capacitance can be obtained from CV measurement by taking the ratio of the current to the voltage scan rate.

3.3.2 Galvanostatic Technique

A galvanostatic method is a specific form of a family of electrochemical techniques called chronopotentiometry. Chronopotentiometry is an electrochemical technique that analyzes the cell under test by controlling the current flow and measuring the effects on its potential over time. There are different types of chronopotentiometry methods based on how the current is controlled. They include constant current chronopotentiometry, linear current chronopotentiometry, current reversal chronopotentiometry, and cyclic chronopotentiometry. When a cyclic constant current chronopotentiometry is applied, the method is called galvanic pulse [74], [76], [77], and [78]. A voltage drop in the galvanic pulse measurement allows the estimation of R_s (Figure 6) by Ohm's law [74]:

$$R_s = \frac{\Delta V_t}{2I} \quad (19)$$

where ΔV_t is the voltage drop across the device and I the amplitude of the current pulse.

3.3.3 Impedance Technique

Impedance measurement techniques are the strongest electrochemical technique. They are often called Electrochemical Impedance Spectroscopy (EIS). During EIS measurement, the impedance of the device under test is analyzed by applying a small alternating current (AC) signal to its terminal. The AC current and voltage are measured as a function of the frequency and used to compute the complex impedance. The EIS impedance data is generally represented using Nyquist and Bode plots. In Bode plot the magnitude and phase angle of the impedance are represented as function of the frequency. Nyquist plot shows the imaginary part of the impedance as a function of the real part [79].

Both Nyquist and Bode plots can give valuable information on the electrical nature of the cell under test (inductive, capacitive, or resistive) as well as the porosity of the working electrode and other electrochemical parameters [80], [81].

3.3.4 Open Circuit Measurements

Open circuit measurement is used to determine the open circuit voltage of the device being tested. During open circuit mode, the instrument used to measure the voltage does not control any electrical parameters (voltage, current etc.) of the device and acts as infinite impedance. The instrument acts essentially as a voltmeter. The open circuit can be used to measure the parallel resistance R_p . The total current i in the supercapacitor (Figure 6) is given by:

$$i = I_{Rp} + I_C \quad (20)$$

where I_C is the current in the capacitance C and I_{Rp} the current in the resistance R_P .

In open circuit mode the supercapacitor is self discharging and $i=0$, (since $I_C=-Cdv/dt$ and $I_{Rp}=V/R_P$) the Equation (20) becomes:

$$0 = \frac{V}{R_P} - C \frac{dv}{dt} \quad (21)$$

The resistance R_P can be obtained by:

$$R_P = \frac{V}{C(dv/dt)} \quad (22)$$

where V is the open circuit voltage at a given time and dv/dt the slope of the self discharge curve at that time.

3.4 Tools and Instruments Used

3.4.1 Electrochemical Instrument

All the electrochemical measurements used in this dissertation (cyclic voltammetry, Galvanostatic pulse, EIS, and open circuit measurements) were performed using the Verstat Potentiostat of Princeton Applied Research (PAR) (Figure 9 (a)).

3.4.2 Solar Simulator

A solar simulator (RST - Radiant Source Technology) coupled with a dark box was used as a setup for testing the response of the photoactive supercapacitors developed in chapter 7 (Appendix D). The solar simulator delivers a light intensity of 80mW cm^{-2} at AM 1.0.

3.4.3 Scanning Electrons Microscope (SEM) and Atomic Force Microscope (AFM)

The supercapacitor electrodes were characterized with Scanning Electron microscope (SEM) and Atomic force Microscope (AFM) to study the topography, structure, and profile of their surfaces. An SEM is an electron microscope that can obtain nanoscale images of conductive surfaces using focused electrons' beams [82]. Atomic Force microscope (AFM) is used to study surfaces morphology and topography by measuring the force on a nanoscale sharp tip mounted on a flexible cantilever induced by the vicinity of the tip to the surface of the electrode being characterized [83]. The intensity of the force is function of the distance of the tip to the surface of the electrode sample. Contrary to the SEM, AFM does not require a conductive surface. An SEM Hitachi S800 and an AFM Dimension 3000 were used to characterize the electrode samples.

3.4.4 Conductivity Measurements

The conductivity tests were recorded using a four point probe technique. A four point probe method uses four aligned probes in contact with the surface under test. A current is flown through the outer probes. A voltage is measured between the two inner probes and the resistivity or conductivity of the surface is computed [84]. The conductivity measurements were performed with a Keithley source meter (model 2602) unit and a four point probe setup (Figure 9 (e) and (f)).

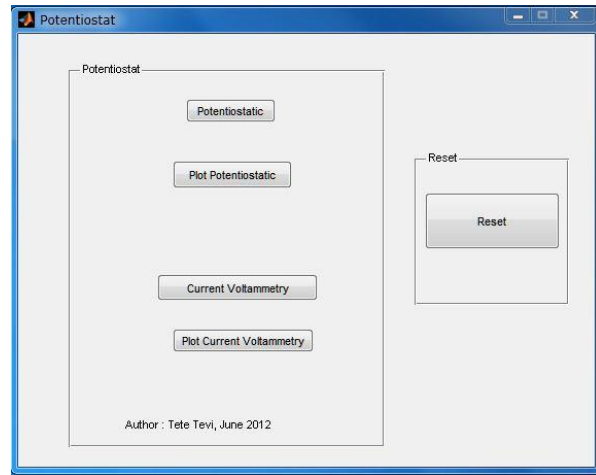
3.4.5 Test Equipment Developed

To complete long time consuming experiments such as self discharge experiments, a two probes Potentiostat device (Figure 8 (a)) was designed and developed. The device uses a National Instrument Data Acquisition tool (USB-1408FS). A code and a graphical user interface

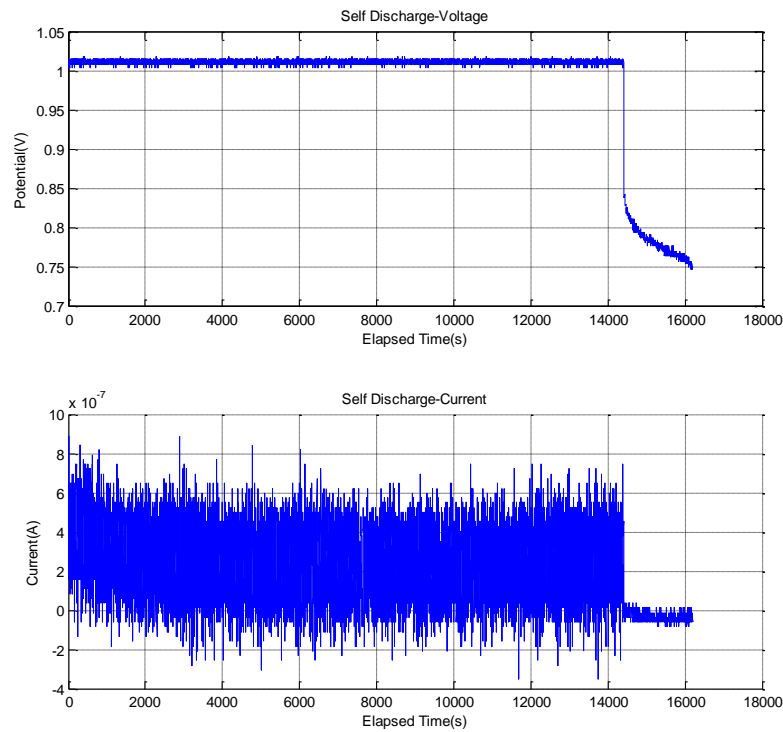
(Figure 8 (b)) were developed in Matlab environment to run the potentiostat. The code is presented in Appendix E.



(a)



(b)



(c)

Figure 8 (a) Developed Potentiostat device, with (b) the graphical user interface, and (c) a sample of real time data obtained with the device.

3.4.6 Other Tools and Instruments Used

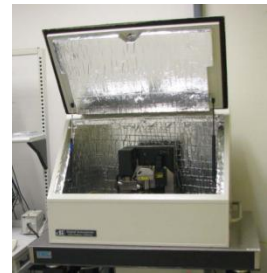
A spin coater (NNRC Laurel Spinner model WS-4008Z-6NPP), a hot plate (Fisher Scientific), and an analytical balance (model GH-252) were also used to prepare the electrode samples. A spincoater is a device that allows uniform and thin coating of liquid films using spinning. As the spin speed is increased, centrifugal forces cause the coating liquid to spread radially over the substrate. A hot plate is used to cure samples at a desired temperature and time. The analytical balance was used in all weight measurements. The balance has a precision of 0.001mg. Figure 9 shows the pictures of the equipment used.



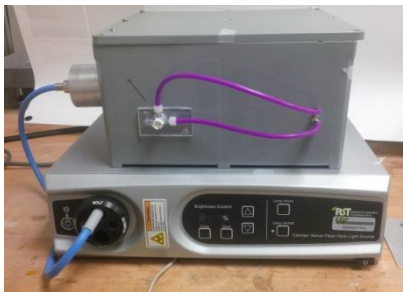
(a)



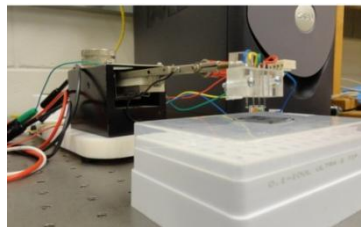
(b)



(c)



(d)



(e)



(f)



(g)



(h)

Figure 9 Equipment used

3.5 Conclusion

The tools and techniques used in this dissertation were presented in this chapter. The techniques include electrochemical methods, spectroscopy methods, conductivity measurements, and simulations methods. The fabrication methods developed for each research activity are presented in the experimental section of each chapter. Supercapacitors possess parameters that can be measured using several analytical methods and test techniques. The specific type of supercapacitor called electric double layer capacitor which is the focus of this dissertation offer some advantages such as high power density compared to the other types of supercapacitors. Nevertheless, although supercapacitors in general have high power density compared to battery and fuel cells, they suffer from high self discharge. The next chapter provides a practical solution to limit the leakage and presents the first research project of this dissertation.

CHAPTER 4: APPLICATION OF POLY (P-PHENYLENE OXIDE) AS BLOCKING LAYER TO REDUCE SELF-DISCHARGE IN SUPERCAPACITORS¹

4.1 Introduction

Application of energy storage devices is growing rapidly due to the demand for more mobile and wireless electronics. Potentially, supercapacitors are suitable alternatives for batteries in applications, where high power density is needed (e.g. wireless devices and electric/hybrid vehicles) [10]. Also, supercapacitors have larger cycle lifetime than batteries. A supercapacitor can be charged and discharged up to a million times, whereas a typical rechargeable battery can be used up to only 1000 cycles [85], [86]. The large cycle lifetime is vital in small electronics which are designed to harvest energy from ambient sources. In fact, the market for wireless sensors equipped with energy harvesting units is growing rapidly for various applications such as structural health and traffic [87]. Despite the advantages, practically, the application of supercapacitors is very limited mainly due to high leakage current in the devices. The leakage current results in self-discharge effect in supercapacitors and inefficient charging/discharging cycles with energy waste during each cycle [86], [88], and [89]. The leakage problem is more serious in devices powered by harvesting solar, thermal, or vibration energy. The amount of harvested power is usually very low (10–1000 μ W [90]). Hence, the amount of current available for charging a supercapacitor is limited. If the current value is less than the leakage current, the supercapacitor cannot be charged at all. The leakage problem has been investigated extensively

¹This chapter was previously published in [52]. Permission is included in Appendix A.

through modeling [91]–[94] and the electrochemical study of the electrode–electrolyte interface [17], [95], [96]. Yet no practical solution has been applied for decreasing the leakage current in supercapacitors. In this work, we have studied the application of an ultra-thin insulating layer (blocking layer) between the electrode and the electrolyte as a potential solution for reducing the leakage current, particularly for wireless sensor applications.

The most popular form of a supercapacitor is the electrochemical double layer capacitor (EDLC) [85]. Figure 10 shows the structure of an EDLC, which is made of two porous electrodes in an electrolyte. When a voltage is applied across the device (charging process), ions move from the bulk electrolyte toward the electrodes and form double layer charges (Figure 11(a)). The double layer mimics a parallel plate capacitor with the solvent material as the dielectric, with permittivity of ϵ_s , between ionic and electronic charges.

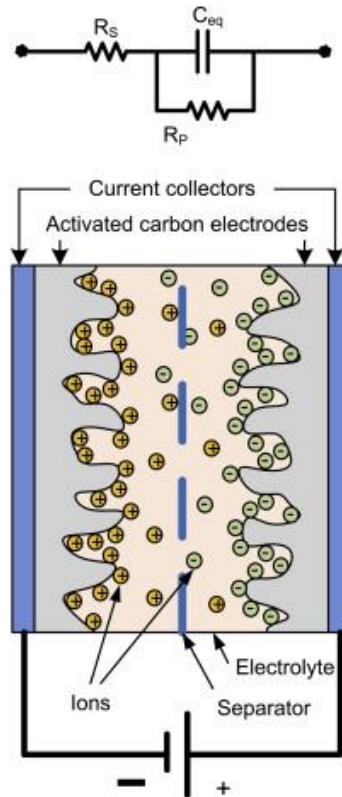


Figure 10 A cross section view and a simplified model for a supercapacitor.

Due to the small distance between the opposite charges (d in Figure 11(a)), the double layer capacitance ($C_{DL} = \epsilon s/d$) is typically in the range of $5\text{--}20\mu\text{Fcm}^{-2}$ [85]. To achieve high specific capacitance, C_{sp} , (capacitance per mass, Fg^{-1} , or capacitance per volume, Fcm^{-3}) in supercapacitors, porous electrodes with extremely large surface area are employed. The energy can be stored in EDLCs by charging the device. Similar to a capacitor, the energy density is equal to $0.5C_{sp}V^2$, where V is the applied charging voltage. Once the device is charged, the charge across the double layer has to be preserved to store the energy. However, as shown in Figure 11(a), a redox reaction (Faradic reaction) may occur at the electrode surface through which electrons pass through the double layer and discharge the capacitor. The effect of the Faradic reactions appears as the leakage current, which results in the self-discharge effect. As a solution, an ultra-thin layer of an insulating material can be employed on the electrode surface to block the electron transfer and reduce the leakage current (Figure 11(b)).

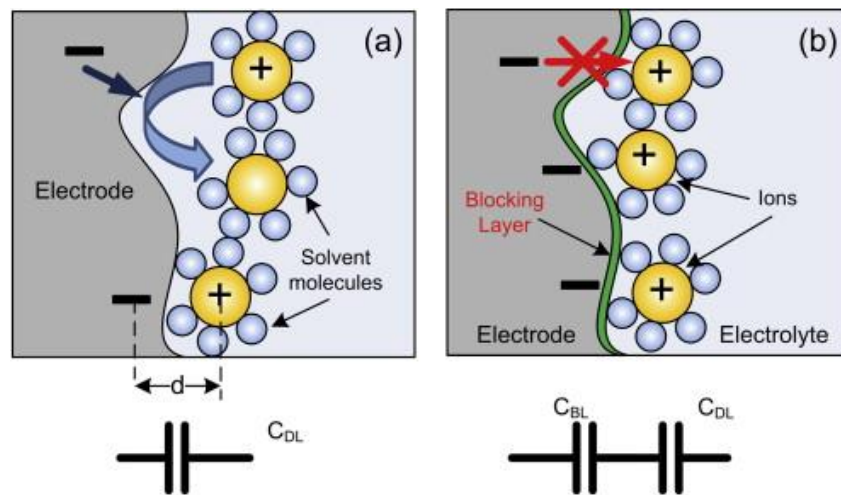


Figure 11 Schematics of the electrode–electrolyte interface (double layer charges) in supercapacitors. The charge arrangement can be modeled with capacitors. (a) Electrochemical reaction at the surface of the electrode results in charge loss. (b) Application of a thin blocking layer decreases the reaction rate and enhances the energy storage capability.

For better understanding the effect of the leakage current, a supercapacitor can be modeled with an ideal capacitance, C_{eq} , a series resistance, R_s , and a parallel

resistance, R_P (Figure 10). Considering a double layer capacitor at each electrode, C_{eq} is the equivalent capacitance of both capacitors in series. R_S includes the contact and the electrolyte resistances, and R_P represents the leakage path. The main source of the leakage current is Faradic reactions at the electrode surface [96]. The amount of the leakage current is proportional to the reaction rate. The rate of the electron transfer depends on the reduction potential of the redox reaction, E_0 , and the applied voltage, V , across the double layer. The difference between V and E_0 is known as the overpotential ($=V - E_0$). According to Tafel equation [31], the Faradic reaction rate is related exponentially to the overpotential, meaning that the leakage current increases exponentially with the increase in the applied voltage. Therefore, R_P is a function of the applied voltage with the lowest value when the device is charged up to the maximum voltage. As a result of the leakage, a typical device loses 10% of the stored energy in less than 1 h [97]. In practice, it is recommended to charge supercapacitors to the voltages lower than the nominal value for controlling the leakage [98]. However, since the energy density is proportional to V^2 , reducing the voltage decreases the amount of stored energy significantly and makes supercapacitors less efficient than batteries for applications with size constraint.

The electrochemical reaction rate can be lowered by application of an insulating layer (blocking layer) on the electrodes. The effect of the blocking layer can be modeled as a capacitance, C_{BL} , in series with the double layer capacitance C_{DL} (Figure 11(b)). It should be noted that the blocking layer is not hindering the double layer capacitance. The coating increases the distance between ionic and electronic charges and provides an energy barrier for Faradic reactions. Therefore, the equivalent capacitance is $C_{eq} = C_{BL}C_{DL}/(C_{BL} + C_{DL})$ which is always smaller than C_{DL} . In order to minimize the capacitance reduction, C_{BL} has to be much larger than C_{DL} . Due to the very small distance between negative and positive charges in a double layer

capacitor, this can happen only if an ultrathin (~ 1 nm) high dielectric material is applied as the blocking layer. It is anticipated to have a C_{DL} in the same range of C_{BL} if a thin layer (1–2 nm) of an insulating polymer ($\epsilon_r \approx 3.5$) is applied. In this case, C_{eq} would be about half of the double layer capacitance. The key point in minimizing the capacitance reduction is to deposit an ultrathin and uniform layer of the polymer on the electrodes. In this work, a thin layer of poly (p-phenylene oxide), PPO, on the electrodes was deposited, acting as the blocking layer. Electrodeposition is an easy method for coating conductive surfaces with conformal thin films [99]. It has been demonstrated that the electrodeposition of PPO can produce a pin-hole free thin-film layer on conductive. Ultra-thin PPO films are stable in organic and aqueous electrolytes, and do not block the formation of an electrical double layer, when deposited on conductive [100]. The mechanism of deposition is based on polymerization of a monomer in an electrochemical reaction. Due to the low conductivity of PPO, the resistance of the polymer chain increases as the film grows. The high resistance leads to formation of a passivation layer, which stops the further growth of PPO. The self-limiting growth mechanism generates an ultra-thin film of PPO with a thickness of about a few nanometers [101]. Figure 12 shows the phenol monomer and the PPO molecule after electropolymerization.

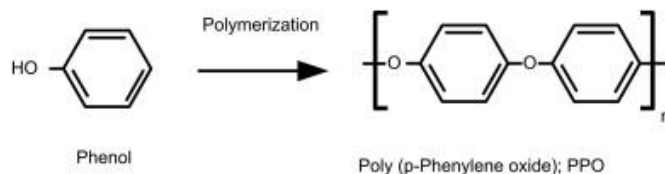


Figure 12 Phenol monomer and PPO polymer.

In order to study the morphology and measure the thickness of the blocking layer, a PPO layer was first deposited on a glassy carbon substrate (flat and smooth surface). Then surface coverage and roughness of the PPO layer were studied using atomic force microscopy (AFM), and the thickness was estimated from an electrochemical impedance spectroscopy (EIS)

experiment. After that, the surface of two activated carbon electrodes was coated with a layer of PPO, and the electrodes were utilized to make a supercapacitor. Also, another capacitor was fabricated with no coating. C_{eq} , R_p and R_s were measured in both devices through electrochemical experiments, including cyclic voltammetry (CV), open circuit voltage measurement, and galvanic pulses. The difference between the parameters in both devices has been discussed, which indicates the effect of the blocking layer on the performance of a supercapacitor.

4.2 Experimental

The electrochemical experiments were performed using a VersaSTAT 4 (Princeton Applied Research) potentiostat. Activated carbon electrodes from Y-Carbon (www.y-carbon.us) and glassy carbons from SPI Supplies (www.2spi.com) were used as the electrodes. All the other chemicals were purchased from Sigma and used without further purification.

4.2.1 PPO Electrodeposition

The developed method explained by Rhodes et al., has been modified for PPO [101]. The phenylene oxide monomer solution was prepared with 50 mM tetramethylammonium hydroxide, 0.1 M tetrabutylammonium perchlorate, and 50 mM phenol solvated in propylene carbonate. The PPO deposition was performed in a three electrode cell configuration with Ag/AgCl reference electrode and a coiled Pt wire as the counter electrode. The working electrode was either a glassy carbon (area of $\sim 0.5 \text{ cm}^2$) or pieces of activated carbon each with apparent surface area of 0.5 cm^2 . Cyclic voltammetry (CV) technique was applied for PPO [101]. The working electrode potential was scanned for 22 cycles between -45 mV and $+955 \text{ mV}$ versus Ag/AgCl with the scan rate of 50 mV s^{-1} . After the electrodeposition, the electrodes were rinsed with propylene carbonate.

4.2.2 Atomic Force Microscopy (AFM)

The morphology of the glassy carbon electrode before and after PPO electrodeposition was studied with tapping mode AFM (Digital Instruments) in air. AFM probes with a resonant frequency of ~300 kHz was employed in the measurements.

4.2.3 Electrochemical Impedance Spectroscopy (EIS)

EIS measurement was performed on the glassy carbon electrode before and after PPO deposition to investigate the effect on capacitance and leakage current, and measure the thickness of the blocking layer. The EIS tests were performed in three probe setup with Ag/AgCl reference and the Pt counter electrodes. The electrolyte was a solution of 1 M tetrabutylammonium hexafluorophosphate (TBAP) in propylene carbonate. The experiments were conducted in the range of 10 mHz–100 kHz with AC amplitude of 10 mV and DC bias of 0 V versus open circuit potential.

4.2.4 Device Fabrication and Characterization

For fabricating supercapacitors, two pieces of activated carbon, each with apparent surface area of 0.5 cm², were used. The glassy carbon electrodes were used as the back contact for current collection. A mesh of polyester was applied as a separator between the activated carbon electrodes. A custom-made Teflon screw-clamp was developed and used to press activated carbons to the back contact electrodes, while the electrodes were immersed into the electrolyte solution containing 1 M TBAP in propylene carbonate. A picture of the setup is shown in Figure 13. To test the effect of the blocking layer, activated carbon electrodes with and without PPO deposited layer were tested. The devices were characterized by multiple cyclic voltammetry, open circuit self-discharge study, and galvanic pulses.

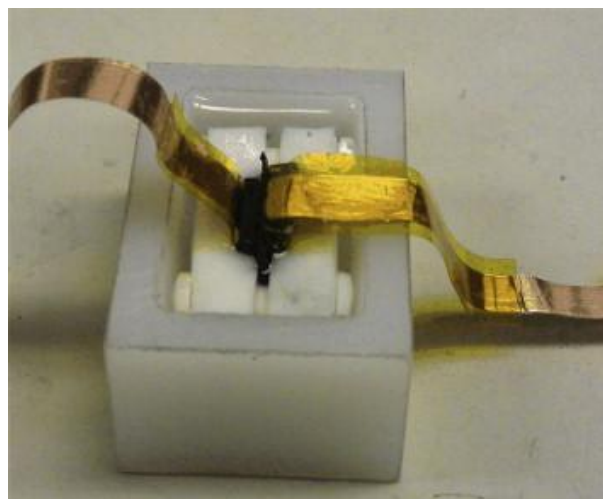


Figure 13 A picture of the fabricated supercapacitor.

4.3 Results and Discussion

4.3.1 PPO Deposition and Characterization

In order to gain high specific capacitance, porous electrodes are commonly employed to fabricate supercapacitors. However, studying the quality and estimating the thickness of the blocking layer on a porous electrode is challenging. Therefore, first we have deposited PPO on a smooth glassy carbon electrode. The blocking layer was deposited on the electrode by multiple cyclic voltammetry (CV) for 22 cycles (Figure 14). The CV result is similar to the previous results reported by Rhodes et al. [101]. The current decrease in every cycle demonstrates the deposition of the PPO layer and the growth of the insulating layer [101]–[103]. The morphology of the glassy carbon electrode before and after PPO deposition was studied using AFM. As shown in Figure 15, the morphologies were quite different. The surface of the glassy carbon electrode showed a smooth microstructure with root-mean-square (RMS) roughness of ~ 1.67 nm, while the roughness is increased to ~ 3.66 nm after the deposition (Figure 15(a) and (b)). The electropolymerized PPO film showed a well-uniform coherent layer on top of the glassy carbon electrode over a 500×500 nm² area (see step height measurement results in the

Supplementary materials in Appendix B). Comparing the phase images of the glassy carbon electrodes with (Figure 15 (d)) and without (Figure 15 (c)) the coating shows a uniform electropolymerization of PPO on the electrode surface. The surface coverage of the glassy carbon electrode was also studied in a $10 \times 10 \mu^2$ area (see the Supplementary material for further details in Appendix B).

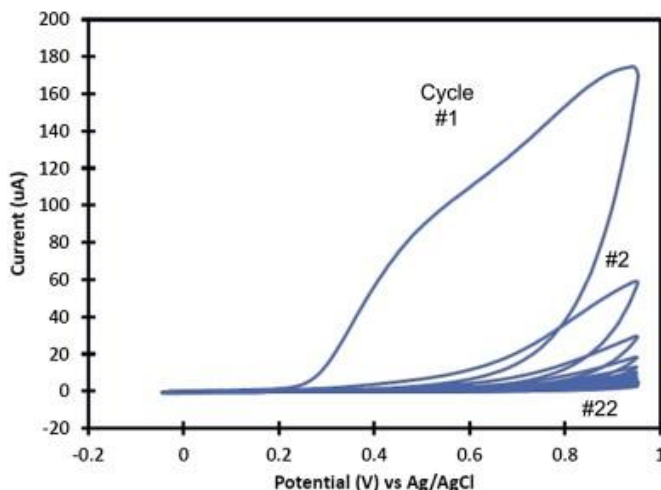


Figure 14 Electrodeposition of PPO on a glassy carbon electrode using CV method (scan rate $50 \text{ mV}\cdot\text{s}^{-1}$); the decrease in the current with subsequent scans indicates the growth of the insulating layer.

The deposited layer was further characterized using the electrochemical impedance spectroscopy (EIS) method. The magnitude and phase of the impedance for the glassy carbon electrode before and after PPO deposition are shown in Figure 16. In order to analyze the frequency response of an electrochemical cell, a more complicated model than the one shown in Figure 10 is required. At very low frequencies, the impedance is under the influence of a non-uniform current [104].

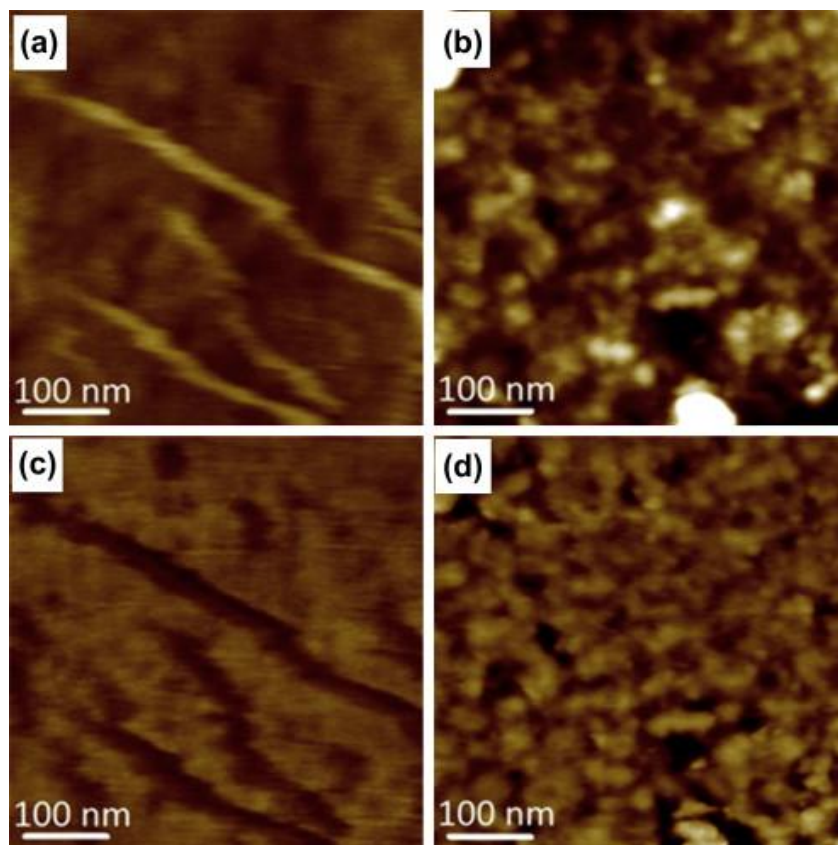


Figure 15 AFM topographic and phase images of: (a) and (c) uncoated glassy carbon surface and (b) and (d) electro-polymerized PPO on a glassy carbon electrode surface. The images were obtained in air using noncontact tapping mode.

This effect cannot be modeled with a resistor–capacitor (RC) circuit, but a constant phase element can be considered in parallel to the double layer capacitor. The detail of the model and the analysis of the impedance for the full spectrum are provided in the Supplementary materials (Appendix B). However, the impedance of the electrode at higher frequencies can still be modeled with the simplified RC circuit in Figure 10 Using ZSimpWin software from Princeton Applied Research, the impedance of the electrodes with and without the coating was simulated for frequencies larger than 10 Hz. The simulation results are also shown in Figure 16. Based on the simulation, the values for C_{eq} , R_P , and R_S are estimated for both electrodes. The values are listed in Table 2.

Table 2 Simulated values for C_{eq} , R_p , and R_s in the glassy carbon electrode with and without the PPO coating. The measured data was obtained from EIS.

C_{eq} [μF]	5.543	0.7719
R_p [$\text{k}\Omega$]	8.49	30.9
R_s [Ω]	207	128

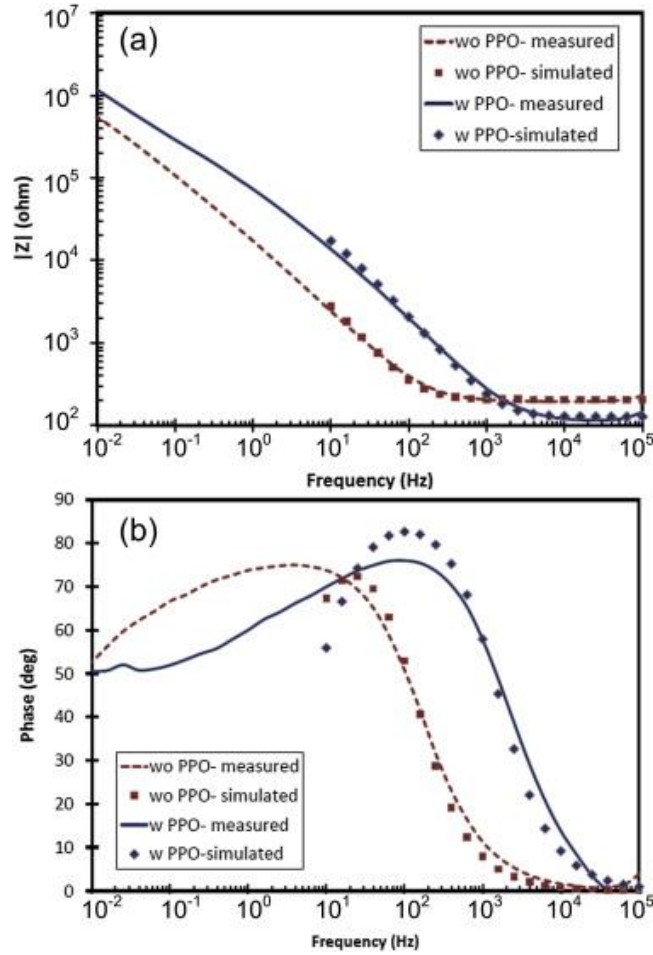


Figure 16 (a) Magnitude and (b) phase of the measured and simulated impedance for the glassy carbon electrodes with and without the PPO layer. Simulations were performed based on the model in Figure 10 for frequencies between 10 Hz and 100 kHz. A more complicated model has been discussed in the Supplementary materials (Appendix B) section which explains the behavior of the cells for the entire spectrum.

The result clearly shows that R_p was increased and C_{eq} was decreased after depositing the blocking layer. The series resistance is also reduced after the deposition. The PPO thickness (t_{BL}) can be estimated from the capacitance change. Considering the model in Figure 11(b), the

blocking layer capacitance is estimated to be $C_{BL} = 0.8967 \mu\text{F}$ based on the measured capacitance ($C_{eq} = 0.7719 \mu\text{F}$) and the double layer capacitance ($C_{DL} = 5.5430 \mu\text{F}$). Since $C_{BL} = \epsilon_{PPO}A/t_{BL}$ (where ϵ_{PPO} is the permittivity of PPO $\epsilon_{PPO} = 3.5 \times 8.85 \times 10^{-12} \text{ F m}^{-1}$ [105] – and $A = 0.5 \text{ cm}^2$ is the surface area of the electrode), the PPO thickness is estimated to be $\sim 1.5 \text{ nm}$. This value is consistent with the previously reported thickness for electrodeposited PPO by other groups [106].

4.3.2 Supercapacitor Characterization

In order to study the effect of the blocking layer on the performance of a supercapacitor, two devices were fabricated and tested: one without PPO coating and the other with electrodeposited PPO on both electrodes. The electrode material was activated carbon with high porosity. The polymer was deposited on the electrodes with the same method applied for the glassy carbon electrode (CV with 22 cycles). As expected, the shape of the curves was similar to the one shown in Figure 14 with much larger current, which was due to the larger surface area of the activated carbon electrode (the result is not presented). The cells were tested at room temperature in a two-electrode configuration using the setup shown in Figure 13. Various electrochemical experiments were carried out to estimate C_{eq} , R_P , and R_S in both devices.

The nominal voltage in a single cell commercial type supercapacitor is between 2.3 V and 2.75 V [107]. To make a device for that voltage range, chemicals with high level of purity should be utilized and a contaminant-free environment is required for the fabrication [106]. Also, supercapacitors must be sealed before testing. Any contaminant in the electrolyte, especially water/moisture, with the redox potential lower than the nominal voltage would affect the device characteristics. Since our experimental setup has not been designed for the best condition, we tested the cells with the voltages less than 2.0 V to avoid damaging the electrodes. Voltage of

2.0 V is sufficient to supply many low power electronics, including wireless devices [90]. However, in this voltage range, a larger leakage current is expected than an off-the-shelf device. Since the test conditions were the same for both devices with and without the blocking layer, the comparison between the results demonstrates the effect of the blocking layer.

4.3.2.1 Specific Capacitance Measurement Using Cyclic Voltammetry

Figure 17 shows the CV curves in the voltage range of ± 2 V across the devices at a scan rate of 50 mV s^{-1} . To obtain the specific current in each cell, the current was normalized to the weight of the activated carbon electrodes. The electrode weight was measured precisely before and after PPO deposition using an analytical balance. The amount of deposited PPO was estimated to be ~ 7 mg. The PPO deposited electrodes were completely dried before the weight measurement. Since both electrodes are similar, it is expected to have a symmetrical response around 0 V. However, the device with the blocking layer is showing small differences between positive and negative voltages. This is likely due to the different amount of phenol residue in two electrodes of the device.

In a CV measurement, the loop width represents the overall capacitance; and the effect of R_p appears in the slope of the loop [31]. As expected, the loop width is smaller in the device with the PPO coating, which indicates lower specific capacitance. Also, the change in the loop slope implies a lower leakage current for the capacitor with the blocking layer. As a rough approximation (assuming R_s is much smaller than R_p), the specific capacitance can be estimated from half of the ratio of the loop width to the scan rate at zero voltage [31]. Using this method, the cell with the blocking layer had a capacitance of 5.70 F g^{-1} whereas the capacitance of the cell with no coating was 12.99 F g^{-1} , which indicates $\sim 44\%$ reduction in the capacitance after

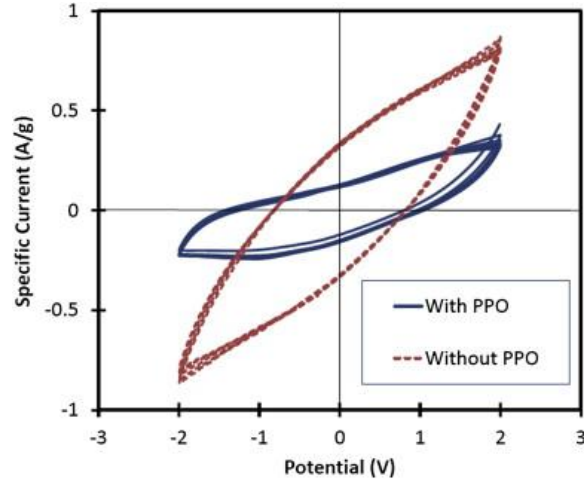


Figure 17 Cyclic voltammograms for two supercapacitors: with and without the PPO blocking layer. The scan rate was 50 mV s^{-1} .

the PPO deposition. In the EIS experiment (Table 2), the capacitance reduced to 14%. The smaller change is likely due to the poor coverage of the PPO layer on the porous activated carbon electrode. In fact, the specific capacitance in the devices with and without the blocking layer implies that the double layer capacitance has to be $\sim 10.16 \text{ F g}^{-1}$ (see the model in Figure 11), while 1.5 nm thickness of the PPO layer suggests specific capacitance of 13.76 F g^{-1} . Hence, the surface coverage is estimated to be $\sim 74\%$ ($=10.16/13.76$), assuming uniformity in the thickness of PPO on the porous electrode. Considering the weight of the electrodes, C_{eq} was measured to be 0.112 F and 0.0897 F for the devices without and with the blocking layers, respectively.

4.3.2.2 Leakage Current Estimation Using Self-Discharge Profile

Since R_p changes with voltage, the leakage current estimation from CV is inaccurate. To measure the leakage current at 2.0 V, both cells with and without the blocking layer were first charged for 18 h at 2.0 V. At the end of the time, the charging currents reached to stable values of $\sim 200 \mu\text{A}$ and $\sim 935 \mu\text{A}$ for the devices with and without the PPO layers, respectively. These current values are considered as the leakage currents required to maintain the capacitor voltage at

2.0 V [107]. In order to investigate how the leakage current drains the stored energy, the self-discharge profile of the devices was studied. Immediately after the charging, the external voltage source was automatically removed and the open circuit voltage at the cells' terminals was monitored. Figure 18 shows the self-discharge profiles of the cells with and without the blocking layers. As expected, the blocking layer reduces the leakage current significantly. After 1 h of self-discharge, the cell with the blocking layer displayed a voltage of 1.43 V compared to 1.22 V for the cell without any coating. The leakage current, i_l , was estimated from $i_l = C_{eq} dV/dt$ (at $t = 0$) where dV/dt is the slope of the self-discharge profile at $t = 0$. The leakage currents in the devices with and without the blocking layer are estimated to be 220 μA and 996 μA , respectively. These values are close to the measured currents at the end of the 18 h charging cycle. Knowing the leakage current, the R_P values at 2 V were obtained from Ohm's law. The resistance values and other parameters in supercapacitors are listed in Table 3.

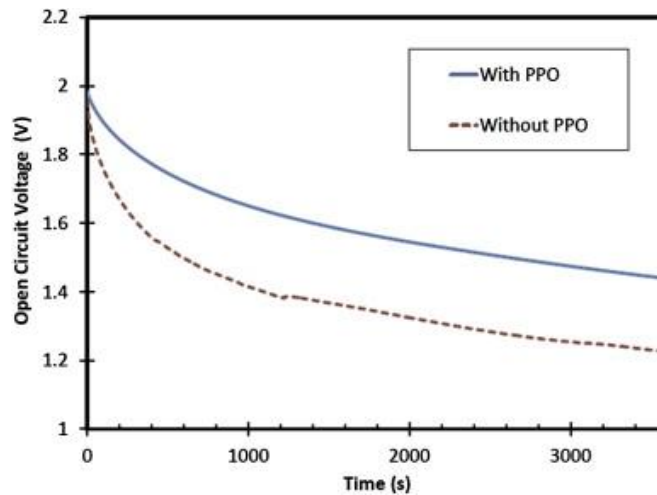


Figure 18 Self-discharge profile in two supercapacitors with and without the blocking layer. Both capacitors were charged at 2.0 V for 18 h prior to open circuit voltage measurement.

Table 3 The characteristics of the supercapacitors without and with the blocking layer.

Characteristics	Without blocking layer	With blocking layer
Specific capacitance [F g^{-1}]	12.99	5.7
Leakage current (at 2.0 V) [μA]	996	220
C_{eq} [F]	0.112	0.0897
RP (at 2.0 V) [$\text{k}\Omega$]	1.97	9.05
RS [Ω]	66	194
Voltage (at $t = 0$ s) [V]	2	2
Voltage (at $t = 3600$ s) [V]	1.23	1.44
Specific energy (at $t = 0$ s) [J g^{-1}]	25.98	11.4
Specific energy (at $t = 3600$ s) [J g^{-1}]	9.76	5.9
Specific energy loss in 1 h [J g^{-1}].	16.22	5.5

It should be noted that the leakage current estimation with this method requires a long charging time (i.e. 18 h) to assure the diffusion of ions into deep nanopores on the electrodes [91]. In a short charging time, only the double layer capacitors at shallow pores are charged. Switching to the open circuit mode, a voltage drop occurs due to the redistribution of charges between shallow and deep pores [91]. This effect is different from the leakage current produced by Faradic reactions at the electrode surfaces.

4.3.2.3 R_S Measurement Using Galvanic Pulses

Galvanostatic charging/discharging is a common method for R_S measurement. In this study, ± 1 mA current pulses (period of 200 s) were applied to charge and discharge the supercapacitors and the voltage across the devices was monitored (Figure 19). The voltage drop at the charge/discharge transition divided by the current difference (2 mA) gives the R_S value (Table 3). The higher resistance in the device with the PPO layer is likely due to the increased series resistance between the activated carbon and the current collector (glassy carbon). For practical applications, a very low series resistance (less than 1 Ω) is required. The devices presented in this work were not optimized for low series resistance. The large observed resistances in both devices are mainly due to the mechanical contacts between the activated

carbon electrode and the glassy carbon. To eliminate this problem, activated carbon electrodes with laminated current collector are recommended for future works.

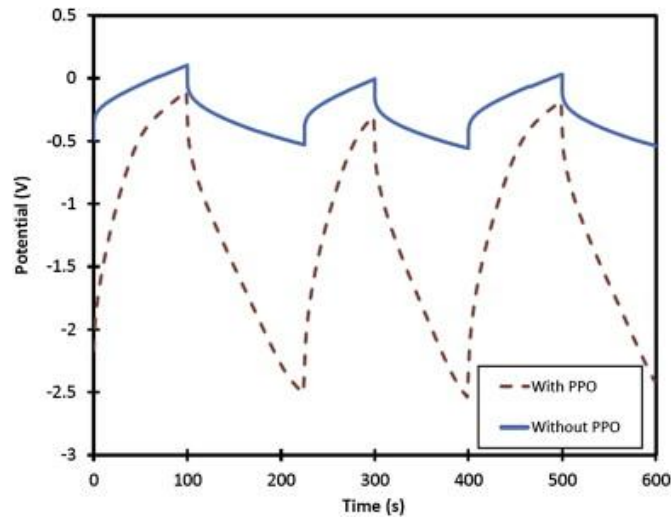


Figure 19 Galvanic pulses for measuring series resistance in supercapacitors with and without PPO layer. Current pulses of ± 1 mA with 200 s period were applied to charge and discharge the devices. The voltage drop at the transition from +1 mA to -1 mA was measured. The resistance was calculated from the voltage difference divided by the 2 mA current difference.

As shown in Figure 19, the voltage increases with time when a supercapacitor is charged with a constant current. A small voltage change, ΔV , is expected for a large capacitor. A ΔV of about 2 V was observed in the capacitor with the blocking layer, while the voltage change was only 0.8 V in the device without any coating. This again confirms the reduction of specific capacitance as the result of the blocking layer.

4.4 Discussion

As shown in Table 3, the application of the blocking layer has reduced the supercapacitor's leakage current by 78%. However, the specific capacitance was decreased from 12.99 F g^{-1} to 5.70 F g^{-1} . As a result, the specific energy, also known as energy density ($C_{sp}V^2/2$), of the supercapacitor with the blocking layer was lower than that in the device without any coating by about 56% at the charging voltage of 2.0 V. As shown in Figure 18, the open

circuit voltage of the capacitor without the coating dropped from 2.0 V to 1.23 V in 1 h, whereas the voltage change in the device with the blocking layer was only 0.56 V in the same period. Therefore, the amounts of the stored energy density after 1 h of self-discharge were 5.90 J g^{-1} and 9.76 J g^{-1} for devices with and without the PPO layer, respectively. The lower energy loss implies that the energy storage efficiency is improved by the application of the blocking layer. It should be noted that the energy loss and leakage current in the devices presented in this work are higher than those values in a typical supercapacitor on the market. This is mainly due to contaminants (e.g. water) in the electrolyte of the devices fabricated in our lab. To avoid contamination, it is recommended to use electrolyte with high purity and do the fabrication and test in a glove box. Nevertheless, the studied approach in this work demonstrates the feasibility of reducing leakage current in any electrolytic double layer capacitor by application of a thin blocking layer.

The energy storage density could be improved if a thinner blocking layer were used. Of course the leakage current would be higher with a thinner PPO layer. Further study is required to investigate the effect of the blocking layer thickness on the specific capacitance, energy density, and leakage current in a device. Due to the self-terminating effect in the electropolymerization of PPO, it is difficult to control the thickness of the deposited layer. A cyclic voltammetry with a fewer number of cycles may produce thinner films, but the layer would likely have defects. Other methods such as atomic layer deposition (ALD) has been planned to be employed for depositing an ultrathin film of an insulator (e.g. Al_2O_3 and Barium Strontium Titanate-BST). The thickness of the layer can be well controlled by using ALD. Also, different insulating materials can be tested.

4.5 Conclusions

As a solution for reducing the leakage current in supercapacitors, application of an ultra-thin blocking layer has been demonstrated. The experimental results from a 1.5 nm thick layer of PPO on activated carbon electrodes of a supercapacitor show that the leakage current was reduced by 78%. However, the specific capacitance and the energy storage density were decreased by 56%. Due to the lower leakage current, the amount of energy waste was significantly lower in the device with the blocking layer, compared to the device with no coating. In conclusion, deposition of the blocking layer can be used to make more efficient supercapacitors for the applications which need longer charge storage time. More study on the thickness and material of the blocking layer is required to optimize the performance of supercapacitors with the blocking layer.. In order to gain a better understanding of the effect of the blocking layer an analytical model has been developed and discussed in the next chapter.

CHAPTER 5: MODELING AND SIMULATION STUDY OF THE SELF-DISCHARGE IN SUPERCAPACITORS IN PRESENCE OF A BLOCKING LAYER²

5.1 Introduction

The depletion of fossil fuels based energies such as oil and natural gas, and the environmental problems linked to their CO₂ emissions, have increased research interests towards renewable sources of energy. Since the captured form of renewable energies (e.g. wind or solar energy) is not readily available all the time, energy storage devices are required for the optimum usage of the energies. The available types of electrical energy storage devices include fuel cells, batteries, and supercapacitors [108]. Although batteries and fuel cells have relatively high energy densities compared to supercapacitors, their power density is lower [8], [9]. Additionally, supercapacitors have high life cycles (typical ~1 million cycles) [109]. The combination of these features make supercapacitors potentially suitable for various applications such as power tools, elevator, energy management systems, electric vehicles [85], [110], wearable and flexible electronics [111], stand-alone severe weather condition systems [112], piezo-electric [113], and renewable energy generation [114], [115].

Most commercial types of supercapacitors are EDLCs (Electric Double Layer Capacitors), in which energy is stored by the formation of a double layer charge at the electrode–electrolyte interface [41], [96]. In a simple form, the electronic charges on the electrode and the

²This chapter was previously published in [116]. Permission is included in Appendix A.

ionic charges at the electrode surface resemble a parallel plate capacitor. The space between the two layers of the charges is limited by the size of the solvent molecules surrounding the ions (Figure 20(a)).

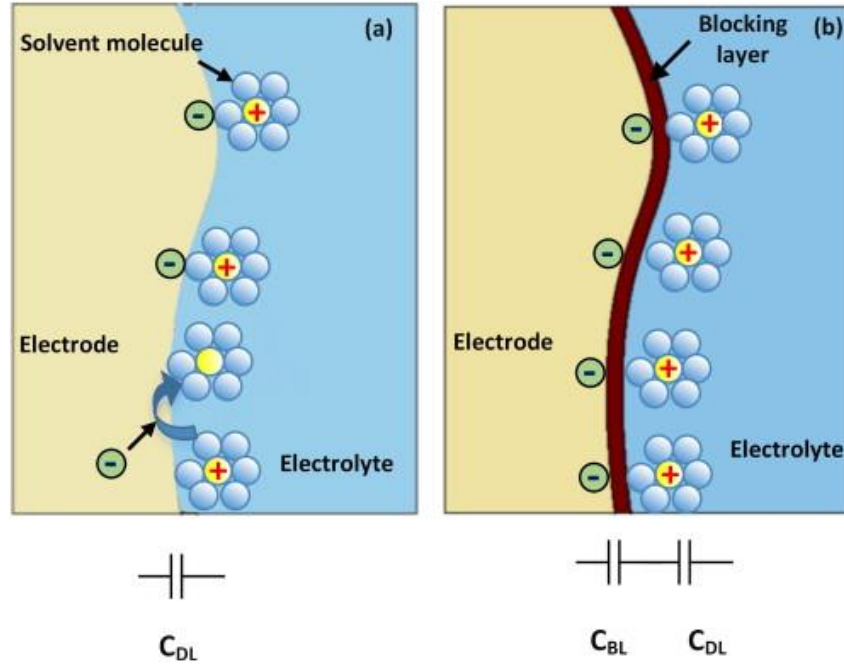


Figure 20 Schematics of the electrode–electrolyte double layer interface in supercapacitors. (a) Charge loss is induced by Faradaic (redox) reactions at the surface of the electrode. (b) Energy storage ability is improved by the application of a thin blocking layer which decreases the kinetics of the redox reactions.

Despite the high power density, supercapacitors suffer from high leakage current [17] which limits their usage in some practical applications. Self discharge or leakage is the inability of supercapacitors to retain stored charge for a long period of time. Faradaic (redox) reactions at the electrode–electrolyte interface are the main reason for the leakage current in EDLCs [18] (see Figure 20(a)).

We have demonstrated that the application of a thin layer of an insulating material (blocking layer) can reduce the leakage current in an EDLC (Figure 20 (b)) [52]. In the previous

work, we coated the surface of the carbon based electrodes with a thin layer (~1.5 nm) of polyphenylene oxide (PPO).

Considering that the leakage current is proportional to the kinetics of the redox reaction, the role of the blocking layer is to decrease the reaction rate by introducing an energy barrier for the electrons passing the electrode–electrolyte interface. In presence of the blocking layer, the electron transfer rate would be limited by the tunneling through the barrier. However, the blocking layer decreases the capacitance because of the increase of the distance between the positive and negative charges in the double layer region [52]. As shown in Figure 20(b), the blocking layer can be modeled as a capacitor (C_{BL}) in series with the double layer capacitor (C_{DL}). Since the decrease in the capacitance affects the energy density in the device, it is important to study the effect of the blocking layer thickness/material on the leakage effect and energy density of the device.

In the current work, we have focused on the theoretical study of the blocking layer. Using the fundamental physical and electrochemical models for redox reactions at an electrode–electrolyte interface, we have developed a model for investigating the blocking layer effect on the device characteristics. It was found that the developed model can explain the experimental results from our previous work) [52]. Based on the model a Matlab code has been developed (Appendix F) to simulate the effect of the barrier thickness and initial voltage on the open circuit voltage and the energy storage of a supercapacitor.

5.2 Modeling

Due the negative impact of the blocking layer on the specific capacitance, a very thin coating layer in the range of nanometer (nm) is recommended to reduce the leakage current. In

this situation, the electrons can still tunnel through the layer (quantum mechanical effect). However, the electron transfer rate reduces exponentially with the thickness of the layer [31].

The modeling study, presented in this work, is limited to investigating the leakage current in an EDLC under the open circuit conditions with the initial voltage of V_0 . It is assumed that prior to the open circuit test, the capacitor was charged for long enough time to form the double layer charge on the entire surface of the electrodes. Hence, the voltage drop in the open circuit would be only due to the electrochemical current, not the rearrangement of ions on the electrode surface [117]. In general, an electrochemical current can be limited by either the reaction rates at the electrode (kinetics) or mass transport (diffusion of ions from the bulk electrolyte to the electrode) [118]. Considering the open circuit conditions, in which there is no external power source during the self-discharge, we have assumed that the current is only kinetics limited. In such a situation, the leakage current is equal to the product of the surface charge and the reaction (electric charge passing the electrode–electrolyte interface per unit of time) rate. However, the rate is a function of the voltage across the double layer. Therefore, the leakage current and the reaction rate decrease as the voltage drops with time (self-discharge).

According to Tafel equation, the electron transfer rate, k_1 , changes exponentially with the over potential (η) [31] and [119]:

$$k_1 = k_0 \cdot \exp(-\alpha\eta F/RT) \quad (23)$$

where k_0 is the rate constant at zero overpotential, α is the charge transfer coefficient ($0 < \alpha < 1$), the portion of the overpotential that shifts the standard free energy of activation level, it also measures the symmetry of the energy barrier [31]), F is the Faraday constant

($\sim 96500 \text{ C mol}^{-1}$), R ($8.314 \text{ J K}^{-1} \text{ mol}^{-1}$) is the gas constant, and T is the absolute temperature in Kelvin.

The overpotential η is the difference between the voltage V across the double layer and the redox potential E_0 of the reaction [120]. As a function of the voltage, Equation (23) then becomes:

$$k_1 = k_0 \cdot \exp[-\alpha F(E_0 - V)/RT] \quad (24)$$

In the presence of a blocking layer, the overall rate, k , is limited by the tunneling rate through the blocking layer. Therefore, k decays exponentially with the thickness of the layer [31].

$$k = k_1 \cdot \exp(-\beta d) \quad (25)$$

In Equation (25) d is the thickness of the blocking layer and β is an exponential coefficient related to the energy barrier of the blocking layer.

From Equations (24) and (25), the electron transfer rate at the surface of an electrode with the blocking layer can be expressed as a function of the voltage and the thickness by:

$$k(V, d) = k_0 \cdot \exp[-\alpha F(E_0 - V)/RT] \cdot \exp(-\beta d) \quad (26)$$

It can be easily noted that for $d = 0$, $k(V, 0) = k_1$. Also it should be noted that Equation (26) is applicable only for devices with a thin blocking layer where the electron can tunnel through (d in the range of a few nanometers). A relatively thick dielectric layer reduces

the overall capacitance to $C_{\text{tot}} \approx C_{\text{BL}}$. In this situation the device is more like a parallel plate capacitor in which the leakage occurs through the defects in the dielectric layer.

Assuming that the leakage current, i , (i.e. Faradic current) is kinetics limited, the current at any time (t) can be expressed by Ref. [31]:

$$i(t) = nFkA\sigma(t) \quad (27)$$

where A is the electrode surface area (cm^2), n is the number of electrons exchanged in the redox reaction, and $\sigma(t)$ is the ions concentration at the surface (mol cm^{-2}) which is a function of the time (during the discharge cycle). It can be noted that the leakage current is proportional to the surface area of the electrode. However, since the double capacitance is directly related to the electrodes surface area, reducing the surface area to decrease the leakage would be detrimental to the storage capability of the device.

The self-discharge current is also given by:

$$i(t) = -C dV / dt \quad (28)$$

where C is the capacitance, V is the voltage across the electrode–electrolyte interface, and t is time. The negative sign is because of the direction of the charge (across the interface) versus the potential of the electrode.

From Equations (27) and (28) we have:

$$i(t) = nFkA\sigma(t) = -C dV / dt \quad (29)$$

In Equation (29), $nFA\sigma(t)$ is equal to the total charge in the double layer $Q_s(t)$ which can be obtained from $Q_s(t) = CV$. Hence, Equation (29) can be rewritten as the following:

$$kQ_s(t) = kCV = -C \, dV / dt \quad (30)$$

Therefore the variation of the voltage with time during the self-discharge process can be obtained from the following differential equation:

$$dV / dt + kV = 0 \quad (31)$$

It is important to notice that Equation (31) suggests that the discharge profile in an EDLC (with or without the blocking layer) is not a function of the capacitance or the electrode surface area. This can be simply explained as both the capacitance and leakage current are proportional to the surface area. So a larger capacitance with larger electrode areas would have a larger leakage current as well, but the discharge profile would be the same regardless of the electrode area or the capacitance value. Finally substituting (23) into (28), the self-discharge voltage is given by:

$$dV / dt + k_0 \cdot \exp[-\alpha F(E_0 - V)/RT] \cdot \exp(-\beta d) \cdot V = 0 \quad (32)$$

Considering $m = k_0 \cdot \exp(-\alpha FE_0/RT)$ as a constant (E_0 is a constant), Equation (32) can be simplified to:

$$dV/dt + m \cdot \exp[\alpha FV/RT] \cdot \exp(-\beta d) \cdot V = 0 \quad (33)$$

The analytical solution of differential Equation (33) involves the use of an inverse function of the exponential integral [121], which cannot be solved easily using analytical methods. Furthermore, solving (33) requires the knowledge of the electrochemical parameters such as m , α , and β . However, the equation can be solved numerically for given conditions. In this approach, the electrochemical parameters can be extracted from experimental results.

5.3 Results and Discussion

5.3.1 Parameter Extraction and Estimation of $k(V, d)$ from Experimental Results

All the numerical studies and simulations were conducted using Matlab. To obtain the self discharge profile in a device with the blocking layer thickness of d (arbitrary) two sets of experimental data were used. The first data was from the self-discharge profile of a carbon electrode without any blocking layer and the second data was from the same electrode with 1.5 nm thick layer of PPO as the blocking layer [52]. The experimental conditions such as charging voltage, charging and discharging times, operating temperature of the two experiments were the same.

Equation (24) suggests that the reaction rate is increasing exponentially with the voltage. The values of $k(V, d)$ have been extracted from the experimental results using the differential equation (31) in this form:

$$k(V, d) = -(\Delta V/\Delta t)/V \quad (34)$$

Figure 21 shows k as a function of voltage for both devices without and with the blocking layer. A linear regression analysis was used to fit exponential functions to the experimental data

[122]. The regression coefficients for Figure 21(a) and b are respectively 0.990 and 0.992. In the absence of the blocking layer, Equation (26) suggests that $k(V,0) = m \cdot \exp(\alpha FV/RT)$. Therefore from the fitted curve in Figure 21(a), we can find that $m = 1.31 \times 10^{-7} \text{ s}^{-1}$ and $\alpha = 0.12$. These values are considered constants for both devices with and without the blocking layer. Since α must be between 0 and 1, the obtained value of α is reasonable [123].

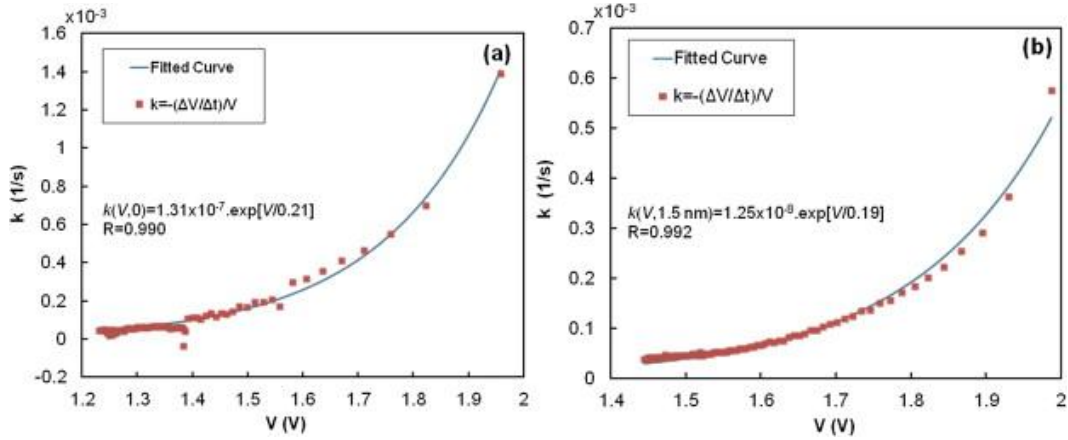


Figure 21 Reaction rates versus voltage in devices (a) without and (b) with the blocking layer. The data points are extracted from the experimental results. The solid curves show the fitting curves. The suggested exponential functions for the fitted curves and the regression coefficient for each fit are shown in the plots.

Using Equation (25), β is extracted from $k(V,0)$ and $k(V,1.5 \text{ nm})$ in Figure 21. It should be noted that β is a function of the voltage as the energy barrier height changes with the voltage across the blocking layer barrier [31]. As explained in detail in the Supplementary Material (see Appendix C), the variation of β with voltage can be approximated with a linear function with $\beta = 0.7473 \text{ nm}^{-1}$ at $V = 2 \text{ V}$. Such a value is in the range of the previously reported electron tunneling coefficient in similar structures (a thin film of an insulator on a conductive electrode) [124], [125] and [126].

The estimated values for m , α , and β were used in Equation (33) to simulate the discharge profile $V(t)$ in hypothetical devices with various thicknesses in the blocking layer (different

values of d). For numerical solution of the differential equation, a variable order Adams–Bashforth–Moulton method (linear multistep method) was used [127], [128] and [129] and the initial condition V_0 (V at $t = 0$) was considered.

5.3.2 Simulation Results for PPO as the Blocking Layer

Estimating the value of $k(V,d)$, Equation (33) was used to calculate the voltage values in a device with and without the blocking layer (1.5 nm of PPO) for $0 \leq t \leq 3600$ s. As shown in Figure 22, the simulation results are in good agreement with the experimental results reported previously [52]. It should be noticed that the simulation results in Figure 22 are not obtained from any direct curve fitting to the experimental data. As mentioned above, it was assumed that the reaction rate is an exponential function of voltage (Equation (26) and the value of k was estimated from the experimental results. Therefore, simulation and experimental results in Figure 22 support the use of Equation (33) to study the discharge profile.

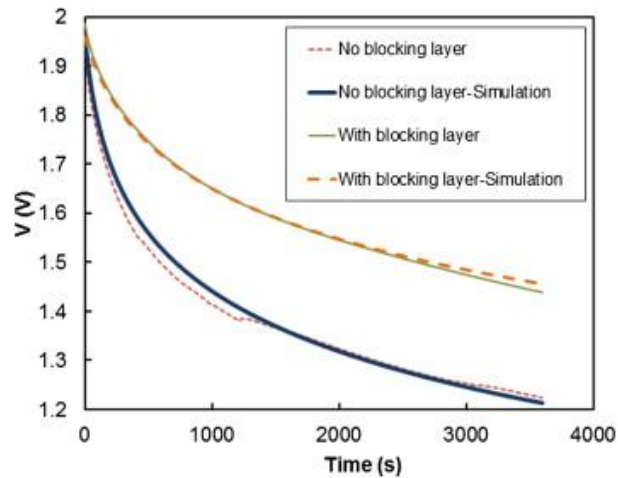


Figure 22 Simulated and experimental self-discharge profiles with 1.5 nm thick PPO as the blocking layer.

5.3.3 Simulation Results for Devices with Various Thickness of the PPO Layer

Using the developed Matlab code (Appendix F) to solve Equation (33), we studied the effect of the blocking layer thickness on the device characteristics. Two different scenarios were considered: a) Constant initial voltage ($V_0 = 2.0$ V), and b) Constant initial energy density.

5.3.3.1 Constant Initial Voltage

To better understand the effect of the thickness of the blocking layer on the leakage, the self discharge voltage profiles for different thicknesses (0.0 nm, 0.5 nm, 1.0 nm, 1.5 nm, 2.0 nm, 2.5 nm, and 3.0 nm) were simulated. The rate constants as a function of the voltage (0–2 V) were calculated for each thickness with the exponential coefficient β obtained from the experimental data. The differential Equation (33) was solved for each thickness and the simulated voltage profiles in Figure 23 were obtained.

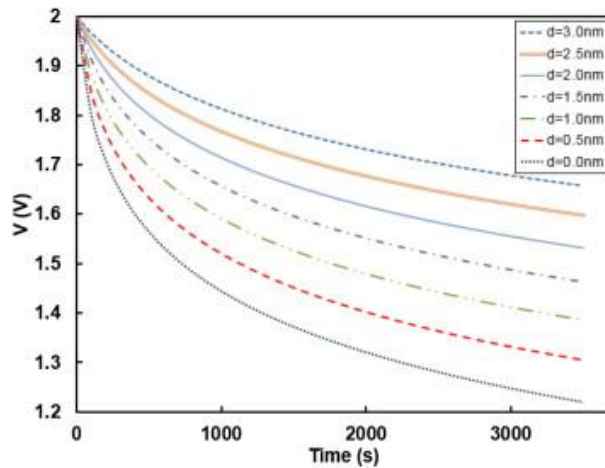


Figure 23 Simulated self-discharge profiles with PPO as the blocking layer for different thicknesses.

As expected, the application of a thicker blocking layer reduced more the leakage current (Figure 23). However, due to the specific capacitance reduction, the profile of the energy density loss was different for different devices. Considering the estimated surface area of the electrode, the thickness and permittivity of PPO, the value of C_{BL} was calculated using the parallel plate

capacitance equation [52]. Then the overall capacitance, C , (C_{DL} in series with C_{BL} - see Figure 20(b)) was calculated for different thickness in the blocking layer. Using the energy equation in a capacitor ($E = 0.5 CV^2$) the change in the stored energy versus time was estimated for different devices. Figure 24 shows the specific energy (energy divided by the mass of the electrodes) versus voltage and the energy versus time for different blocking layer thicknesses. As shown, the energy loss was less in devices with the thicker blocking layer. For the device with no blocking layer, the estimated energy loss in 1 h was 15.27 J g^{-1} whereas in the device with 1.5 nm of the blocking layer, it was only 4.86 J g^{-1} (see Table 4). Those estimated values were in agreement with the experimental values reported in Ref. [52] (16.22 J g^{-1} and 5.5 J g^{-1}). The estimated energy loss in the device with 3.0 nm of the blocking layer was the smallest ($\sim 2.02 \text{ J g}^{-1}$), however due to the effect of the blocking layer thickness on the capacitance, the initial energy density for $V_0 = 2.0 \text{ V}$ was also the lowest. Nevertheless, the energy loss in the device with no blocking layer was the highest with more than half of the initial energy loss in an hour. The specific capacitance, the specific energy at $t = 0 \text{ s}$ and 3600 s (initial specific energy and after 1 h of self-discharge), and the amount of energy loss in 1 h were calculated and listed in Table 4.

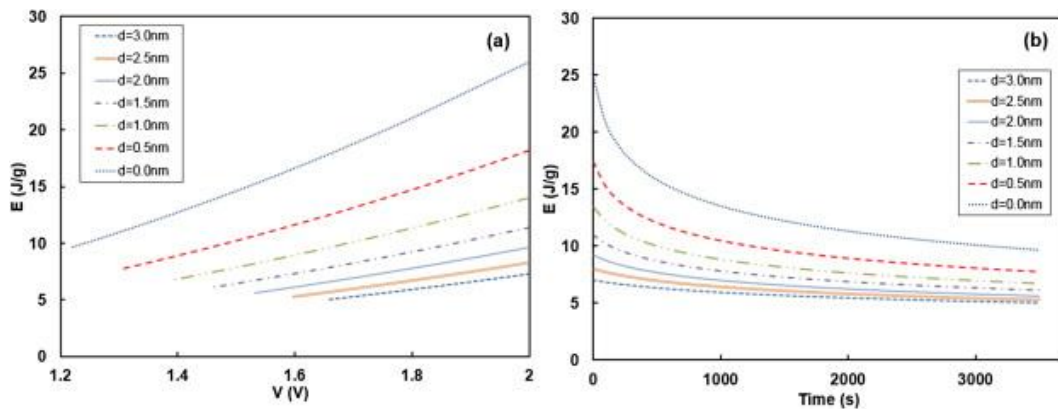


Figure 24 Simulated specific energy profiles with PPO as the blocking layer for different thicknesses. Specific energy versus (a) voltage and (b) time.

Table 4 Simulated characteristics of the supercapacitors for different thicknesses of the blocking layer (PPO) with the same initial voltage.

Blocking layer thickness [nm]	0	0.5	1	1.5	2	2.5	3
Specific capacitance [$F g^{-1}$]	12.99	9.11	7.01	5.7	4.8	4.15	3.65
Voltage (at $t = 0$ s) [V]	2	2	2	2	2	2	2
Voltage (at $t = 3600$ s) [V]	1.21	1.3	1.38	1.46	1.53	1.59	1.65
Specific energy (at $t = 0$ s) [$J g^{-1}$]	24.92	17.47	13.45	10.93	9.21	7.96	7
Specific energy (at $t = 3600$ s) [$J g^{-1}$]	9.64	7.75	6.73	6.08	5.62	5.27	4.98
Specific energy loss in 1 h [$J g^{-1}$].	15.28	9.72	6.72	4.86	3.59	2.69	2.02

5.3.3.2 Constant Initial Energy Density

Although the application of a blocking layer reduces the specific capacitance, the device voltage range can be expanded due to the voltage drop across the blocking layer. Since the energy of a supercapacitor is a function of the capacitance and the voltage, the question is if the voltage expansion can compensate the capacitance reduction to make a low leakage device with the same energy density? We have used the developed Matlab code (Appendix F) to study the self-discharge profile and the change in the energy density of the simulated devices with various thickness of the blocking layer. It was assumed that each device was charged to an initial voltage to store a specific amount of energy (specific energy of a device without any blocking layer with the initial voltage of $2 V = 24.92 J g^{-1}$ was selected). Figure 25 shows the voltage drop and the change in the specific energy with time for devices with the same initial specific energy storage.

The summary of the important parameters is also listed in Table 5.

Table 5 Simulated characteristics of the supercapacitors for different thicknesses of the blocking layer (PPO) at different charging voltages and same initial specific energy.

Blocking layer thickness [nm]	0	0.5	1	1.5	2	2.5	3
Voltage (at $t = 0$ s) [V]	2	2.34	2.67	2.96	3.22	3.47	3.69
Voltage (at $t = 3600$ s) [V]	1.21	1.3	1.39	1.46	1.54	1.61	1.67
Specific energy (at $t = 0$ s) [$J g^{-1}$]	24.92	24.92	24.92	24.92	24.92	24.92	24.92
Specific energy (at $t = 3600$ s) [$J g^{-1}$]	9.6	7.77	6.77	6.13	5.69	5.36	5.11
Specific energy loss in 1 h [$J g^{-1}$].	15.31	17.14	18.15	18.78	19.22	19.55	19.81

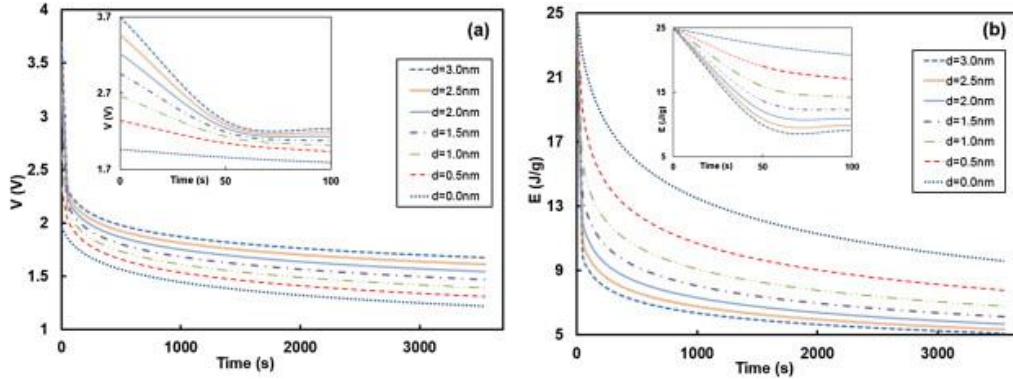


Figure 25 (a) Self discharge voltage and (b) specific energy profiles in devices with various thickness of the blocking layer. The initial energy density was the same in all the devices. The inset figures show the detail of the plots from $t = 0$ s to $t = 100$ s.

Although the self discharge voltage profile was improved for higher thicknesses compared to 0.0 nm, the energy loss in the device with no blocking layer was the lowest. This was due to the sharp voltage drop observed for charging voltages above the initial charging voltage of 2.0 V (see Figure 25).

It should be noticed that in presence of the blocking layer the device voltage can be extended to a limited value. The upper limit in the voltage would be determined by the breakdown effect from the voltage across the blocking layer. Considering the dielectric strength of 1.7 MV cm^{-1} [101] for a PPO layer, the largest potential across a 3 nm thick film is only 0.51 V. This implies that the device voltage can be expanded only by 1.02 V (2×0.51 V for the voltage drop on the blocking layers on both electrodes).

Although the presented work was limited to study devices with PPO blocking layer at different thicknesses, the analytical and computational methods can be applied to study other dielectric materials. A larger specific capacitance can be achieved if a material with higher permittivity (e.g. Al_2O_3) was used instead of PPO. Also, the energy density can be improved if the breakdown strength in the new dielectric layer is larger than that in PPO.

5.4 Conclusion

In this work, we have demonstrated an analytical model to explain the self discharge profile of a supercapacitor for different thicknesses of the blocking layer. This was achieved by considering the rate constant of the faradic reactions responsible for the leakage and the tunneling of the electrons through the blocking layer. The simulated self discharge profiles are compatible with the experimental results reported in the previous work. In this study the effect of the charging voltage on the self discharge and the impact of the thickness on the capacitance reduction and the energy losses were also evaluated for a specific type of blocking layer. The model developed in this work could be utilized as a tool to predict the electrochemical behaviors (capacitance, leakage current, self discharge voltage, and specific energy) of a double layer capacitor in the presence of a blocking layer for any given thickness. This could contribute in the choice of the optimum blocking layer material and thickness to reduce the leakage for specific applications. The optimized thickness of the blocking layer could be predicted based on the specific application and the values obtained from the simulation results compared to defined figure of merits of the supercapacitor relative to the application. One needs to define the limitations in the application (e.g. energy loss or voltage drop in 1 h or more) to use the developed simulation tool for estimating the best thickness of the blocking layer and study the effect of that on the energy density and the discharge profile. The next chapter explores the enhancement of PEDOT: PSS double layer capacitance by altering its structure with the optimum amount of a surfactant.

**CHAPTER 6: EFFECT OF TRITON X-100 ON THE DOUBLE LAYER
CAPACITANCE AND CONDUCTIVITY OF POLY(3,4-
ETHYLENEDIOXYTHIOPHENE):POLY(STYRENESULFONATE) (PEDOT:PSS)
FILMS³**

6.1 Introduction

As an alternative to batteries, supercapacitors have attracted a lot of interests in applications where fast charging and long life cycle capabilities are needed [71], [130], and [131]. Supercapacitors are electrochemical devices with two separated electrodes in an electrolyte. The main mechanism of energy storage in supercapacitors is based on the formation of double layer capacitance at the electrode–electrolyte interface [96]. In addition to the double layer formation, energy storage can be achieved by redox reactions at the surface of the electrodes in a pseudo supercapacitor [43], [132]. In spite of high power density, the application of supercapacitors, as primary energy storage devices, is limited mainly due to their low energy density which is at least one order of magnitude lower than batteries [10]. To increase the energy density, highly porous electrodes with high specific capacitance are required [20]. Different structures and electrode materials have been investigated to increase the specific capacitance [20]. Among different materials, the application of conducting polymers is generally attractive because of low-cost material and simple fabrication processing [20], [133]. A thin film of a

³This chapter was previously published in [74]. Permission is included in Appendix A

conducting polymer can be deposited on an electrode using simple techniques such as spin coating or inkjet printing [134], [135], [136] and [137].

Despite their ability to be easily processed and fabricated at large scales, when used as primary or sole electrode material, conducting polymers have low double layer specific capacitance due to the compact structure of the polymer film [133]. Previous studies have shown that the combination of a conducting polymer with other materials (e.g. carbon nanotubes and graphene) can significantly enhance conductivity and the specific capacitance of the composite polymers [133], [19], [138], [21] and [22]. However, the high cost and complexity of synthesizing composite materials are drawbacks for the large scale production of the devices.

Among conducting polymers, poly(3,4-ethylenedioxythiophene):poly(styrenesulfonate) (PEDOT:PSS) is a promising material for supercapacitors due to stability, conductivity, and aqueous solution processability of the polymer [135], [136], [139] and [140]. PEDOT:PSS is widely used in many organic electronic devices including, solar cells, light emitting diodes [141], [142], [23], [24] and [143], Schottky diodes [25], and supercapacitors [144], [145]. PEDOT:PSS is obtained by the polymerization of EDOT monomers in the presence of PSS anions which serve as oxidative agents [140]. Although PEDOT alone is unstable and insoluble in most solvents [146], PEDOT:PSS is well stable and can be dissolved in water [147] and [148]. To further enhance the stability and conductivity, PEDOT:PSS can be treated with ethylene glycol (EG). The addition of EG increases phase separation between PSS chains and PEDOT oligomers, which provides better conductivity through the charge transporting species (PEDOT) of the conducting polymer [149] and [150]. Similar stability and conductivity enhancement has been observed when dimethyl sulfoxide (DMSO) was used instead of EG [137] and [151].

The non-ionic surfactant polymer of polyethylene glycol and *p*-t-octylophenol (Triton X-100) has also been utilized to increase PEDOT:PSS films conductivity by stabilizing PEDOT nanosized particles [152] and to enhance the stability by decreasing surface tension [153]. Furthermore, Fic et al. have shown that the application of Triton X-100 in the electrolyte of a supercapacitor can enhance the specific capacitance by increasing the wettability of the electrode [153]. The decrease in the surface tension is achieved due to the molecular structure of Triton X-100, which has amphiphilic properties (hydrophilic ‘head’ and hydrophobic ‘tail’) [153]. Moreover, it is found that the electrical and optical properties of a PEDOT:PSS film improve by mixing a small percentage of a surfactant to the PEDOT:PSS solution before depositing the polymer film [152]. In this case, Triton X-100 can change the structure of the polymer film to increase the porosity of PEDOT:PSS films [154]. Also, it was shown that the addition of a small amount of Triton X-100 (0.3 wt%) to PEDOT:PSS increases the capacitance of an all-printed supercapacitor [136]. However the correlation between the concentration of Triton X-100 and the specific capacitance of the conducting polymer has not been studied. In this paper we present the effects of different concentrations of Triton X-100 on the double layer capacitance of PEDOT:PSS supercapacitors. We have found that the specific capacitance of the polymer film can be increased by a factor of 10 when mixing 3.0 wt% of Triton X-100 with the PEDOT:PSS solution before depositing the polymer. Higher concentration of the surfactant resulted in lower specific capacitance, likely due to change in the structural integrity of the polymer film.

To understand the electrical behavior of a supercapacitor, the simple Randles model including a capacitor (C) with a parallel resistor (and R_p) and an equivalent series resistor (R_s) can be used for large signal applications [155]. However, for small signal analysis, the ideal capacitance can be replaced by a Constant Phase Element (CPE) which takes into consideration

the surface morphology and uniformity of the charge distribution on the electrode [156], [157], [158] and [159].

6.2 Experimental

A Princeton Applied Research Potentiostat-VersaSTAT4 was used to perform all electrochemical experiments. The conductivity tests were conducted with a four point-probe setup using a Keithley source meter unit (model 2602). All chemicals were purchased from Sigma–Aldrich and used without additional purification. All weight measurements were recorded using an analytical balance (model GH-252) with a precision of 0.001 mg.

6.2.1 Electrode Fabrication

Separate PEDOT:PSS composite solutions were prepared by mixing pristine PEDOT:PSS with 5 wt% of EG and different percentages of Triton-X 100 (0.0, 0.3, 0.5, 1.5, 2.0, 2.5, 3.0, 3.3, 4.0, 5.0 wt%). Before using, the pristine PEDOT:PSS solutions were filtered through polytetrafluoroethylene (PTFE) membrane syringe filters with 0.22 μm pore size. The mixed samples were then sonicated for 40 min to dissolve any particle and to achieve homogeneous solutions.

Indium tin oxide (ITO) coated on polyethylene terephthalate (PET) with a surface resistivity of $60 \Omega/\square$ (Sigma) was used as the substrate and the back contact for the polymer film. The electrodes were fabricated by spin coating 2 mL of each polymer mixture on the ITO substrate ($2 \text{ cm} \times 1 \text{ cm}$) for 30 s at 1000 rpm. After the coating, the samples were cured on a hot plate for 15 min at $120 \text{ }^\circ\text{C}$. To enhance the conductivity, the cured films were further post-treated by putting the surface of the spin-coated films in contact with an EG bath for 5 min followed by another hot plate annealing at $120 \text{ }^\circ\text{C}$ for 40 min [160]. Figure 26 shows a fabricated electrode. The mass of composite PEDOT:PSS films were measured before and after each stage of

electrode and cell fabrication in order to accurately determine the mass of treated/composite PEDOT:PSS on the 2 cm × 1 cm ITO substrates.

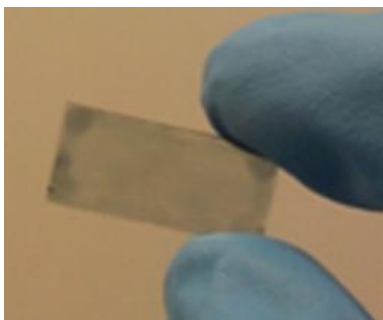


Figure 26 Treated PEDOT–PSS film on ITO substrate.

It was noted that samples with low levels of Triton X-100 (i.e. 0.3 wt%, 0.5 wt%) yielded non-uniform coatings. Also, it was observed that the solution of PEDOT:PSS with 5.0 wt% of the surfactant was viscous (gel form) which resulted in an adhesive film when it was spin coated on the substrate.

6.2.2 Cell Fabrication and Characterization

Experimental cells were fabricated for each sample from the above electrodes by inserting exactly 1.0 cm of the electrode into the electrolyte of the cell (electrode apparent surface area of 1 cm × 1 cm). The layers of the PEDOT:PSS composite at the upper part of the substrates were removed using isopropanol, to expose the ITO active layer which served as the current collector in the fabricated cells. A solution of 1 M tetrabutylammonium hexafluorophosphate (TBAP) solvated in propylene carbonate (PC) was used as the electrolyte for all tests. The three-electrode cell configuration with a coiled Pt wire as the counter electrode, Ag/AgCl as the reference electrode, and the treated PEDOT:PSS on ITO as the working electrode was used for all experiments except for the stability test which was performed under a

two-electrode configuration. All the samples were tested under the same experimental conditions at room temperature.

To study the performance of the PEDOT:PSS films with various Triton X-100 percentages, electrochemical tests including Cyclic Voltammetry (CV), Galvanostatic, and Electrochemical Impedance Spectroscopy (EIS) measurements were conducted. The specific capacitance of each electrode was measured by the CV method, in which the working electrode potential was swept with a scan rate of 25 mV/s between -500 mV and $+500$ mV versus Ag/AgCl for 5 cycles. The series resistances of the films and the effect of charging and discharging on the electrodes' performances, as the percentage of Triton X-100 varies, were analyzed using fast galvanic pulses of ± 1.0 μ A. To determine the effects of Triton X-100 on the impedance of the treated PEDOT:PSS films, EIS tests were also performed for a frequency range of 10 mHz to 100 kHz. The stability test was carried out by doing 3000 cycle of CV test (two-electrode) in the voltage range of -1.0 V to $+1.0$ V (50 mV/s) across a cell with two similar electrodes soaked in the TBAP electrolyte.

The conductivity of the PEDOT:PSS films was measured using a four point-probe setup (Keithley 2602). The treated PEDOT:PSS samples were spin-coated under the same experimental conditions as described in Section 2.1, on the non-conductive side of the substrates. The thicknesses of the films were estimated based on the recorded mass of treated PEDOT:PSS on the substrates, the surface area of the substrates, and the density of the dried coating of PEDOT:PSS (1.011 g/cm³) from the product information (Sigma). The structure and morphology of selected PEDOT:PSS treated films with Triton X-100 (0.0, 3.0, and 5.0 wt%) were studied using SEM (HITACHI S-800).

6.3 Results and Discussion

6.3.1 Specific Capacitance Measurements Using Cyclic Voltammetry

Figure 27 shows the CV curves of selected treated PEDOT:PSS films with 0.0, 0.3, 3.0, and 5.0 wt% of Triton X-100. The CVs were performed at a scan rate of 25 mV/s in the voltage range of ± 0.5 V versus reference electrode (Ag/AgCl). The current was normalized to the weight of treated PEDOT:PSS films on the $1\text{ cm} \times 1\text{ cm}$ portion of the ITO substrates which was immersed into the electrolyte. The rectangular shape of the voltammograms indicated that the capacitances recorded arise from double layer effect (no pseudo capacitance) [161]. It can be noted that the presence of Triton X-100 has a significant effect on the specific capacitance of the treated PEDOT:PSS films. The specific capacitance, C_{sp} , can be estimated from the difference of specific currents, ΔI_{sp} , at zero voltage and the scan rate ν ($C_{sp} = 0.5 \times \Delta I_{sp} / \nu$). A conducting polymer film with no surfactant (0.0 wt%) showed ~ 2.0 F/g capacitance which is consistent with previously reported values [162]. The specific capacitance was almost the same (~ 1.7 F/g) with low concentration of Triton X (0.3 wt%). However, the specific capacitance was increased to almost 10 times higher (20 F/g) for 3.0 wt% of Triton X-100. Using 5.0 wt% of the surfactant.

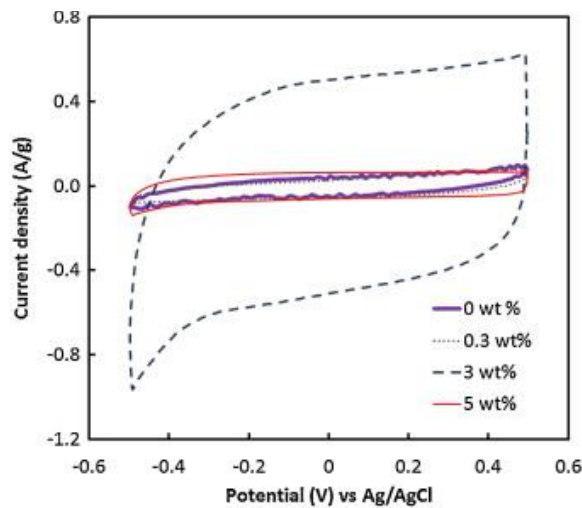


Figure 27 Cyclic voltammetry curves for different values of Triton X-100 percentage. The capacitance was reduced to the same level as the polymer without the surfactant (~ 2.5 F/g).

The specific capacitance of all samples was measured separately. As shown in Figure 28, the peak specific capacitance was achieved in the sample with 3.0 wt% concentration of Triton X-100. The increase in the capacitance from 0.0 to 3.0% of the surfactant is likely due to the increase in the porosity of the PEDOT:PSS films with the addition of the Triton X-100 [154]. Also, a part of the capacitance change can be because of the reduction in the surface tension of the electrode [153]. As shown in Figure 28, the increase in the surfactant concentration, beyond 3.0 wt%, resulted in a decrease of the specific capacitance. It was observed that the PEDOT:PSS solution became very viscous (gel form) when the Triton X-100 concentration was higher than 3.0 wt%. As the result, the quality of spin coated films was lower with some defects.

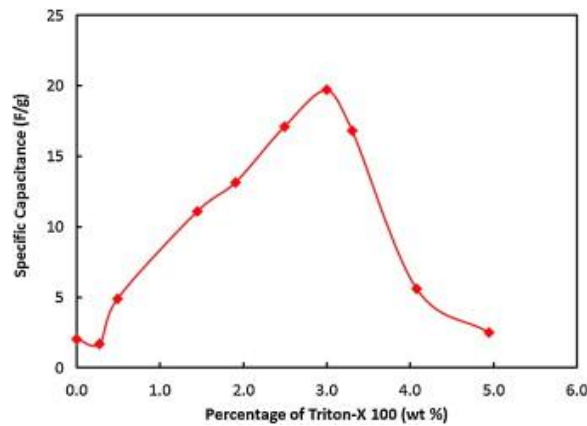


Figure 28 Specific capacitance as a function of Triton X-100 percentage.

6.3.2 Fast Galvanic Pulse Measurements

In order to study the effect of Triton X-100 on the series resistance, galvanic pulse measurements were performed by applying $\pm 1 \mu\text{A}$ current pulses to the cells (3-probe configuration) for 40 s (20 s to charge and 20 s to discharge). Figure 29 shows the voltage change in the electrode with 3.0 wt% surfactant. The linear potential variation during charge and discharge of the capacitor implies that the effect of R_p is negligible for this voltage range [163]. Also the slope of the potential represents the capacitance of the electrode. As expected, the

specific capacitances measured with this method were the same as the values reported from the CV measurement (Figure 28).

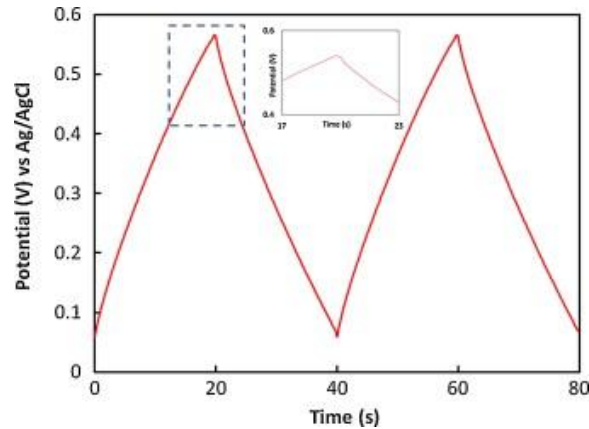


Figure 29 Galvanic pulses for PEDOT–PSS electrodes with 3.0 wt% Triton X-100. Current pulses of $\pm 1 \mu\text{A}$ with 40 s period were applied to charge and discharge the supercapacitors. (Inset) The voltage drops at the transition from charging to discharging.

As shown in the inset plot (Figure 29), the transition from $+1 \mu\text{A}$ to $-1 \mu\text{A}$ resulted in a voltage drop, ΔV , due to the series resistance, R_s . The value of the resistance can be estimated from $R_s = \Delta V / 2 \mu\text{A}$. The series resistance has been measured in all the electrodes with different concentrations of the surfactant. The results of the measurements are shown in Figure 30. Although the values of the series resistance of the cells were not significantly affected by the concentration level of Triton X-100, the series resistance was at the lowest value for the samples with $\sim 3.0 \text{ wt\%}$ in the surfactant concentration. The variation in the series resistance can be due to the difference in the surface area and thickness of the films [140]. Also, the conductivity of the polymer can be affected by the presence of the surfactant.

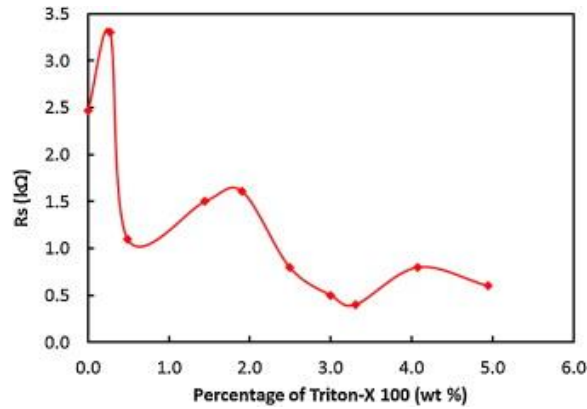


Figure 30 Series resistances for different values of Triton-X 100 percentage.

In order to study the effect of Triton X-100 on the conductivity of the polymer films, the polymer solutions with various concentrations of the surfactant was spin coated on the nonconductive side of the substrates. The lateral conductivity of the samples was measured using the 4-probe technique. The results are shown in Figure 31. The conductivities recorded ranged between 0.7 S/cm and 33 S/cm. The films with no surfactant presented the lowest conductivity of 0.7 S/cm. The addition of surfactant increased the conductivity of the film by at least 20 times. Although a local peak was observed at 3.0 wt%, the variation in the conductivity does not show any correlation with the concentration of Triton X-100.

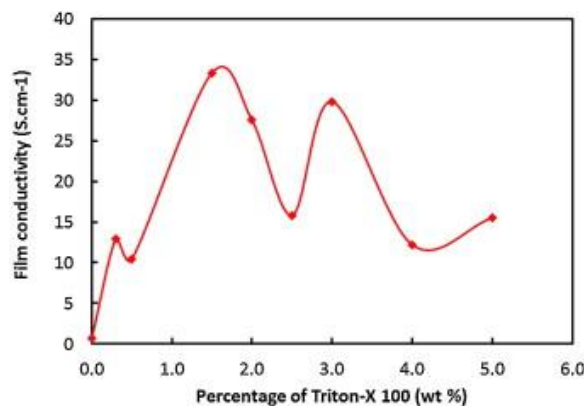


Figure 31 Film conductivity as a function of Triton-X 100 percentage.

The trend of the resistance change in Figure 30 and the conductivity of the samples in Figure 31 reveal that in addition to the polymer conductivity, the surfactant concentration affects the contact resistance between the polymer film and the back contact ITO. This was also observed particularly for the sample with 0.3 wt%, which had a low quality film (nonuniform film with defects) when spin coated on ITO.

6.3.3 Electrochemical Impedance Spectroscopy

The results from CV and galvanic pulse measurements show the large signal behavior of the polymer film. In order to understand the effect of the surfactant on the small signal response of the PEDOT:PSS films, electrochemical impedance spectroscopy tests were performed with no DC voltage bias and a sinusoidal signal of 20 mV, in the frequency range of 10 mHz to 100 kHz. The Nyquist plots for different levels of Triton X-100 are shown in Figure 32. The plots show that the parallel resistance (RP) of the electrode was higher for 3.0 wt% and 5.0 wt% of Triton X-100. The slopes of the Nyquist plots for low frequencies, when the charging is diffusion limited, were smaller for low concentrations of Triton X-100.

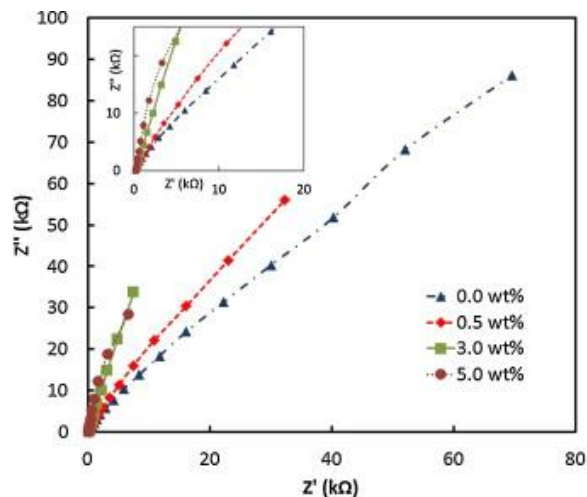


Figure 32 Nyquist plots of electrodes made with PEDOT:PSS with different percentages of Triton X-100. (Inset) Nyquist plot at high frequencies.

The Bode plot of the measured impedance for the electrode of 3.0 wt% surfactant is shown in Figure 33. The plots show both the magnitude and phase of the impedance for a frequency range from 10 mHz to 100 kHz. To explain the behavior of an electrode in different frequencies a more complicated model than the Randles model is required. Due to the porous structure of the electrode, instead of the double layer capacitor, a distributed capacitance–resistance model (transmission line model) can be applied which is usually presented with a constant phase element (CPE) instead of the capacitor [136]. The small signal model of the electrode with CPE is shown in Figure 33 (inset). Using ZSimpWin software from Princeton Applied Research, the model was applied to find the best fit to the experimental results. Table 6 shows the estimated parameters for the electrodes with 0.0, 3.0, and 5.0 wt% of Triton X-100. Also the measured masses for the samples have been listed in the table.

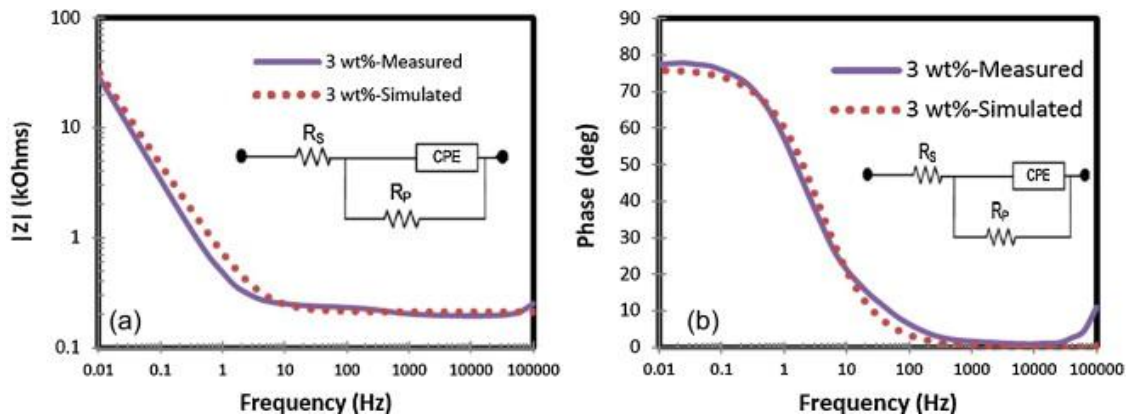


Figure 33 (a) Magnitude and (b) phase of impedance from the electrode made of PEDOT:PSS containing 3.0 wt% of Triton X-100. Both experimental and simulation results are shown. The simulation results were obtained using the inset models.

Table 6 Simulated values for CPE, R_p , and R_s in the of 0.0, 3.0, and 5.0 wt% Triton-X 100 electrode.

Characteristics	Value (0 wt%)	Value (3.0 wt%)	Value (5.0 wt%)
R_s [Ω]	150.8	210.3	219
Q [$S \text{ sec}^n$]	4.492×10^{-5}	3.250×10^{-4}	4.591×10^{-4}
Frequency power, n [$0 < n < 1$]	0.7214	0.8508	0.9197
R_p [Ω]	2.70×10^5	3.69×10^6	3.41×10^8
Polymer mass [mg]	7.5×10^{-2}	2.5×10^{-2}	2.7×10^{-2}

CPE is a complex impedance with the frequency power of n . The CPE impedance in angular frequency of ω is specified with Q and n : $Z_{CPE} = Q^{-1}(j\omega)^{-n}$ where $j = \sqrt{-1}$ [155]. The value of n depends on the nature of the electrode and varies from 0 to 1. A CPE with $n = 1$ is practically a double layer capacitor. Lower values of n indicate the porosity, surface roughness, and inhomogeneity of the charge distribution in the electrode [136]. The high value of n for the electrode containing 5.0 wt% of Triton X-100 implies low porosity of the electrode and relatively uniform charge distribution. This is consistent with the observation from the gel form of the solution with 5.0 wt% surfactant. In contrast, the electrode with no surfactant demonstrated the lowest value of n , which could be due to more distributed pores in the polymer film. However, the lower value of Q and larger mass in the sample with no surfactant suggests smaller pore (lower surface area) in the film with 0% surfactant. Additionally, the low specific capacitance in the absence of Triton X-100 measured by CV (Figure 27 and Figure 28) indicates low surface area (small pores). Although the pores may not be well distributed in the volume of the polymer with 3.0 wt% of Triton X-100, the larger specific capacitance implies the existence of larger pores with large overall surface area. The structure of the films was further studied with SEM. The results in Figure 35 confirm the structural differences.

6.3.4 Stability Study

To study the stability of the electrode, a symmetrical supercapacitor was fabricated by inserting two ITO electrodes coated with PEDOT:PSS (3.0 wt% Triton-X 100) in a beaker containing the electrolyte (1 M TBAP in propylene carbonate). The device was tested by charging and discharging the cell for 3000 cycles from -1.0 V to $+1.0$ V (50 mV/s). The CV results for the device before and after 3000 cycles are shown in Figure 34. The capacitance dropped from 0.486 mF to 0.431 mF which could be partly due to the solvent evaporation from the beaker and partly from polymer film detachment (defect). For device applications, it is recommended to seal the cell in vacuum [159]. Also, air and water molecules in air can be removed by vacuuming which enhances the stability of the device and expands the voltage range to much higher values (3.0 V) [159]. Using an unsealed setup, we observed exponential changes in the current when the scan window was expanded beyond 1.0 V (the result is not presented here). Hence, the stability test was performed in the limited voltage range to avoid damaging the polymer film. Nevertheless, the result in Figure 34 shows that the stability of the polymer film with the surfactant is reasonable.

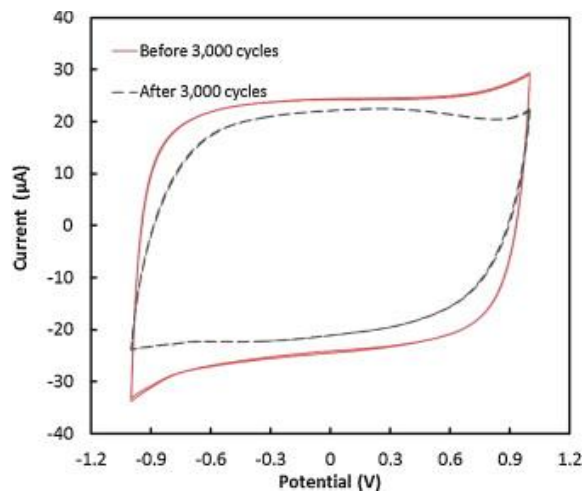


Figure 34 Cyclic voltammetry curves before and after 3000 cycles of charging and discharging a symmetrical cell with polymer electrodes containing 3.0 wt% Triton X-100.

6.3.5 Surface Morphology

Figure 35 shows the surface morphology of different electrodes. The images were taken with a HITACHI S-800 SEM machine. The film with no Triton X-100 showed no significant feature with a compact structure, which implies nanoscale pores. The treated PEDOT:PSS film with 3.0 wt% of Triton X-100 presented more porosity compared to the other electrodes.

The film obtained with 3.0 wt% showed opening gaps in its structure. The gaps indicated a lamellar structure with 2 μm wide alternating bands. The structure of the 3.0 wt% film is in agreement with the impedance spectroscopy measurements. The 5.0 wt% film showed less porosity, than the 3.0 wt%, with individual randomly distributed pores in the micrometer scale. The SEM images showed that the addition of the surfactant changed the morphology of the surface of the PEDOT:PSS films by augmentation of porosity.

6.4 Conclusion

In this chapter, we presented the influence of Triton X-100 on the double layer capacitance of a PEDOT:PSS based electrode. A peak specific capacitance of ~ 20 F/g was achieved when 3.0 wt% of the surfactant was mixed with the polymer solution. The series resistances of the samples and the films' conductivities were measured which showed that the addition of Triton X-100 to PEDOT:PSS increased the film conductivity, but the level of the non-anionic surfactant did not affect significantly the conductivity of PEDOT:PSS films. The surface morphology and EIS study revealed that the surfactant has produced larger pores in the polymer film. The porosity structure was changed by the formation of gaps on the surface of the film with 3.0 wt% of the surfactant. Overall, the addition of the optimum concentration of Triton X-100 can increase the large signal double layer capacitance of PEDOT:PSS, allowing the conductive polymer to be utilized in electrochemical capacitor applications where double layer

capacitance is preferred to pseudocapacitive effect. The next chapter presents the final research project in which PEDOT:PSS modified with 3 wt% of Triton X-100 is used in addition to dyes to develop a photoactive supercapacitor.

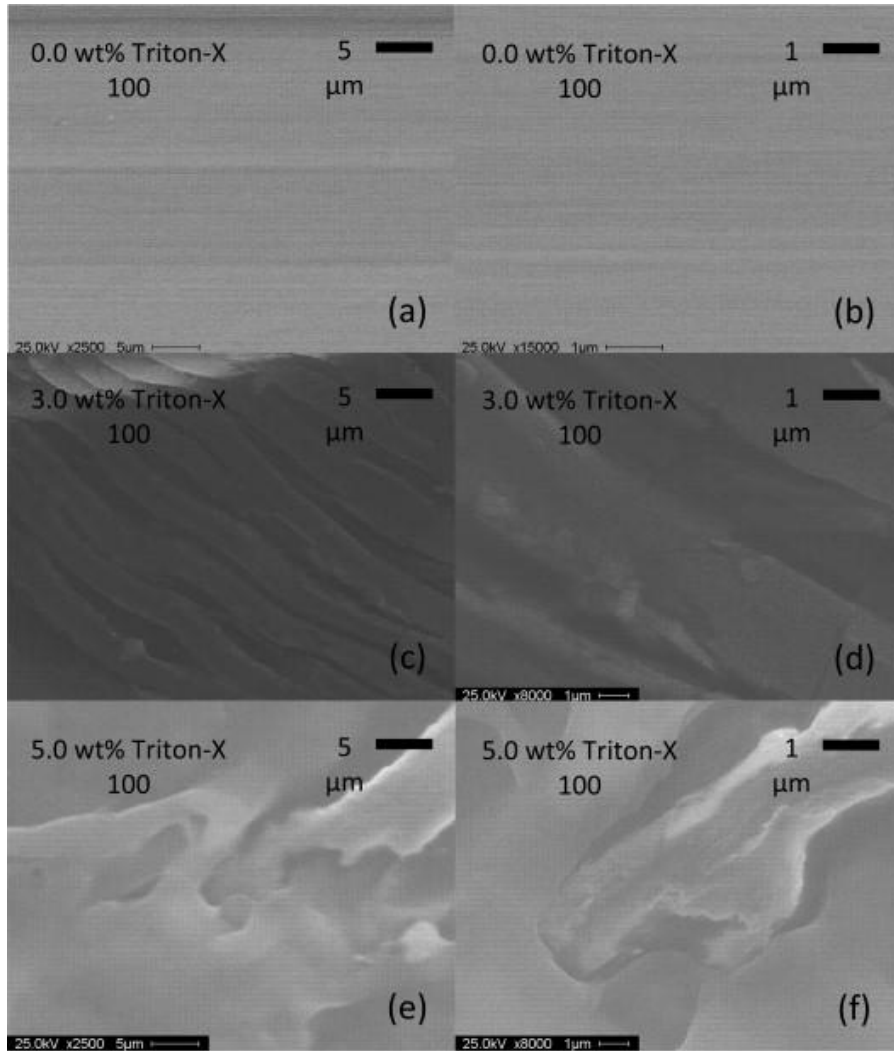


Figure 35 SEM images of PEDOT-PSS on ITO electrodes with (a) and (b) 0.0 wt%; (c) and (d) 3.0 wt%; and (e) and (f) 5.0 wt% Triton X-100. All samples were also treated with 5 wt% ethylene glycol.

CHAPTER 7: PHOTOACTIVE SUPERCAPACITORS FOR SOLAR ENERGY HARVESTING AND STORAGE⁴

7.1 Introduction

Due to the intermittent nature of solar energy, energy storage is essential in systems which are powered by harvesting solar energy [164]. Conventionally, external energy storage devices such as batteries and supercapacitors are employed in conjunction with solar cells [165]. In the attempt to store energy in a photovoltaic device, various hybrid devices were fabricated and tested before [166]–[178]. In a simple form, demonstrated by several groups [166]–[172], [174]–[178], a cell with two compartments can be designed for accommodating a dye sensitized solar cell (DSSC) and a supercapacitor in a device. Most of those devices are essentially a solar cell and a supercapacitor in one package with three electrodes (one electrode is shared between the capacitor and solar cell). An external circuit, such as a diode switch, is required to connect the solar cell to the capacitor during energy harvesting cycle and prevent the capacitor discharge through the DSSC [166], [167]. In a different approach, Zhang et al., have used a modified counter electrode in a DSSC which demonstrated ~ 100 mV open circuit voltage with a few minutes energy storage in a two terminal device [173].

Photogalvanic cells (invented in 1970s) are also capable of harvesting and storing energy by using two different ions (positive and negative charge carriers) in the electrolyte of a two

⁴This chapter was previously published in [179]. Permission is included in Appendix A.

terminal device [180]. Different types of photogalvanic cells have been investigated, so far [181], [182]. However, the experimental studies and the theoretical analysis show that the storage time is limited to the recombination rate of the positive and negative ions in the electrolyte [183]. Charge storage time in the range of a few minutes can be achieved in a photogalvanic cell by reducing the recombination rate in a cell using semiconducting electrodes [181].

We have devised a new structure which can convert photons to electric charges and at the same time store the charges in the device under the open circuit conditions. As shown in Figure 36 (a), the new device is an electrochemical cell with porous working and counter electrodes. The working electrode is a composite film of a conducting polymer (Poly(3,4-ethylenedioxythiophene) Polystyrene sulfonate and – PEDOT:PSS) and a dye deposited on a transparent indium tin oxide (ITO) electrode. The counter electrode is made of a porous activated carbon. Using porous conducting polymer (CP) and activated carbon electrodes, the device is essentially a supercapacitor which can store charges [20],[74], [184]. As shown in this work, application of the dye molecules can enhance the photovoltaic effect in the conducting polymer.

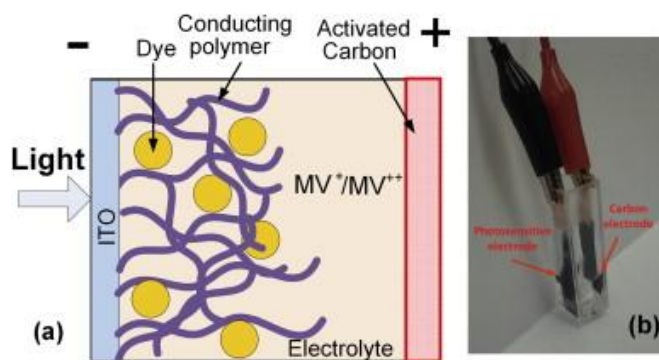


Figure 36 (a) Schematic of an electrochemical device with a composite of a conducting polymer and a dye as the photosensitive anode electrode (– terminal). Methyl viologen (MV^+/MV^{++}) was applied as the redox material in the electrolyte. (b) A fabricated photoelectrochemical cell using the composite film as the photosensitive electrode.

A photograph of the fabricated cell is shown in Figure 36(b). The presented work includes both the photovoltaic response and energy storage effect in the new device. Composite electrodes of CP with two different dyes and various concentration of the dye have been investigated. The results show a promising energy storage feature for a photovoltaic device.

7.2 Experimental

7.2.1 Materials and Equipment

Indium tin oxide coated PET (polyethylene terephthalate plastic), porphyrin dye (5,10,15,20-tetraphenyl-21h,23h-porphine-Zinc), also known as ZnTPP, PEDOT:PSS (1.3 wt% dispersion in water), Triton X-100, ethylene glycol, methyl viologen (MV) and Tris were all purchased from Sigma–Aldrich. The carbon paper, as the counter electrode, was purchased from Y-carbon. The Ru based dye (triisothiocyanato-(2,2':6',6''-terpyridyl-4,4',4''-tricarboxylato) ruthenium(II) tris(tetra-butylammonium)) also known as N749 was from Solaronix. The electrical and electrochemical measurements, including open circuit voltage test, current measurement, cyclic voltammetry (CV) and electrochemical impedance spectroscopy (EIS), were carried out using a desktop computer connected to a VersaSTAT 4 potentiostat. The cells were placed in a dark box connected via an optical fibre to a solar simulator (RST, Radiant Source Technology) with an internal AM 1.0 optical filter which delivered light intensity of 80 mW cm^{-2} at its output. For the experiments, the illumination time was controlled manually by turning on and off the instrument shutter. The experimental setup, including the dark box and the shutter mechanism, was designed to eliminate the effect of stray light in the experiment. A picture of the setup is presented in the supplementary data section (see Figure SD1 in Appendix D). The optical absorption spectrum was measured using a Thermo Scientific (Evolution 201) UV–Vis spectrophotometer.

7.2.2 Electrode Fabrication

1.25 mg of ZnTPP (or N749) was dissolved in 2.5 ml isopropanol (acetonitrile for N749). 2.5 ml of the conducting polymer solution was made by mixing 5 wt% ethylene glycol and 3 wt% Triton X-100 in the PEDOT:PSS [74]. Different ratio (1:0, 1:1, 1:2, 2:1, and 0:1) of the conducting polymer and dye solutions were mixed and sonicated for 5–20 min to achieve a homogeneous solution. Kapton tape was used to make a rectangular mask (1.0 cm × 0.5 cm) on the ITO electrode. 10 µl of the mixed solution was drop casted on the electrode and dried on a hotplate for 5 min at 120 °C to make the composite film on the transparent electrode. The electrode and a piece of Y-carbon (as the counter electrode) were placed in a disposable cuvette and it was filled with the electrolyte (1 mM MV in 0.1 M Tris buffer solution) to cover the composite film. The apparent surface area of the carbon electrode in the solution was estimated to 1.0 cm × 0.5 cm. The fabricated cells were not sealed.

7.3 Results and Discussion

First a composite film was made by drop casting a mixed solution of 1:1 ratio of PEDOT and porphyrin dye solutions on an ITO electrode. The molecular structure of the dye (ZnTPP) is shown in Figure 37(a). The electrode with 1:1 CP-dye was used as the working electrode in a cell with a porous carbon electrode (counter electrode) and an electrolyte with 1 mM methyl viologen (MV) in Tris buffer. The cell was kept in the dark for about one hour until a stable open circuit voltage was achieved. Then the cell was illuminated for 400 s, using the solar simulator. As shown in Figure 37(a), the open circuit voltage across the cell in the dark was 405 mV (the negative value shows that the composite film was the negative terminal of the device—see Figure 36). The cell voltage (absolute value) was increased gradually from 405 mV to 431 mV in 400 s of illumination. After turning off the light, unlike conventional DSSCs [185],

the voltage was not dropped to the dark value immediately. Instead a gradual change was observed and the magnitude of the cell voltage reached to 421 mV in 580 s after the cessation of light. The gradual increase in the cell voltage in light implies the energy storage effect (charging the supercapacitor). A simple explanation is that, under the open circuit condition, the photoexcited charges (generated in the composite) accumulate on the conducting polymer and charge the working electrode. The interaction between MV^+ ions in the electrolyte and the positive charge on the composite can also oxidized the ions and convert them to MV^{++} ($MV^+ \rightarrow MV^{++} + e^-$). The oxidized ions (MV^{++}) diffuse to the counter electrode where a double layer charge can be formed on the surface of the carbon electrode. The slow change in the voltage after illumination shows the leakage effect in the supercapacitor [52]. Nevertheless, the device was able to store a part of the photogenerated charges after ~ 10 min. The photovoltaic and energy storage effects were further studied in the device by illuminating the cell for another 400 s under the open circuit conditions. Immediately after turning off the light, the short circuit current was recorded. As shown in Figure 37(b), the stored charges in the device resulted in a dark current which was decreased from 30 μA to 18 μA in 50 s. The low short circuit current and gradual discharge of the device indicates a relatively large internal resistance. While the short circuit current was monitored, the light source was turned on for 90 s. The current was increased to 23 μA at the end of the illumination cycle and decreased again when the light was turned off. The positive current and negative open circuit voltage indicate a photovoltaic power generation by the device. The increase in the short circuit current under illumination also shows the feasibility of delivering a part of the photogenerated charges directly to a load and store some of the charges. It should be mentioned that due to the storage effect, the conventional current–voltage test (scanning voltage and recording the current) cannot be applied to characterize the

photovoltaic effect and estimate the efficiency, short circuit current, open circuit voltage, and the fill-factor (FF) of the device. As shown in Figure 37(c), the voltage scan shows a large current even in dark, because of the supercapacitive characteristic of the device ($I = C \cdot dV/dt$ – where I is the current, C is the device capacitance, and dV/dt is the scan rate). However, in the current form, with relatively low short circuit current, the photo conversion efficiency is very low.

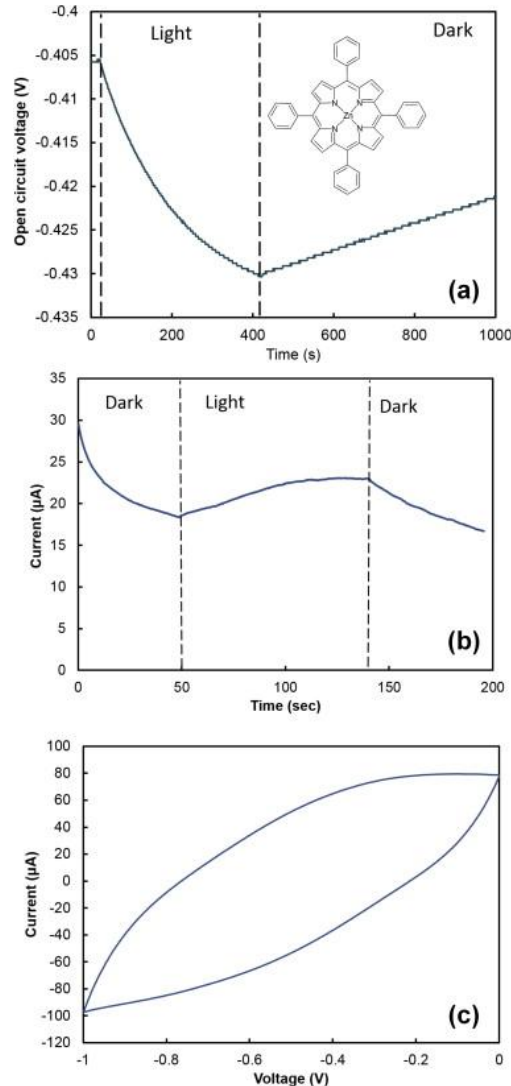


Figure 37 Photovoltaic and energy storage effect in the cell with PEDOT:PSS- porphyrin dye composite electrode. (a) Open circuit voltage and (b) short circuit current in the dark and light. (c) CV in the dark with scan rate of 50 mV s^{-1} . The voltages were measured with respect to the counter electrode (carbon electrode) potential. The molecular structure of the porphyrin dye (ZnTPP) is shown in the inset of Figure 37(a).

The storage capacitance of the device was measured using CV method. Since the working electrode voltage was negative, the voltage range in the CV measurement was set between 0 V and -1 V (Figure 37(c)). The value of the capacitance was estimated to be ~ 1.04 mF from the width of the CV loop at -0.5 V.

To investigate the effect of dye concentration on the energy storage and photovoltaic effect of the device, various composite electrodes were fabricated with CP-dye ratios of 1:0 (only CP), 1:1, 1:2, 2:1, and 0:1 (only dye). Figure 38(a) shows the CV results from the devices with those electrodes. As expected the electrode with only dye coating had very negligible capacitance likely due to the lack of porosity. Although due to the higher amount of CP it was expected to achieve the highest capacitance in the device with only CP, the electrode with one part CP and two parts dye showed the largest capacitance of 1.76 mF and the electrode with only CP had a capacitance of only 0.19 mF. To understand the capacitance increase in the composite electrode, SEM (Scanning Electron Microscopy) images were taken (Figure 38(b) and (c)) which clearly showed the structural difference between the composite and the CP films. It is likely that the micro cracks on the composite material enhanced the film porosity.

The photovoltaic effect in different electrodes was studied by monitoring the change in the open circuit voltages in the dark and light (Figure 40). Since the capacitance of the electrode with only dye was negligible (Figure 38(a)), only the electrodes with the conducting polymers were considered in the photovoltaic test. Due to the energy storage effect, different devices showed different open circuit voltages in the dark, even after keeping devices in the short circuit (in the dark) mode for a few hours. Therefore, for a comparative study, only the change in the open circuit voltage from the dark (ΔV) is presented in Figure 40. The cell open circuit voltages are demonstrated in Figure S2 in the supplementary data (see Appendix D). The largest

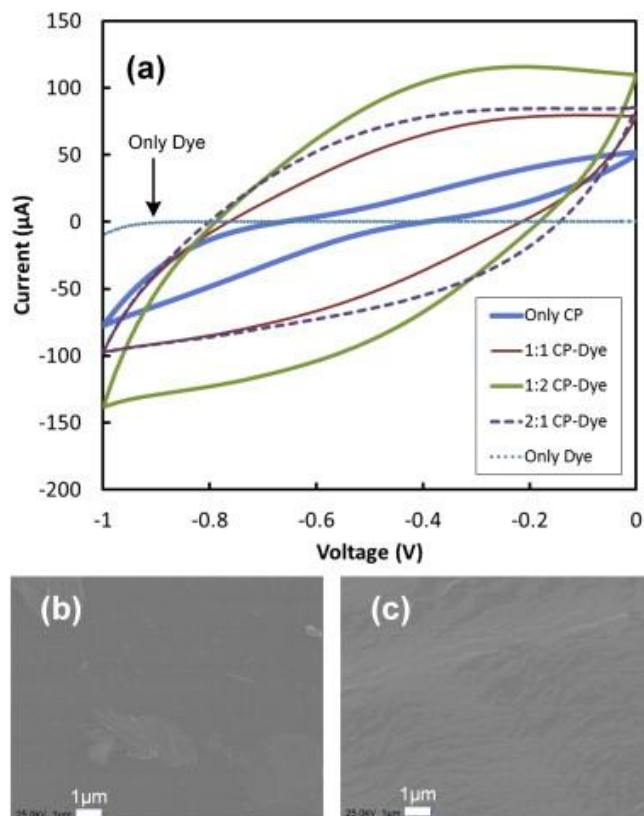


Figure 38 (a) CV results from devices with only CP, only dye, and 1:1, 1:2, 2:1 CP-dye composite electrodes. The scan rate was 50 mV s^{-1} and the experiment was performed in the dark. SEM images of electrodes with (b) only CP and (c) 1:2 CP-dye composite films.

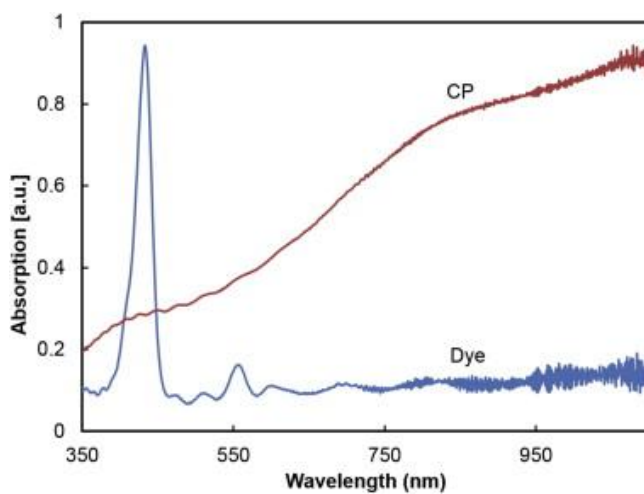


Figure 39 Optical absorption of the films of only CP and only dye on two ITO electrodes.

ΔV was -27 mV from the device with 2:1 CP-dye composite. The electrode with only CP showed the lowest ΔV (-12 mV). Considering the absorption spectrum in Figure 39, it seems that the absorption of high energy photons by the dye molecules enhances the photovoltaic effect. However, the larger ΔV in the composite of 2:1 CP-dye than the electrodes with higher dye concentration (1:1 and 1:2 CP-dye) shows the importance of the ratio between the dye and the conducting polymer for the photovoltaic effect.

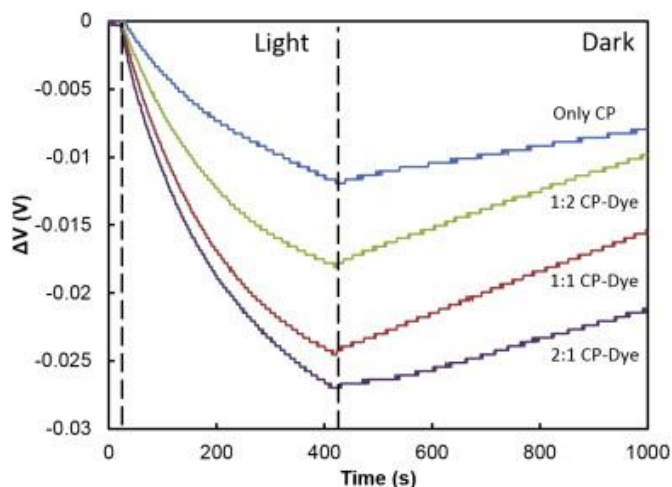


Figure 40 The change in the open circuit voltage in different cells under illumination and after cessation of light.

Considering the semiconducting properties of conducting polymers, the structure of the device is similar to a DSSC in which a porous layer of TiO_2 nanoparticles (semiconducting material) and a layer of dye molecules are applied as the photoactive electrode. However, there is [185], [186]. The mechanism of the photogenerated charge storage in the composite film is not known yet, but it is likely that the charge is stored on the polymer chains by changing the oxidation state of the polymer film (pseudo capacitive charge storage) [133]. The CV experiment with very low scan rate (2 mV s^{-1}) was performed in the dark and light on the cell (two probe experiment) with 2:1 CP-dye electrode to investigate the oxidation state of the composite film. As shown in Figure 41(a), an oxidation peak was observed at -0.78 V. Also, a very broad

reduction peak can be seen around -245 mV (the peak is more pronounced in the CV of the dark experiment-inset Figure 41 (a)). The reduction peak is under influence of the knee current. Due to the small peak amplitudes, the redox peaks could not be seen in the CV with fast scan rate (Figure 38). Nevertheless, the open circuit voltage of the cell (Figure 37(a)) is between the redox peaks. Hence, it is possible to change the redox state by shifting the composite electrode voltage to more negative value [187]. The voltage of the oxidation peak did not change in the dark and light, but the knee in the current was sharper under illumination, which suggests faster charge transfer in light than in the dark. The effect of light on the electrode properties was further studied by performing EIS on the cell with the 2:1 CP-dye electrode. The Nyquist plot is presented in Figure 41(b). The impedance at high frequencies showed a resistive behaviour with the series resistance of 1.52 k Ω . Such a large resistance explains the limited short circuit current in the cell (Figure 37(b)). To reduce the resistance, an electrolyte with higher ion concentration can be used. Also the contact resistance between the composite film and the ITO electrode has to be improved. The semi-circle with almost linear tail in the Nyquist plot suggests that the polarization is due to a combination of diffusion and kinetic processes [155]. The presented equivalent circuit model (inset Figure 41(b)) was applied to simulate the cell response in the dark and light using ZSim software. In the model, RS represents the series resistance, CD is the double layer capacitance, RP is the parallel resistance, R_{ct} is the charge transfer resistance, and Q is the constant phase element with power of n . The estimated values of the elements in the model are listed in Table 7. In both the dark and light cases, the estimated value for n is close to 1 which implies a capacitive behaviour (transmission line model) [136] and [188]. The values of CD , Q , and n were almost the same in the dark and light. Hence, as expected, the effect of light on the capacitive behaviour of the cell was negligible. The largest difference was observed

in R_{ct} and RP , which again shows higher charge transfer rate in light than in the dark and larger cell current in light.

Table 7 Comparison between impedance parameters in the dark and light.

Description	R_s (k Ω)	C_D (μ F)	R_P (k Ω)	R_{ct} (k Ω)	Q (S sec ⁿ)	n
Dark	1.52	4.1	9.11	1.77	8.26E-04	0.92
Light	1.52	4.02	6.89	1.51	8.28E-04	0.96

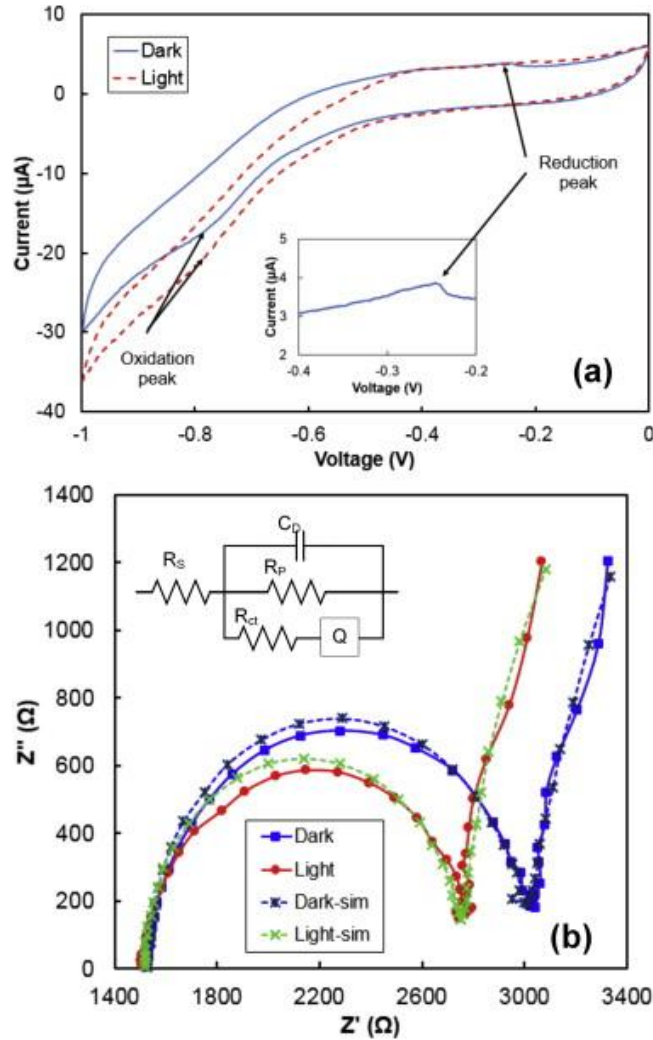


Figure 41 Photoelectric study of the cell with 2:1 CP-dye composite electrode (a) CVs in dark and light with slow scan rate (2 mV s^{-1}). (Inset) the reduction peak under influence of the current knee. (b) Electro impedance spectroscopy in the dark and light. The proposed model for the cell is shown inside the figure. The simulated results for the dark and light are also presented.

The concept of using a CP-dye composite for making photovoltaic devices with embedded energy storage was further developed by using a Ru based dye molecule (see Figure 42 for the molecular structure of N749) instead of the porphyrin dye in a 1:1 CP-dye composite. The photovoltaic test of the device showed a much slower charging cycle with a large potential difference under illumination. As shown in Figure 42, the cell voltage (absolute value) was increased from 42 mV to 240 mV in 2500 s ($\Delta V = 198$ mV). Also, the cell showed an incredibly high charge storage stability. After turning off the light the open circuit voltage was reduced by only 20 mV ($\sim 10\%$ of ΔV) in 2 h. However, the short circuit current was in sub micro amp range (the result is not presented). In addition, Ru based dyes are relatively expensive and, potentially, they are not suitable for low cost devices such as the photoactive supercapacitor studied in this work.

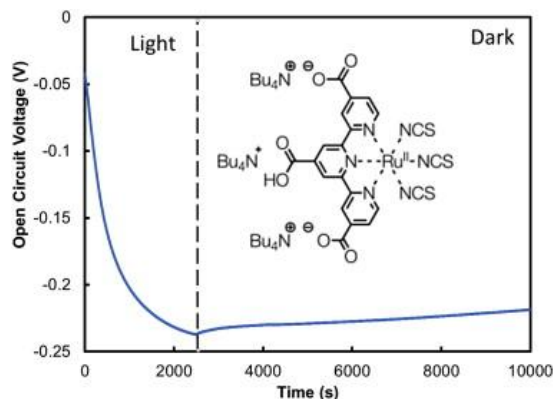


Figure 42 Open circuit voltage of a cell with CP and N749 dye composite electrode in light and dark. Long storage time of more than 7500 s was achieved with only 20 mV cell voltage change in the dark. The inset Figure shows the molecular structure of N749.

The energy diagram in Figure 43 has been presented to suggest the charge cycle in the devices with ZnTPP/N749 dye molecule. Similar to a DSSC, absorbed photons by the dye molecules (or CP) generate excited states. The electron in the excited state can reduce the PEDOT:PSS polymer. In this situation the electron is not mobile. This resembles a localized

charge in a higher energy state in the polymer. Also, the dye molecules receive electrons from methyl viologen through another redox reaction ($MV^+ \rightarrow MV^{++} + e^-$) and MV^{++} ions diffuse toward the counter electrode. Under the open circuit conditions, the reduced polymer at the composite electrode and the oxidized methyl viologen at the counter electrode generate a potential difference across the cell. In the short circuit mode, the carbon electrode delivers electrons to methyl viologen in the electrolyte and ITO removes electrons from PEDOT:PSS. Since holes are more mobile than electrons in the polymer, the generated hole can travel through the polymer film where the stored electron can be released through a recombination process. The energy levels in Figure 43 have been obtained from reported values in other publications [189]–[194]. The significant difference between the two dyes is in the LUMO level. The excited electrons in ZnTPP can be transferred to the conduction band of the polymer and from there, they would be trapped in the localized states. However, the excited electrons in N749 move directly to the localized states. This can explain the slow increase in the voltage (Figure 42) and low current in the device with the Ru dye, as the direct electron transfer to the localized states has likely lower probability than trapping the charges from the conduction band in the ZnTPP case. Nevertheless, a bottleneck in the electron cycle is the redox potential of MV. A redox mediator with lower energy than methyl viologen would facilitate the charge circulation. A detail energy study of the composite material is required for better understanding of the mechanism of charge cycle and storage in the device.

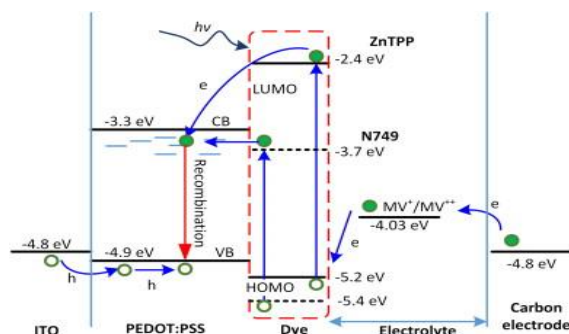


Figure 43 Energy diagram of the photoactive supercapacitor. The energy levels are versus the vacuum level. The localized states below the conduction band of the polymer show the energy states when the polymer is reduced. The diagram shows the energy levels for both ZnTPP and N749 dyes.

7.4 Conclusions

Using composite materials of a conducting polymer and dye molecules, a new photoelectrochemical device was introduced which demonstrated an internal energy storage capability. The effect of dye concentration on the energy storage and photovoltaic effects were investigated. It was found that the addition of the dye increases the capacitance in the conducting polymer and enhances the photovoltage in the device. Slow scan CV and EIS study revealed that the electrical properties of the composite electrode changes in presence of light by facilitating the charge transfer. Also, application of N749 dye molecule showed significant improvement in the photovoltage and charge stability in the cell. Further study is required to investigate the effect of materials and concentrations on the photovoltaic and energy storage properties of the device. Additionally, for practical applications, there are technical issues, such as sealing the device, which must be addressed after device development.

7.5 Acknowledgements

This work was supported by a grant from Sunvault Energy Inc. The SEM images, presented in this work, were taken at NREC (Nanotechnology Research & Education Center) at the University of South Florida.

CHAPTER 8: CONCLUSIONS AND FUTURE WORKS

As part of this work, different projects including the self-discharge reduction of supercapacitors, the modeling of self-discharge knowing the blocking layer thickness and their simulation for various thicknesses, the enhancement of PEDOT:PSS double layer capacitance, and the study of photoactive dyes and PEDOT:PSS as electrode material for photoelectrochemical supercapacitors were completed. The research activities contributed to the enhancement of supercapacitors energy storage for renewable energy applications.

Supercapacitor leakage problem has been intensively studied and documented in literature. It has been found that the main cause of supercapacitor self-discharge reside in electrochemical reactions in the electrolyte on the surface of the electrodes. Electrons in the electrode cross the interface between the electrode and the electrolyte, to engage in the Faradic reactions. In this work we have successfully reduced the leakage current by ~78% in a carbon based supercapacitor by coating the surface of the electrodes with a thin PPO insulating film with an approximate thickness of ~1.5 nm. Although the self discharge was reduced, the capacitance was also decreased. A mathematical model was then developed to study how the thickness and type of blocking layer affects the self-discharge and the energy density of the device. The tunneling of the electrons engaging in the electrochemical reactions and the kinetics of those reactions were considered to develop the model. Following the model, a computational code was written in Matlab to simulate the leakage and energy profiles of different thicknesses of the blocking layer (Appendix F). The second research project confirmed the first and showed that the tool developed can be used to predict the self-discharge behaviors of hypothetical

devices with different layers of different thicknesses. A third research discovered the optimal concentration of Triton- X 100 in a spin coated PEDOT:PSS electrode that enhanced the conducting polymer's double layer capacitance. The capacitance was increased to 20 F/g for a concentration of 3 wt % triton- X 100. The polymer was pretreated with 5 wt % ethylene glycol. The addition of the right amount of the surfactant not only increased the conductivity of the polymer, but also modified its surface structure increasing the capacitance. It was also found that different concentration of the surfactant yielded different porosity changes of the polymer. A final research project developed a photoelectrochemical device made with a composite material of dye and PEDOT:PSS. The PEDOT: PSS was pre-treated with 3 wt % of Triton X-100. The study of the effect of dye concentration on the device showed that their addition improved the capacitance and the photovoltage. The counter electrode of the device was a carbon-based electrode.

To continue this work, future works based on the following ideas can be explored:

- Use a semiconducting material that would be able to act as a blocking layer when the device is not connected to any external load but switch to non-blocking mode when the device is recharging or connected to a load. This would allow the reduction of the self-discharge not only in EDLCs but also in pseudocapacitive devices.
- Use a multi-layer structure of PEDOT:PSS where different superimposed spin coated layers of the conducting polymer are treated with different Triton X-100 concentrations. This study will shed more light on how the diffusion of ions is affected by the pores size and morphology of a supercapacitor electrode.
- Study how the ratio of the polymer to dye concentration increases the open circuit voltage

and photocurrent as well as the capacitance of the photoelectrochemical device. Different types of carbon counter electrodes can also be studied for an optimum operation of the device.

REFERENCES

- [1] J. P. Holdren, "Population and the energy problem," *Popul. Environ.*, vol. 12, pp. 231–255, 1991.
- [2] C. C. D. US EPA, "Greenhouse Gas Emissions: Greenhouse Gases Overview." [Online]. Available: <http://www.epa.gov/climatechange/ghgemissions/gases.html>. [Accessed: 28-May-2015].
- [3] A. H. MacDougall and P. Friedlingstein, "The origin and limits of the near proportionality between climate warming and cumulative CO₂ emissions," *J. Clim.*, 2015.
- [4] Z. Zou, J. Cao, B. Cao, and W. Chen, "Evaluation strategy of regenerative braking energy for supercapacitor vehicle," *ISA Trans.*, vol. 55, no. 0, pp. 234–240, Mar. 2015.
- [5] H. Yang and Y. Zhang, "A study of supercapacitor charge redistribution for applications in environmentally powered wireless sensor nodes," *J. Power Sources*, vol. 273, no. 0, pp. 223–236, Jan. 2015.
- [6] B. C. Steele and A. Heinzl, "Materials for fuel-cell technologies," *Nature*, vol. 414, pp. 345–352, 2001.
- [7] M. D. Anderson and D. S. Carr, "Battery energy storage technologies," *Proc. IEEE*, vol. 81, pp. 475–479, 1993.
- [8] M. F. El-Kady, V. Strong, S. Dubin, and R. B. Kaner, "Laser Scribing of High-Performance and Flexible Graphene-Based Electrochemical Capacitors," *Science*, vol. 335, pp. 1326–1330, 2012.
- [9] A. F. Burke, "Batteries and Ultracapacitors for Electric, Hybrid, and Fuel Cell Vehicles," *Proc. IEEE*, vol. 95, pp. 806–820, 2007.
- [10] M. Winter and R. J. Brodd, "What Are Batteries, Fuel Cells, and Supercapacitors?," *Chem. Rev.*, vol. 104, pp. 4245–4270, 2004.
- [11] Y. Zhang, H. Feng, X. Wu, L. Wang, A. Zhang, T. Xia, H. Dong, X. Li, and L. Zhang, "Progress of electrochemical capacitor electrode materials: A review," *Int. J. Hydrog. Energy*, vol. 34, no. 11, pp. 4889 – 4899, 2009.
- [12] S. Faraji and F. N. Ani, "The development supercapacitor from activated carbon by electroless plating—A review," *Renew. Sustain. Energy Rev.*, vol. 42, no. 0, pp. 823 – 834, 2015.

- [13] J. Schindall, "The Charge of the Ultra - Capacitors," 01-Nov-2007. [Online]. Available: <http://spectrum.ieee.org/transportation/advanced-cars/the-charge-of-the-ultra-capacitors>. [Accessed: 07-Jun-2015].
- [14] L. I. Schultz and N. P. Querques, "Tracing the ultracapacitor commercialization pathway," *Renew. Sustain. Energy Rev.*, vol. 39, no. 0, pp. 1119 – 1126, 2014.
- [15] "Ultracapacitor Market Forecast 2015-2020," *Market Research Media*. [Online]. Available: <http://www.marketresearchmedia.com/?p=912>. [Accessed: 07-Jun-2015].
- [16] "Supercapacitor Market by Materials & Products - 2020 | MarketsandMarkets." [Online]. Available: <http://www.marketsandmarkets.com/Market-Reports/supercapacitor-market-37140453.html>. [Accessed: 07-Jun-2015].
- [17] B. W. Ricketts and C. Ton-That, "Self-discharge of carbon-based supercapacitors with organic electrolytes," *J. Power Sources*, vol. 89, pp. 64–69, Jul. 2000.
- [18] E. Bakhoun, "New mega-farad ultracapacitors," *Ultrason. Ferroelectr. Freq. Control IEEE Trans. On*, vol. 56, pp. 14–21, 2009.
- [19] L. Chen, Z. Song, G. Liu, J. Qiu, C. Yu, J. Qin, L. Ma, F. Tian, and W. Liu, "Synthesis and electrochemical performance of polyaniline–MnO₂ nanowire composites for supercapacitors," *J. Phys. Chem. Solids*, vol. 74, no. 2, pp. 360–365, 2013.
- [20] G. Wang, L. Zhang, and J. Zhang, "A review of electrode materials for electrochemical supercapacitors," *Chem. Soc. Rev.*, vol. 41, pp. 797–828, Jan. 2012.
- [21] H. Gómez, M. K. Ram, F. Alvi, P. Villalba, E. Stefanakos, and A. Kumar, "Graphene-conducting polymer nanocomposite as novel electrode for supercapacitors," *J. Power Sources*, vol. 196, pp. 4102–4108, 2011.
- [22] F. Alvi, M. K. Ram, P. A. Basnayaka, E. Stefanakos, Y. Goswami, and A. Kumar, "Graphene–polyethylenedioxythiophene conducting polymer nanocomposite based supercapacitor," *Electrochimica Acta*, vol. 56, no. 25, pp. 9406–9412, 2011.
- [23] W. Zhang, B. Zhao, Z. He, X. Zhao, H. Wang, S. Yang, H. Wu, and Y. Cao, "High-Efficiency ITO-Free Polymer Solar Cells Using Highly Conductive PEDOT: PSS/Surfactant Bilayer Transparent Anodes," *Energy Env. Sci*, 2013.
- [24] J. G. Tait, B. J. Worfolk, S. A. Maloney, T. C. Hauger, A. L. Elias, J. M. Buriak, and K. D. Harris, "Spray coated high-conductivity PEDOT: PSS transparent electrodes for stretchable and mechanically-robust organic solar cells," *Sol. Energy Mater. Sol. Cells*, vol. 110, pp. 98–106, 2013.
- [25] M. Tahir, M. H. Sayyad, F. Wahab, and F. Aziz, "The electrical characterization of Ag/PTCDA/PEDOT: PSS/p-Si Schottky diode by current–voltage characteristics," *Phys. B Condens. Matter*, vol. 415, pp. 77–81, 2013.

- [26] J. Miller, "A brief history of supercapacitors," *Battery Energy Storage Technol.*, p. 61, 2007.
- [27] H. A. Andreas and B. E. Conway, "Examination of the double-layer capacitance of an high specific-area C-cloth electrode as titrated from acidic to alkaline pHs," *Electrochimica Acta*, vol. 51, no. 28, pp. 6510–6520, Sep. 2006.
- [28] R. Kötz and M. Carlen, "Principles and applications of electrochemical capacitors," *Electrochimica Acta*, vol. 45, pp. 2483–2498, 2000.
- [29] H. I. Becker, "Low voltage electrolytic capacitor," Jul. 1957.
- [30] P. Pattathil, N. Sivakumar, and T. S. Sonia, "Capacitor to Supercapacitor: An Introduction," *Nanostructured Ceram. Oxides Supercapacitor Appl.*, p. 1, 2014.
- [31] A. J. Bard and L. R. Faulkner, *Electrochemical methods: fundamentals and applications*, vol. 2. Wiley New York, 1980.
- [32] S. Peiffer, O. Klemm, K. Pecher, and R. Hollerung, "Redox measurements in aqueous solutions — A theoretical approach to data interpretation, based on electrode kinetics," *J. Contam. Hydrol.*, vol. 10, no. 1, pp. 1–18, Jun. 1992.
- [33] I. Grenthe, W. Stumm, M. Laaksoharju, A. C. Nilsson, and P. Wikberg, "Redox potentials and redox reactions in deep groundwater systems," *Chem. Geol.*, vol. 98, no. 1–2, pp. 131–150, Jul. 1992.
- [34] J. O. Bockris and A. K. Reddy, *Modern electrochemistry: an introduction to an interdisciplinary area*. Springer Science & Business Media, 2012.
- [35] J. Wang, *Analytical electrochemistry*. John Wiley & Sons, 2006.
- [36] S. Owerre and M. Paranjape, "Macroscopic quantum tunneling and quantum–classical phase transitions of the escape rate in large spin systems," *Phys. Rep.*, vol. 546, pp. 1–60, 2015.
- [37] S. K. Kulkarni, "Introduction to Quantum Mechanics," in *Nanotechnology: Principles and Practices*, Springer, 2015, pp. 1–29.
- [38] H. Chaluvadi, Z. N. Ozer, M. Dogan, C. Ning, J. Colgan, and D. Madison, "Observation of two-center interference effects for electron impact ionization of N₂," *J. Phys. B At. Mol. Opt. Phys.*, vol. 48, no. 15, p. 155203, 2015.
- [39] G. Muga, R. S. Mayato, and I. Egusquiza, *Time in quantum mechanics*, vol. 1. Springer Science & Business Media, 2007.
- [40] E. Schrödinger, "An undulatory theory of the mechanics of atoms and molecules," *Phys. Rev.*, vol. 28, no. 6, p. 1049, 1926.

- [41] B. E. Conway, *Electrochemical Supercapacitors-Scientific Fundamentals and Technological Applications*. New York: Kluwer Academic/Plenum Publishers, 1999.
- [42] B. E. Conway, "Transition from 'supercapacitor' to 'battery' behavior in electrochemical energy storage," *J. Electrochem. Soc.*, vol. 138, no. 6, pp. 1539–1548, 1991.
- [43] B. E. Conway, V. Birss, and J. Wojtowicz, "The role and utilization of pseudocapacitance for energy storage by supercapacitors," *J. Power Sources*, vol. 66, pp. 1–14, Jun. 1997.
- [44] X. Wang, C. Yan, J. Yan, A. Sumboja, and P. S. Lee, "Orthorhombic niobium oxide nanowires for next generation hybrid supercapacitor device," *Nano Energy*, vol. 11, no. 0, pp. 765–772, Jan. 2015.
- [45] H. Ji, X. Zhao, Z. Qiao, J. Jung, Y. Zhu, Y. Lu, L. L. Zhang, A. H. MacDonald, and R. S. Ruoff, "Capacitance of carbon-based electrical double-layer capacitors," *Nat Commun*, vol. 5, Feb. 2014.
- [46] E. Skúlason, "Modeling Electrochemical Reactions at the Solid-liquid Interface Using Density Functional Calculations," *Int. Conf. Comput. Sci. ICCS 2015 Comput. Sci. Gates Nat.*, vol. 51, no. 0, pp. 1887–1896, 2015.
- [47] G. Feng, G. Hu, R. Qiao, and N. R. Aluru, "Structure of the Electrical Double Layers: Insights from Continuum and Atomistic Simulations," *Comput. Bioeng.*, p. 327, 2015.
- [48] B. Giera, N. Henson, E. M. Kober, M. S. Shell, and T. M. Squires, "Electric Double-Layer Structure in Primitive Model Electrolytes: Comparing Molecular Dynamics with Local-Density Approximations," *Langmuir*, vol. 31, no. 11, pp. 3553–3562, 2015.
- [49] B. J. Akle, "Characterization and modeling of the ionomer-conductor interface in ionic polymer transducers," 2005.
- [50] A. Velikonja, V. Kralj-Iglič, and A. Iglič, "On Asymmetric Shape of Electric Double Layer Capacitance Curve," *Int J Electrochem Sci*, vol. 10, pp. 1–7, 2015.
- [51] S. Senthilkumar, K. V. Sankar, J. Melo, A. Gedanken, and R. K. Selvan, "Carbon-Based Hybrid Composites as Advanced Electrodes for Supercapacitors," *Adv. Funct. Mater.*, p. 399, 2015.
- [52] T. Tevi, H. Yaghoubi, J. Wang, and A. Takshi, "Application of poly (p-phenylene oxide) as blocking layer to reduce self-discharge in supercapacitors," *J. Power Sources*, vol. 241, pp. 589–596, 2013.
- [53] V. Augustyn, P. Simon, and B. Dunn, "Pseudocapacitive oxide materials for high-rate electrochemical energy storage," *Energy Environ. Sci.*, vol. 7, no. 5, pp. 1597–1614, 2014.

- [54] V. Augustyn, J. Come, M. A. Lowe, J. W. Kim, P.-L. Taberna, S. H. Tolbert, H. D. Abruña, P. Simon, and B. Dunn, “High-rate electrochemical energy storage through Li+ intercalation pseudocapacitance,” *Nat Mater*, vol. 12, no. 6, pp. 518–522, Jun. 2013.
- [55] C. Cheng and A. H. Ngan, “Reversible Electrochemical Actuation of Metallic Nanohoneycombs Induced by Pseudocapacitive Redox Processes,” *ACS Nano*, 2015.
- [56] J. S. Wang, *Pseudocapacitive Effects in Nanostructured Transition Metal Oxide Materials*. ProQuest, 2008.
- [57] P. A. Basnayaka, *Development of Nanostructured Graphene/Conducting Polymer Composite Materials for Supercapacitor Applications*. University of South Florida, 2013.
- [58] J. Oh, M. E. Kozlov, B. G. Kim, H.-K. Kim, R. H. Baughman, and Y. H. Hwang, “Preparation and electrochemical characterization of porous SWNT–PPy nanocomposite sheets for supercapacitor applications,” *Synth. Met.*, vol. 158, no. 15, pp. 638–641, Sep. 2008.
- [59] A. K. Sharma, Y. Sharma, R. Malhotra, and J. Sharma, “Solvent tuned PANI-CNT composites as advanced electrode materials for supercapacitor application,” *Adv. Mater. Lett.*, vol. 3, no. 2, pp. 82–86, 2012.
- [60] L. Hu, J. Tu, S. Jiao, J. Hou, H. Zhu, and D. J. Fray, “In situ electrochemical polymerization of a nanorod-PANI–Graphene composite in a reverse micelle electrolyte and its application in a supercapacitor,” *Phys. Chem. Chem. Phys.*, vol. 14, no. 45, pp. 15652–15656, 2012.
- [61] Q. Wu, Y. Xu, Z. Yao, A. Liu, and G. Shi, “Supercapacitors based on flexible graphene/polyaniline nanofiber composite films,” *ACS Nano*, vol. 4, no. 4, pp. 1963–1970, 2010.
- [62] K. Zhang, L. L. Zhang, X. Zhao, and J. Wu, “Graphene/polyaniline nanofiber composites as supercapacitor electrodes,” *Chem. Mater.*, vol. 22, no. 4, pp. 1392–1401, 2010.
- [63] H. Wang, Q. Hao, X. Yang, L. Lu, and X. Wang, “A nanostructured graphene/polyaniline hybrid material for supercapacitors,” *Nanoscale*, vol. 2, no. 10, pp. 2164–2170, 2010.
- [64] F. Alvi, M. K. Ram, P. A. Basnayaka, E. Stefanakos, Y. Goswami, and A. Kumar, “Graphene–polyethylenedioxythiophene conducting polymer nanocomposite based supercapacitor,” *Electrochimica Acta*, vol. 56, no. 25, pp. 9406–9412, 2011.
- [65] S. Bose, N. H. Kim, T. Kuila, K. Lau, and J. H. Lee, “Electrochemical performance of a graphene–polypyrrole nanocomposite as a supercapacitor electrode,” *Nanotechnology*, vol. 22, no. 29, p. 295202, 2011.

- [66] H.-H. Chang, C.-K. Chang, Y.-C. Tsai, and C.-S. Liao, "Electrochemically synthesized graphene/polypyrrole composites and their use in supercapacitor," *Carbon*, vol. 50, no. 6, pp. 2331–2336, 2012.
- [67] Z. Li, Y. Mi, X. Liu, S. Liu, S. Yang, and J. Wang, "Flexible graphene/MnO₂ composite papers for supercapacitor electrodes," *J. Mater. Chem.*, vol. 21, no. 38, pp. 14706–14711, 2011.
- [68] J. An, J. Liu, Y. Ma, R. Li, M. Li, M. Yu, and S. Li, "Fabrication of graphene/polypyrrole nanotube/MnO₂ nanotube composite and its supercapacitor application," *Eur. Phys. J. Appl. Phys.*, vol. 58, no. 03, p. 30403, 2012.
- [69] D. Pech, M. Brunet, H. Durou, P. Huang, V. Mochalin, Y. Gogotsi, P.-L. Taberna, and P. Simon, "Ultrahigh-power micrometre-sized supercapacitors based on onion-like carbon," *Nat Nano*, vol. 5, no. 9, pp. 651–654, Sep. 2010.
- [70] X. Feng, *Nanocarbons for Advanced Energy Storage*, vol. 1. John Wiley & Sons, 2015.
- [71] A. Chu and P. Braatz, "Comparison of commercial supercapacitors and high-power lithium-ion batteries for power-assist applications in hybrid electric vehicles I. Initial characterization," *J. Power Sources*, vol. 112, pp. 236–246, Oct. 2002.
- [72] F. Scholz, U. Schröder, R. Gulaboski, and A. Doménech-Carbó, "Earlier Developed Techniques," in *Electrochemistry of Immobilized Particles and Droplets*, Springer, 2015, pp. 1–10.
- [73] W. Vielstich, "Cyclic voltammetry," in *Handbook of Fuel Cells*, John Wiley & Sons, Ltd, 2010.
- [74] T. Tevi, S. W. Saint Birch, S. W. Thomas, and A. Takshi, "Effect of Triton X-100 on the double layer capacitance and conductivity of poly (3, 4-ethylenedioxythiophene): poly (styrenesulfonate)(PEDOT: PSS) films," *Synth. Met.*, vol. 191, pp. 59–65, 2014.
- [75] S. Roldan, D. Barreda, M. Granda, R. Menendez, R. Santamaria, and C. Blanco, "An approach to classification and capacitance expressions in electrochemical capacitors technology," *Phys. Chem. Chem. Phys.*, vol. 17, no. 2, pp. 1084–1092, 2015.
- [76] V. S. Bagotsky, *Fundamentals of electrochemistry*, vol. 44. John Wiley & Sons, 2005.
- [77] S.-I. Pyun, H.-C. Shin, J.-W. Lee, and J.-Y. Go, *Electrochemistry of Insertion Materials for Hydrogen and Lithium*. Springer Science & Business Media, 2012.
- [78] P. J. Lingane and D. G. Peters, "Chronopotentiometry," *C R C Crit. Rev. Anal. Chem.*, vol. 1, no. 4, pp. 587–634, Jan. 1971.
- [79] M. E. Orazem and B. Tribollet, *Electrochemical impedance spectroscopy*, vol. 48. John Wiley & Sons, 2011.

- [80] A. ter Heijne, O. Schaetzle, S. Gimenez, L. Navarro, B. Hamelers, and F. Fabregat-Santiago, "Analysis of bio-anode performance through electrochemical impedance spectroscopy," *Bioelectrochemistry*, no. 0.
- [81] E. Taer, M. Deraman, I. Talib, R. Farma, M. Ishak, R. Omar, B. Dolah, N. Basri, M. Othman, and S. Kanwal, "Impedance spectroscopic analysis of composite electrode from activated carbon/conductive materials/ruthenium oxide for supercapacitor applications," presented at the THE 5TH ASIAN PHYSICS SYMPOSIUM (APS 2012), 2015, vol. 1656, p. 030004.
- [82] J. Goldstein, D. E. Newbury, P. Echlin, D. C. Joy, A. D. Romig Jr, C. E. Lyman, C. Fiori, and E. Lifshin, *Scanning electron microscopy and X-ray microanalysis: a text for biologists, materials scientists, and geologists*. Springer Science & Business Media, 2012.
- [83] G. Binnig, C. F. Quate, and C. Gerber, "Atomic Force Microscope," *Phys. Rev. Lett.*, vol. 56, no. 9, pp. 930–933, Mar. 1986.
- [84] I Miccoli and F Edler and H Pfnür and C Tegenkamp, "The 100th anniversary of the four-point probe technique: the role of probe geometries in isotropic and anisotropic systems," *J. Phys. Condens. Matter*, vol. 27, no. 22, p. 223201, 2015.
- [85] P. Simon and Y. Gogotsi, "Materials for electrochemical capacitors," *Nat. Mater.*, vol. 7, pp. 845–54, Nov. 2008.
- [86] A. Burke, "Ultracapacitors: why, how, and where is the technology," *J. Power Sources*, vol. 91, no. 1, pp. 37–50, Nov. 2000.
- [87] G. Park, T. Rosing, M. Todd, C. Farrar, and W. Hodgkiss, "Energy Harvesting for Structural Health Monitoring Sensor Networks," *J. Infrastruct. Syst.*, vol. 14, no. 1, pp. 64–79, Mar. 2008.
- [88] Xiaofan Jiang, J. Polastre, and D. Culler, "Perpetual environmentally powered sensor networks," in *Information Processing in Sensor Networks, 2005. IPSN 2005. Fourth International Symposium on*, 2005, pp. 463–468.
- [89] V. V. N. Obreja, "On the performance of supercapacitors with electrodes based on carbon nanotubes and carbon activated material—A review," *Proc. E-MRS 2007 Symp. M Electron Transp. Low-Dimens. Carbon Struct. Sci. Technol. Nanotub. Nanowires*, vol. 40, no. 7, pp. 2596–2605, May 2008.
- [90] V. C. Gungor and G. P. Hancke, "Industrial Wireless Sensor Networks: Challenges, Design Principles, and Technical Approaches," *Ind. Electron. IEEE Trans. On*, vol. 56, no. 10, pp. 4258–4265, Oct. 2009.
- [91] H. Yang and Y. Zhang, "Self-discharge analysis and characterization of supercapacitors for environmentally powered wireless sensor network applications," *J. Power Sources*, vol. 196, pp. 8866–8873, 2011.

- [92] F. Belhachemi, S. Rael, and B. Davat, "A physical based model of power electric double-layer supercapacitors," in *Industry Applications Conference, 2000. Conference Record of the 2000 IEEE*, 2000, vol. 5, pp. 3069–3076 vol.5.
- [93] D. Petreus, D. Moga, R. Galatus, and R. A. Munteanu, "Modeling and sizing of supercapacitors," *Adv. Electr. Comput. Eng.*, vol. 8, no. 2, pp. 15–22, 2008.
- [94] Y. Diab, P. Venet, H. Gualous, and G. Rojat, "Self-Discharge Characterization and Modeling of Electrochemical Capacitor Used for Power Electronics Applications," *Ieee Trans. Power Electron.*, vol. 24, pp. 510–517, Feb. 2009.
- [95] J. Niu, B. E. Conway, and W. G. Pell, "Comparative studies of self-discharge by potential decay and float-current measurements at C double-layer capacitor and battery electrodes," *J. Power Sources*, vol. 135, pp. 332–343, 2004.
- [96] B. E. Conway, W. G. Pell, and T. C. Liu, "Diagnostic analyses for mechanisms of self-discharge of electrochemical capacitors and batteries," *J. Power Sources*, vol. 65, pp. 53–59, Apr. 1997.
- [97] CAP-XX, *Application Note AN1005 Rev 2.2, Simple Measurement of Supercapacitor Parameters*. 2009.
- [98] *How Supercapacitors Solve LED Flash Power Issues in High Res Camera Phones*, *EE Times Design*. .
- [99] G. Injeti, B. Leo, "Science and Technology of Advanced Materials," 2008, vol. 9, p. 043001.
- [100] R. L. McCarley, E. A. Irene, and R. W. Murray, "Permeant molecular sieving with electrochemically prepared 6-nm films of poly(phenylene oxide)," *J. Phys. Chem.*, vol. 95, no. 6, pp. 2492–2498, Mar. 1991.
- [101] C. P. Rhodes, J. W. Long, M. S. Doescher, J. J. Fontanella, and D. R. Rolison, "Nanoscale Polymer Electrolytes: Ultrathin Electrodeposited Poly(Phenylene Oxide) with Solid-State Ionic Conductivity," *J. Phys. Chem. B*, vol. 108, no. 35, pp. 13079–13087, Sep. 2004.
- [102] C. P. Rhodes, J. W. Long, M. S. Doescher, B. M. Dening, and D. R. Rolison, "Charge insertion into hybrid nanoarchitectures: mesoporous manganese oxide coated with ultrathin poly(phenylene oxide)," *Aerogels 7 Proc. 7th Int. Symp. Aerogels 7th Int. Symp. Aerogels*, vol. 350, no. 0, pp. 73–79, Dec. 2004.
- [103] H. L. Jason Kanga, "Electrodeposition of Poly(phenylene oxide) Nanoscale Patterns with Nanosphere Lithography," 2009.
- [104] M. Paunovic and M. Schlesinger, *Fundamentals of electrochemical deposition*, vol. 45. john wiley & sons, 2006.

- [105] D. Ionescu and I. Ciobanu, "Study in microwave range of some HF board materials for lead-free technologies," *Romanian Rep. Phys.*, vol. 61, no. 4, pp. 676–688, 2009.
- [106] A. Izadi-Najafabadi, "Carbon nanotube and polypyrrole supercapacitors," 2006.
- [107] "FreedomCAR Ultracapacitor Test Manual." .
- [108] I. Hadjipaschalis, A. Poullikkas, and V. Efthimiou, "Overview of current and future energy storage technologies for electric power applications," *Renew. Sustain. Energy Rev.*, vol. 13, no. 6–7, pp. 1513–1522, Aug. 2009.
- [109] C. T. Goh and A. Cruden, "Automated high current cycling test system for supercapacitor characterisation," presented at the Power Electronics, Electrical Drives, Automation and Motion (SPEEDAM), 2012 International Symposium on, 2012, pp. 748–753.
- [110] J. R. Miller and P. Simon, "Electrochemical capacitors for energy management," *Sci. Mag.*, vol. 321, pp. 651–652, 2008.
- [111] K. Jost, L. Haverhals, D. Durkin, J. McDonough, C. R. Perez, C. Hugh, P. C. Trulove, G. Dion, and Y. Gogotsi, "Knitted electrochemical capacitors for applications in smart garments," presented at the 224th ECS Meeting (October 27–November 1, 2013), 2013.
- [112] C. Lecoeur, B. Daffos, R. Lin, L. Divay, P. Le Barny, M. P. Thi, P.-L. Taberna, and P. Simon, "Self-standing electrochemical double layer capacitors for operation in severe temperature conditions," *Mater. Renew. Sustain. Energy*, vol. 2, no. 2, pp. 1–7, Apr. 2013.
- [113] H. Ebrahimi, H. Yaghoubi, F. Giammattei, and A. Takshi, "Electrochemical Detection of Piezoelectric Effect from Misaligned Zinc Oxide Nanowires Grown on a Flexible Electrode," *Electrochimica Acta*, vol. 134, pp. 435–441, 2014.
- [114] W. Lee and H. Cha, "A supercapacitor remaining energy control method for smoothing a fluctuating renewable energy power," presented at the ECCE Asia Downunder (ECCE Asia), 2013 IEEE, 2013, pp. 398–403.
- [115] G. L. Park, A. I. Schäfer, and B. S. Richards, "Renewable energy-powered membrane technology: Supercapacitors for buffering resource fluctuations in a wind-powered membrane system for brackish water desalination," *Renew. Energy*, vol. 50, pp. 126–135, 2013.
- [116] T. Tevi and A. Takshi, "Modeling and simulation study of the self-discharge in supercapacitors in presence of a blocking layer," *J. Power Sources*, vol. 273, pp. 857–862, 2015.
- [117] J. Black and H. A. Andreas, "Effects of charge redistribution on self-discharge of electrochemical capacitors," *Electrochimica Acta*, vol. 54, pp. 3568–3574, May 2009.

- [118] J. Black and H. A. Andreas, "Prediction of the self-discharge profile of an electrochemical capacitor electrode in the presence of both activation-controlled discharge and charge redistribution," *J. Power Sources*, vol. 195, pp. 929–935, Feb. 2010.
- [119] T. M. Nahir, R. A. Clark, and E. F. Bowden, "Linear-Sweep Voltammetry of Irreversible Electron Transfer in Surface-Confined Species Using the Marcus Theory," *Anal. Chem.*, vol. 66, pp. 2595–2598, Aug. 1994.
- [120] S. Brankovic and K. Rajeshwar, "Electrodeposition for Energy Applications," 2008.
- [121] D. A. Barry, J. Y. Parlange, and L. Li, "Approximation for the exponential integral (Theis well function)," *J. Hydrol.*, vol. 227, pp. 287–291, 2000.
- [122] H. Dette, I. M. Lopez, I. M. Ortiz Rodriguez, and A. Pepelyshev, "Maximin efficient design of experiment for exponential regression models," *J. Stat. Plan. Inference*, vol. 136, pp. 4397–4418, 2006.
- [123] J. Grimshaw, *Electrochemical reactions and mechanisms in organic chemistry*. Elsevier, 2000.
- [124] E. Katz, N. Itzhak, and I. Willner, "Electron transfer in self-assembled monolayers of N-methyl-N'-carboxyalkyl-4, 4'-bipyridinium linked to gold electrodes," *Langmuir*, vol. 9, pp. 1392–1396, 1993.
- [125] H. O. Finklea, S. Avery, M. Lynch, and T. Furtch, "Blocking oriented monolayers of alkyl mercaptans on gold electrodes," *Langmuir*, vol. 3, pp. 409–413, 1987.
- [126] Xu, H. Li, and Y. Zhang, "Relationship between electronic tunneling coefficient and electrode potential investigated by using self-assembled alkanethiol monolayers on gold electrodes," *J. Phys. Chem.*, vol. 97, pp. 11497–11500, 1993.
- [127] L. F. Shampine and M. K. Gordon, *Computer solution of ordinary differential equations: the initial value problem*. WH Freeman San Francisco, 1975.
- [128] R. Garrappa, "On some explicit Adams multistep methods for fractional differential equations," *J. Comput. Appl. Math.*, vol. 229, pp. 392–399, 2009.
- [129] A. Rios Neto and K. Rama Rao, "A stochastic approach to global error estimation in ODE multistep numerical integration," *J. Comput. Appl. Math.*, vol. 30, pp. 257–281, 1990.
- [130] H. Chen, T. N. Cong, W. Yang, C. Tan, Y. Li, and Y. Ding, "Progress in electrical energy storage system: A critical review," *Prog. Nat. Sci.*, vol. 19, no. 3, pp. 291–312, Mar. 2009.
- [131] F. I. Simjee and P. H. Chou, "Efficient Charging of Supercapacitors for Extended Lifetime of Wireless Sensor Nodes," *Power Electron. IEEE Trans. On*, vol. 23, no. 3, pp. 1526–1536, May 2008.

- [132] B. E. Conway and W. G. Pell, "Double-layer and pseudocapacitance types of electrochemical capacitors and their applications to the development of hybrid devices," *J. Solid State Electrochem.*, vol. 7, no. 9, pp. 637–644, Sep. 2003.
- [133] G. A. Snook, P. Kao, and A. S. Best, "Conducting-polymer-based supercapacitor devices and electrodes," *J. Power Sources*, vol. 196, pp. 1–12, 2011.
- [134] S. K. M. Jönsson, J. Birgerson, X. Crispin, G. Greczynski, W. Osikowicz, A. W. Denier Van Der Gon, W. R. Salaneck, and M. Fahlman, "The effects of solvents on the morphology and sheet resistance in poly (3, 4-ethylenedioxythiophene)–polystyrenesulfonic acid (PEDOT–PSS) films," *Synth. Met.*, vol. 139, pp. 1–10, 2003.
- [135] C. Mid-Eum and S. Seung-Woo, "Robust energy management of a battery/supercapacitor Hybrid Energy Storage System in an electric vehicle," presented at the Electric Vehicle Conference (IEVC), 2012 IEEE International, 2012, pp. 1–5.
- [136] D. S. Yoo, A. Mahmoudzadeh, E. C. W. Fok, K. Walus, and J. D. W. Madden, "Multiple time constant modelling of a printed conducting polymer electrode," *Electrochimica Acta*, vol. 56, no. 13, pp. 4711–4716, May 2011.
- [137] P. Wilson, C. Lekakou, and J. F. Watts, "A comparative assessment of surface microstructure and electrical conductivity dependence on co-solvent addition in spin coated and inkjet printed poly (3, 4-ethylenedioxythiophene): polystyrene sulphonate (PEDOT: PSS)," *Org. Electron.*, vol. 13, no. 3, pp. 409–418, 2012.
- [138] T. Elze and T. G. Tanner, "Temporal properties of liquid crystal displays: Implications for vision science experiments," *PloS One*, vol. 7, no. 9, p. e44048, 2012.
- [139] T. A. Skotheim and J. Reynolds, *Conjugated polymers: processing and applications*, vol. 2. CRC, 2006.
- [140] X. Crispin, F. L. E. Jakobsson, A. Crispin, P. C. M. Grim, P. Andersson, A. Volodin, C. Van Haesendonck, M. Van der Auweraer, W. R. Salaneck, and M. Berggren, "The origin of the high conductivity of poly (3, 4-ethylenedioxythiophene)-poly (styrenesulfonate)(PEDOT-PSS) plastic electrodes," *Chem. Mater.*, vol. 18, pp. 4354–4360, 2006.
- [141] D. Gupta, M. M. Wienk, and R. A. Janssen, "Efficient Polymer Solar Cells on Opaque Substrates with a Laminated PEDOT: PSS Top Electrode," *Adv. Energy Mater.*, 2013.
- [142] C. H. Manathunga and V. P. S. Perera, "Quasi-solid State Dye Sensitized Solar Cells Constructed using PEDOT: PSS as the Hole Conductor," presented at the Proceedings of Technical Sessions, 2013, vol. 29, pp. 23–27.
- [143] M. Sessolo, D. Tordera, and H. J. Bolink, "Ionic Iridium Complex and Conjugated Polymer Used To Solution-Process a Bilayer White Light-Emitting Diode," *ACS Appl. Mater. Interfaces*, vol. 5, no. 3, pp. 630–634, Feb. 2013.

- [144] M. E. Plonska-Brzezinska, M. Lewandowski, M. Błaszcyk, A. Molina-Ontoria, T. Luciński, and L. Echegoyen, "Preparation and Characterization of Carbon Nano-Onion/PEDOT:PSS Composites," *ChemPhysChem*, vol. 13, no. 18, pp. 4134–4141, Dec. 2012.
- [145] A. K. Cuentas Gallegos and M. E. Rincón, "Carbon nanofiber and PEDOT-PSS bilayer systems as electrodes for symmetric and asymmetric electrochemical capacitor cells," *J. Power Sources*, vol. 162, pp. 743–747, 2006.
- [146] P. Park, "Application of nano-structured conducting polymers to humidity sensing," 2008.
- [147] Y. H. Kim, C. Sachse, M. L. Machala, C. May, L. Muller-Meskamp, and K. Leo, "Highly Conductive PEDOT:PSS Electrode with Optimized Solvent and Thermal Post-Treatment for ITO-Free Organic Solar Cells," *Adv. Funct. Mater.*, vol. 21, pp. 1076–1081, Mar. 2011.
- [148] S. Timpanaro, M. Kemerink, F. J. Touwslager, M. M. De Kok, and S. Schrader, "Morphology and conductivity of PEDOT/PSS films studied by scanning–tunneling microscopy," *Chem. Phys. Lett.*, vol. 394, pp. 339–343, 2004.
- [149] G. M. Suppes, B. A. Deore, and M. S. Freund, "Porous Conducting Polymer/Heteropolyoxometalate Hybrid Material for Electrochemical Supercapacitor Applications," *Langmuir*, vol. 24, pp. 1064–1069, Feb. 2008.
- [150] M. Vosgueritchian, D. J. Lipomi, and Z. Bao, "Highly Conductive and Transparent PEDOT:PSS Films with a Fluorosurfactant for Stretchable and Flexible Transparent Electrodes," *Adv. Funct. Mater.*, vol. 22, pp. 421–428, 2012.
- [151] J. Y. Kim, J. H. Jung, D. E. Lee, and J. Joo, "Enhancement of electrical conductivity of poly(3,4-ethylenedioxythiophene)/poly(4-styrenesulfonate) by a change of solvents," *Synth. Met.*, vol. 126, no. 2–3, pp. 311–316, Feb. 2002.
- [152] J. S. Choi, J.-H. Yim, D.-W. Kim, J.-K. Jeon, Y. S. Ko, and Y. Kim, "Effects of various imidazole-based weak bases and surfactant on the conductivity and transparency of poly(3,4-ethylenedioxythiophene) films," *Synth. Met.*, vol. 159, pp. 2506–2511, 2009.
- [153] K. Fic, G. Lota, and E. Frackowiak, "Electrochemical properties of supercapacitors operating in aqueous electrolyte with surfactants," *Electrochimica Acta*, vol. 55, pp. 7484–7488, 30 2010.
- [154] D. S. Yoo, "Fabrication and modelling of an all-printed PEDOT: PSS supercapacitor on a commercial paper," 2010.
- [155] A. J. Bard and L. R. Faulkner, *Electrochemical Methods: Fundamentals and Applications, 2nd Edition*. Wiley New York, 2001.
- [156] Z. Kerner and T. Pajkossy, "Impedance of rough capacitive electrodes: the role of surface disorder," *J. Electroanal. Chem.*, vol. 448, pp. 139–142, 1998.

- [157] J. B. Bates and Y. T. Chu, "Surface topography and electrical response of metal-electrolyte interfaces," *Solid State Ion.*, vol. 28–30, Part 2, pp. 1388–1395, 1988.
- [158] G. J. Brug, A. L. G. van den Eeden, M. Sluyters-Rehbach, and J. H. Sluyters, "The analysis of electrode impedances complicated by the presence of a constant phase element," *J. Electroanal. Chem. Interfacial Electrochem.*, vol. 176, pp. 275–295, 1984.
- [159] C. Lei, P. Wilson, and C. Lekakou, "Effect of poly (3, 4-ethylenedioxythiophene)(PEDOT) in carbon-based composite electrodes for electrochemical supercapacitors," *J. Power Sources*, vol. 196, no. 18, pp. 7823–7827, 2011.
- [160] B. Yoo, A. Dodabalapur, D. C. Lee, T. Hanrath, and B. A. Korgel, "Germanium nanowire transistors with ethylene glycol treated poly (3, 4-ethylenedioxythiophene): poly (styrene sulfonate) contacts," *Appl. Phys. Lett.*, vol. 90, pp. 072106–072106–3, 2007.
- [161] B. Xu, F. Wu, R. Chen, G. Cao, S. Chen, G. Wang, and Y. Yang, "Room temperature molten salt as electrolyte for carbon nanotube-based electric double layer capacitors," *J. Power Sources*, vol. 158, pp. 773–778, 2006.
- [162] S. Ghosh and O. Inganäs, "Conducting polymer hydrogels as 3D electrodes: applications for supercapacitors," *Adv. Mater.*, vol. 11, no. 14, pp. 1214–1218, 1999.
- [163] G. L. Bullard, H. B. Sierra-Alcazar, H. L. Lee, and J. L. Morris, "Operating principles of the ultracapacitor," *Magn. IEEE Trans. On*, vol. 25, pp. 102–106, 1989.
- [164] R. A. Messenger and J. Ventre, *Photovoltaic systems engineering*. CRC press, 2003.
- [165] L. M. Fraas and L. D. Partain, *Solar cells and their applications*, vol. 236. John Wiley & Sons, 2010.
- [166] C.-Y. Hsu, H.-W. Chen, K.-M. Lee, C.-W. Hu, and K.-C. Ho, "A dye-sensitized photo-supercapacitor based on PProDOT-Et₂ thick films," *Sel. Pap. Present. 4th Int. Conf. Polym. Batter. Fuel Cells*, vol. 195, no. 18, pp. 6232–6238, Sep. 2010.
- [167] P. Liu, H. X. Yang, X. P. Ai, G. R. Li, and X. P. Gao, "A solar rechargeable battery based on polymeric charge storage electrodes," *Electrochem. Commun.*, vol. 16, no. 1, pp. 69–72, Mar. 2012.
- [168] T. Miyasaka, H. Ina, and M. Ikegami, "Dye-sensitized photocapacitors fabricated with ionic liquid electrolytes for power generation and storage," presented at the Meeting Abstracts, 2012, pp. 2864–2864.
- [169] H. Nagai and H. Segawa, "Energy-storable dye-sensitized solar cell with a polypyrrole electrode," *Chem. Commun.*, no. 8, pp. 974–975, 2004.

- [170] Y. Saito, A. Ogawa, S. Uchida, T. Kubo, and H. Segawa, "Energy-storable Dye-sensitized Solar Cells with Interdigitated Nafion/Polypyrrole-Pt Comb-like Electrodes," *Chem. Lett.*, vol. 39, no. 5, pp. 488–489, 2010.
- [171] M. Skunik-Nuckowska, K. Grzejszczyk, P. J. Kulesza, L. Yang, N. Vlachopoulos, L. Häggman, E. Johansson, and A. Hagfeldt, "Integration of solid-state dye-sensitized solar cell with metal oxide charge storage material into photoelectrochemical capacitor," *J. Power Sources*, vol. 234, no. 0, pp. 91–99, Jul. 2013.
- [172] P. A. Mini, S. V. Nair, and K. R. V. Subramanian, "Design and development of an integrated device consisting of an independent solar cell with electrical storage capacity," *Prog. Photovolt. Res. Appl.*, vol. 21, no. 5, pp. 1153–1157, Aug. 2013.
- [173] X. Zhang, X. Huang, C. Li, and H. Jiang, "Dye-Sensitized Solar Cell with Energy Storage Function through PVDF/ZnO Nanocomposite Counter Electrode," *Adv. Mater.*, vol. 25, no. 30, pp. 4093–4096, 2013.
- [174] X. Huang, X. Zhang, and H. Jiang, "Energy storage via polyvinylidene fluoride dielectric on the counterelectrode of dye-sensitized solar cells," *J. Power Sources*, vol. 248, no. 0, pp. 434–438, Feb. 2014.
- [175] J. Bae, Y. J. Park, M. Lee, S. N. Cha, Y. J. Choi, C. S. Lee, J. M. Kim, and Z. L. Wang, "Single-Fiber-Based Hybridization of Energy Converters and Storage Units Using Graphene as Electrodes," *Adv. Mater.*, vol. 23, no. 30, pp. 3446–3449, Aug. 2011.
- [176] W. Guo, X. Xue, S. Wang, C. Lin, and Z. L. Wang, "An Integrated Power Pack of Dye-Sensitized Solar Cell and Li Battery Based on Double-Sided TiO₂ Nanotube Arrays," *Nano Lett.*, vol. 12, no. 5, pp. 2520–2523, May 2012.
- [177] P. Liu, Y. Cao, G. Li, X. Gao, X. Ai, and H. Yang, "A Solar Rechargeable Flow Battery Based on Photoregeneration of Two Soluble Redox Couples," *ChemSusChem*, vol. 6, no. 5, pp. 802–806, 2013.
- [178] Y. Saito, S. Uchida, T. Kubo, and H. Segawa, "Surface-oxidized tungsten for energy-storable dye-sensitized solar cells," *Thin Solid Films*, vol. 518, no. 11, pp. 3033–3036, 2010.
- [179] A. Takshi, H. Yaghoubi, T. Tevi, and S. Bakhshi, "Photoactive supercapacitors for solar energy harvesting and storage," *J. Power Sources*, vol. 275, pp. 621–626, 2015.
- [180] W. Albery and M. Archer, "Photogalvanic Cells II. Current-Voltage and Power Characteristics," *J. Electrochem. Soc.*, vol. 124, no. 5, pp. 688–697, 1977.
- [181] W. J. Albery, "Development of photogalvanic cells for solar energy conservation," *Acc. Chem. Res.*, vol. 15, no. 5, pp. 142–148, May 1982.

- [182] G. Chen, J. M. Zen, F. R. F. Fan, and A. J. Bard, "Electrochemical investigation of the energetics of irradiated FeS₂ (pyrite) particles," *J. Phys. Chem.*, vol. 95, no. 9, pp. 3682–3687, 1991.
- [183] W. J. Albery and M. D. Archer, "Optimum efficiency of photogalvanic cells for solar energy conversion," *Nature*, vol. 270, no. 5636, pp. 399–402, Dec. 1977.
- [184] A. Laforgue, P. Simon, J. Fauvarque, M. Mastragostino, F. Soavi, J. Sarrau, P. Lailler, M. Conte, E. Rossi, and S. Saguatti, "Activated carbon/conducting polymer hybrid supercapacitors," *J. Electrochem. Soc.*, vol. 150, no. 5, pp. A645–A651, 2003.
- [185] C. C. Wamser, H.-S. Kim, and J.-K. Lee, "Solar cells with porphyrin sensitization," *Opt. Mater.*, vol. 21, no. 1–3, pp. 221–224, Jan. 2003.
- [186] M. Grätzel, "Dye-sensitized solar cells," *J. Photochem. Photobiol. C Photochem. Rev.*, vol. 4, no. 2, pp. 145–153, Oct. 2003.
- [187] J. T. Mefford, W. G. Hardin, S. Dai, K. P. Johnston, and K. J. Stevenson, "Anion charge storage through oxygen intercalation in LaMnO₃ perovskite pseudocapacitor electrodes," *Nat. Mater.*, vol. 13, no. 7, pp. 726–732, 2014.
- [188] M. R. Warren and J. D. Madden, "Electrochemical switching of conducting polymers: A variable resistance transmission line model," *J. Electroanal. Chem.*, vol. 590, no. 1, pp. 76–81, May 2006.
- [189] T. Brown, J. Kim, R. Friend, F. Cacialli, R. Daik, and W. Feast, "Built-in field electroabsorption spectroscopy of polymer light-emitting diodes incorporating a doped poly (3, 4-ethylene dioxythiophene) hole injection layer," *Appl. Phys. Lett.*, vol. 75, no. 12, pp. 1679–1681, 1999.
- [190] K. Nagamatsu, S. Avasthi, J. Jhaveri, and J. C. Sturm, "A 12% efficient silicon/PEDOT: PSS heterojunction solar cell fabricated at < 100 C," *Photovolt. IEEE J. Of*, vol. 4, no. 1, pp. 260–264, 2014.
- [191] K. K. Cline, M. T. McDermott, and R. L. McCreery, "Anomalously Slow Electron Transfer at Ordered Graphite Electrodes: Influence of Electronic Factors and Reactive Sites," *J. Phys. Chem.*, vol. 98, no. 20, pp. 5314–5319, May 1994.
- [192] S. M. Khan, M. Kaur, J. R. Heflin, and M. H. Sayyad, "Fabrication and characterization of ZnTPP:PCBM bulk heterojunction (BHJ) solar cells," *J. Phys. Chem. Solids*, vol. 72, no. 12, pp. 1430–1435, Dec. 2011.
- [193] M. Shiraishi and M. Ata, "Work function of carbon nanotubes," *Carbon*, vol. 39, no. 12, pp. 1913–1917, Oct. 2001.

- [194] T. Funaki, H. Funakoshi, O. Kitao, N. Onozawa-Komatsuzaki, K. Kasuga, K. Sayama, and H. Sugihara, "Cyclometalated Ruthenium(II) Complexes as Near-IR Sensitizers for High Efficiency Dye-Sensitized Solar Cells," *Angew. Chem. Int. Ed.*, vol. 51, no. 30, pp. 7528–7531, Jul. 2012.

APPENDIX A: COPYRIGHT PERMISSIONS

Below is permission for the use of material in Chapter 4.

ELSEVIER LICENSE TERMS AND CONDITIONS

Jun 29, 2015

This is an Agreement between Tete Tevi ("You") and Elsevier ("Elsevier"). It consists of your order details, the terms and conditions provided by Elsevier, and the payment terms and conditions.

All payments must be made in full to CCC. For payment instructions, please see information listed at the bottom of this form.

Supplier	Elsevier Limited The Boulevard, Langford Lane Kidlington, Oxford, OX5 1GB, UK
Registered Company Number	1982084
Customer name	Tete Tevi
Customer address	2208 Fitness club Way Apt 201 TAMPA, FL 33612
License number	3658290344892
License date	Jun 29, 2015
Licensed content publisher	Elsevier
Licensed content publication	Journal of Power Sources
Licensed content title	Application of poly (p-phenylene oxide) as blocking layer to reduce self-discharge in supercapacitors
Licensed content author	Tete Tevi, Houman Yaghoubi, Jing Wang, Arash Takshi
Licensed content date	1 November 2013
Licensed content volume number	241
Licensed content issue number	n/a
Number of pages	8
Start Page	589
End Page	596
Type of Use	reuse in a thesis/dissertation
Portion	full article
Format	both print and electronic
Are you the author of this Elsevier article?	Yes
Will you be translating?	No
Title of your thesis/dissertation	Enhancement of Supercapacitor Energy Storage by Leakage Reduction and Electrode Modification
Expected completion date	Aug 2015
Estimated size (number of pages)	100
Elsevier VAT number	GB 494 6272 12
Price	0.00 USD
VAT/Local Sales Tax	0.00 USD / 0.00 GBP

Below is permission for the use of material in Chapter 5.

ELSEVIER LICENSE TERMS AND CONDITIONS

Jun 29, 2015

This is an Agreement between Tete Tevi ("You") and Elsevier ("Elsevier"). It consists of your order details, the terms and conditions provided by Elsevier, and the payment terms and conditions.

All payments must be made in full to CCC. For payment instructions, please see information listed at the bottom of this form.

Supplier	Elsevier Limited The Boulevard, Langford Lane Kidlington, Oxford, OX5 1GB, UK
Registered Company Number	1982084
Customer name	Tete Tevi
Customer address	2208 Fitness club Way Apt 201 TAMPA, FL 33612
License number	3658290461578
License date	Jun 29, 2015
Licensed content publisher	Elsevier
Licensed content publication	Journal of Power Sources
Licensed content title	Modeling and simulation study of the self-discharge in supercapacitors in presence of a blocking layer
Licensed content author	Tete Tevi, Arash Takshi
Licensed content date	1 January 2015
Licensed content volume number	273
Licensed content issue number	n/a
Number of pages	6
Start Page	857
End Page	862
Type of Use	reuse in a thesis/dissertation
Intended publisher of new work	other
Portion	full article
Format	both print and electronic
Are you the author of this Elsevier article?	Yes
Will you be translating?	No
Title of your thesis/dissertation	Enhancement of Supercapacitor Energy Storage by Leakage Reduction and Electrode Modification
Expected completion date	Aug 2015
Estimated size (number of pages)	100
Elsevier VAT number	GB 494 6272 12

Below is permission for the use of material in Chapter 6.

ELSEVIER LICENSE TERMS AND CONDITIONS

Jul 21, 2015

This is an Agreement between Tete Tevi ("You") and Elsevier ("Elsevier"). It consists of your order details, the terms and conditions provided by Elsevier, and the payment terms and conditions.

All payments must be made in full to CCC. For payment instructions, please see information listed at the bottom of this form.

Supplier	Elsevier Limited The Boulevard, Langford Lane Kidlington, Oxford, OX5 1GB, UK
Registered Company Number	1982084
Customer name	Tete Tevi
Customer address	2208 Fitness club Way Apt 201 TAMPA, FL 33612
License number	3658840222793
License date	Jun 29, 2015
Licensed content publisher	Elsevier
Licensed content publication	Synthetic Metals
Licensed content title	Effect of Triton X-100 on the double layer capacitance and conductivity of poly(3,4-ethylenedioxythiophene):poly(styrenesulfonate) (PEDOT:PSS) films
Licensed content author	Tete Tevi, Shantonio W. Saint Birch, Sylvia W. Thomas, Arash Takshi
Licensed content date	May 2014
Licensed content volume number	191
Licensed content issue number	n/a
Number of pages	7
Start Page	59
End Page	65
Type of Use	reuse in a thesis/dissertation
Intended publisher of new work	other
Portion	full article
Format	both print and electronic
Are you the author of this Elsevier article?	Yes
Will you be translating?	No
Title of your thesis/dissertation	Enhancement of Supercapacitor Energy Storage by Leakage Reduction and Electrode Modification
Expected completion date	Aug 2015
Estimated size (number of pages)	
Elsevier VAT number	GB 494 6272 12

Below is permission for the use of material in Chapter 7.

ELSEVIER LICENSE TERMS AND CONDITIONS

Jul 21, 2015

This is an Agreement between Tete Tevi ("You") and Elsevier ("Elsevier"). It consists of your order details, the terms and conditions provided by Elsevier, and the payment terms and conditions.

All payments must be made in full to CCC. For payment instructions, please see information listed at the bottom of this form.

Supplier	Elsevier Limited The Boulevard, Langford Lane Kidlington, Oxford, OX5 1GB, UK
Registered Company Number	1982084
Customer name	Tete Tevi
Customer address	2208 Fitness club Way Apt 201 TAMPA, FL 33612
License number	3660830836152
License date	Jul 02, 2015
Licensed content publisher	Elsevier
Licensed content publication	Journal of Power Sources
Licensed content title	Photoactive supercapacitors for solar energy harvesting and storage
Licensed content author	Arash Takshi, Houman Yaghoubi, Tete Tevi, Sara Bakhshi
Licensed content date	1 February 2015
Licensed content volume number	275
Licensed content issue number	n/a
Number of pages	6
Start Page	621
End Page	626
Type of Use	reuse in a thesis/dissertation
Intended publisher of new work	other
Portion	full article
Format	both print and electronic
Are you the author of this Elsevier article?	Yes
Will you be translating?	No
Title of your thesis/dissertation	Enhancement of Supercapacitor Energy Storage by Leakage Reduction and Electrode Modification
Expected completion date	Aug 2015
Estimated size (number of pages)	100
Elsevier VAT number	GB 494 6272 12
Price	0.00 USD

APPENDIX B: SUPPLEMENTARY MATERIAL FOR CHAPTER 4

Supplementary Materials

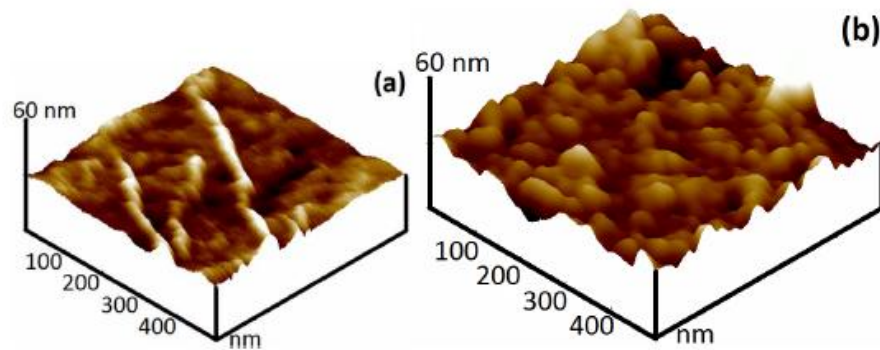
Application of Poly (p-Phenylene Oxide) as blocking layer to reduce self discharge in supercapacitors

Tete Tevi^a, Houman Hyaghoubi^b, Jing Wang^c, Arash Takshi^d

Department of Electrical Engineering, University of South Florida, Tampa FL 33620, U.S.A.

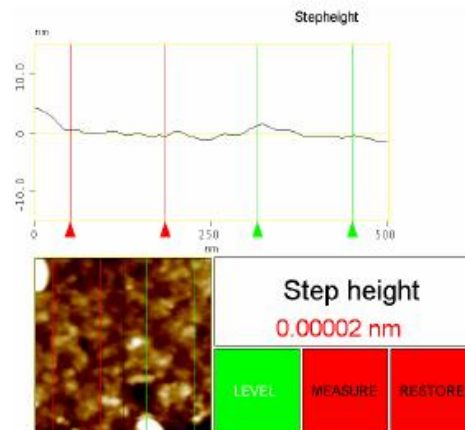
tete@mail.usf.edu, hyaghoubi@mail.usf.edu, jingw@usf.edu, atakshi@usf.edu

Section 1: The detail of the Atomic Force Microscopy results



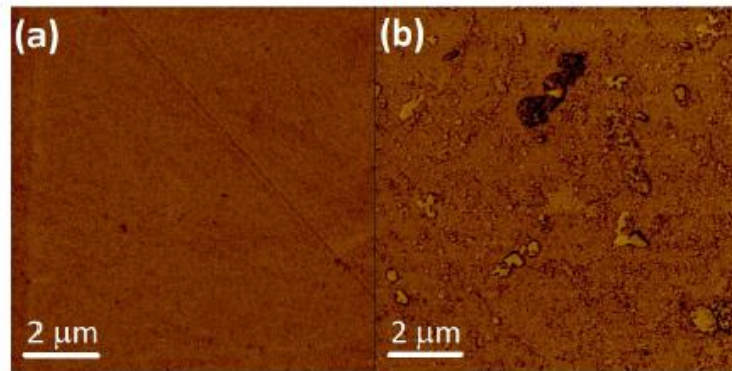
Supplementary Figure 1. (a) 3D AFM topographic images of: (a) uncoated glassy carbon surface and (b) electro-polymerized PPO on a glassy carbon electrode surface. The images were obtained in air using noncontact tapping mode.

As supplementary Figure 1 demonstrates the RMS roughness of the glassy carbon surface would be increased from ~1.67 nm to ~3.66 nm after electrodeposition of PPO. The deposited PPO film shows a well-uniform coherent layer on top of the glassy carbon electrode as it was shown in supplementary Figure 2.



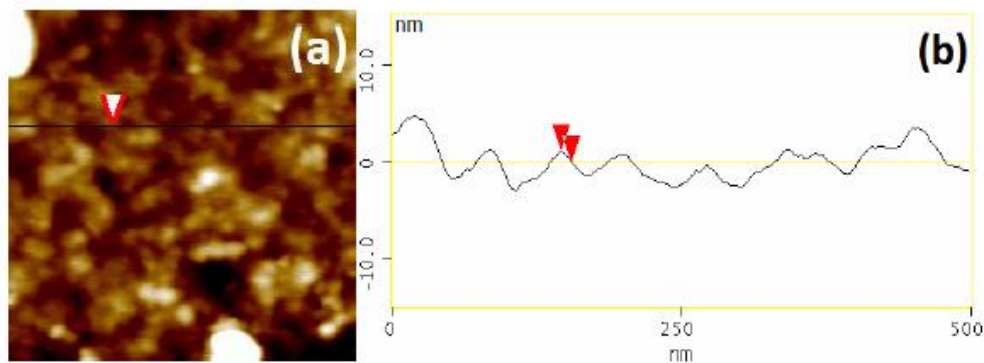
Supplementary Figure 2. Step height measurement for uniformity estimation of the electropolymerized (phenol) film over a 500 x 500 nm area.

The comparison of the AFM phase images for the coated and uncoated glassy carbon electrode over a large 10 by 10 μm surface area also, shows a well coverage of the surface as supplementary Figure 3 shows. The visible large features in supplementary Figure 3 (b) show the aggregation of polymer molecules on some part of the coated glassy carbon surface.



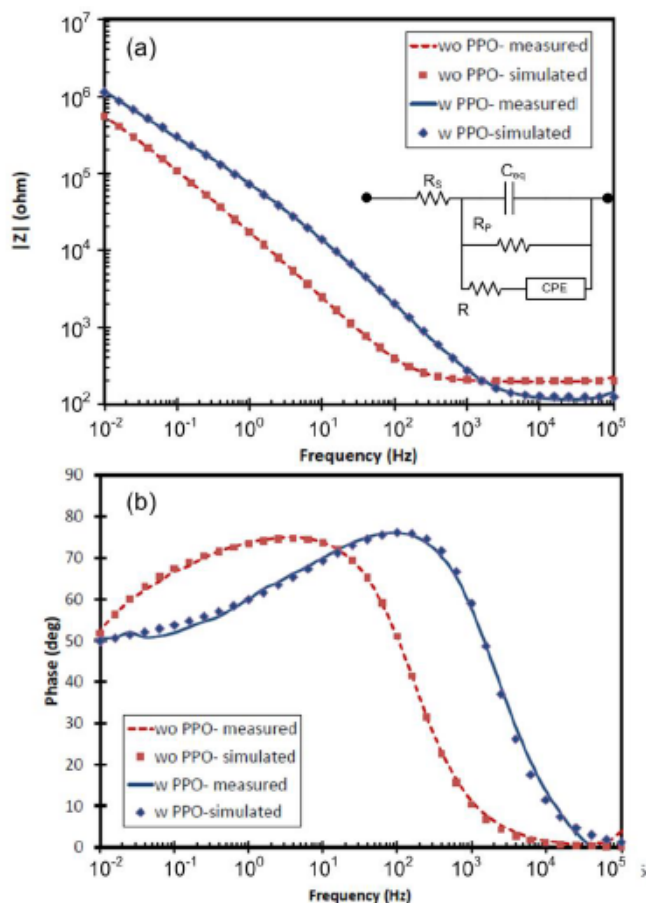
Supplementary Figure 3. AFM topographic phase images of: (a) uncoated glassy carbon surface and (b) electropolymerized PPO on a glassy carbon electrode surface for a 10 by 10 μm surface area. The images were obtained in air using noncontact tapping mode.

Morphology and section analysis of the electropolymerized layer indicates polymer particles with a height of ~ 1.0 nm.



Supplementary Figure 4. Morphology and section analysis of the electro-polymerized layer over a 500 by 500 nm surface area. The image was obtained in air using noncontact tapping mode.

Section 2: EIS Simulation results for glassy carbon electrodes with and without the PPO layer for frequencies from 10 mHz to 100 kHz.



Supplementary Figure 5. (a) Magnitude and (b) phase of the measured and simulated impedance for the glassy carbon electrodes with and without the PPO layer. Simulations were performed based on the model shoed in the inset figure for frequencies between 10 mHz and 100 kHz.

At very low frequencies, the impedance of an electrochemical cell is under influence of non-uniform current distribution at the electrodes. This effect can be modeled with a constant phase element (CPE) and a series resistance, all in parallel with the double layer capacitance (see the inset of supplementary Figure 5). The admittance of CPE, Y_{CPE} , is equal to $Q(j\omega)^n$ where Q and n are frequency independent parameters. ω is the frequency in radian and j is the imaginary unit equal to $\sqrt{-1}$.

Using ZSimpWin software from Princeton Applied Research, the impedance of the electrodes with and without the coating was simulated for frequencies from 10 mHz to 100 kHz. The simulation results are in good agreement with the measured impedances (supplementary Figure 5). Based on the simulation, the values for C_{dl} , R_p , R_s , Q , n , and R are estimated for both electrodes and listed in supplementary Table 1.

APPENDIX C: SUPPLEMENTARY MATERIAL FOR CHAPTER 5

Supplementary Materials

Modeling and Simulation Study of the Self-discharge in Supercapacitors in Presence of a Blocking Layer

Tete Tevi^a and Arash Takshi^b

Department of Electrical Engineering, University of South Florida, Tampa FL 33620, U.S.A.

^atete@mail.usf.edu, ^batakshi@usf.edu

The voltage dependence of the tunneling coefficient

In general for a rectangular energy barrier, the tunneling coefficient is given as a function of the energy barrier [1] by:

$$\beta = \frac{4\pi(2m^*)^{1/2}E^{1/2}}{h} \quad (s1)$$

where m^* is the effective electron mass (kg), E is the height of the barrier in J, and h is Planck's constant ($6.626 \times 10^{-34} \text{ m}^2 \text{ kg s}^{-1}$). However, in presence of an electric field across the barrier (i.e. charged supercapacitor with the blocking layer) the rectangular energy barrier model is not accurate. In this situation, Poole-Frenkel model is usually applied in which β is a function of the voltage (i.e. electric field) [2]. Xu et al., have suggested a linear approximation for β in an electrochemical interface with an insulating interfacial layer on the electrode ($\beta=aV+b$, where a and b are the linear coefficient and offset value, respectively) [3]. Also, in our study, the ratio of $k(V,d)/k(V,0)$, which is equal to $\exp(-\beta d)$, suggests that β has to be a linear function of the voltage. From Fig. 2 in the manuscript we have

$$k(V,0)=1.31 \times 10^{-7} \cdot \exp(V/0.21) \quad (s2)$$

and

$$k(V,1.5 \text{ nm})=1.25 \times 10^{-8} \cdot \exp(V/0.19) \quad (s3)$$

Therefore, $\exp(-\beta \times 1.5 \text{ nm}) = 0.095 \exp(V/1.995)$ and $\beta \text{ (nm}^{-1}\text{)}$ is expressed by:

$$\beta = -0.4118 V + 1.5693 \quad (\text{s4})$$

Considering $V=2 \text{ V}$ the value of β is 0.7473 nm^{-1} . To verify if such a value is physically realistic, one can use equation (s1) to estimate the height of energy barrier. Assuming that the effective mass of electron is ~ 0.1 [4] of the electron mass in free space ($9.1 \times 10^{-31} \text{ kg}$), the energy barrier of the blocking layer is estimated to be 0.053 eV which is a reasonable value. It should be emphasized that calculating the energy barrier height from this method is not accurate due to the over simplified model of the rectangular energy barrier and estimation of the effective mass of electron. However, the reasonable estimated energy barrier height confirms that the calculated β can be physically realistic.

Supplementary References

- [1] T.E. Hartman, *Journal of Applied Physics*, 35 (1964) 3283-3294.
- [2] C.P. Rhodes, J.W. Long, M.S. Doescher, J.J. Fontanella, D.R. Rolison, *The Journal of Physical Chemistry B*, 108 (2004) 13079-13087.
- [3] J. Xu, H. Li, Y. Zhang, *The Journal of Physical Chemistry*, 97 (1993) 11497-11500.
- [4] G. Hutchison, Y.-J. Zhao, B. Delley, A. Freeman, M. Ratner, T. Marks, *Physical Review B*, 68 (2003) 035204.

APPENDIX D: SUPPLEMENTARY MATERIAL FOR CHAPTER 7

Supplementary Materials

Photoactive Supercapacitors for Solar Energy Harvesting and Storage

Arash Takshi^a, Houman Yaghoubi^b, Tete Tevi^c, Sara Bakhshi^d

Department of Electrical Engineering, University of South Florida, Tampa FL 33620, U.S.A.

^aatakshi@usf.edu, ^bhyaghoubi@mail.usf.edu, ^ctete@mail.usf.edu, ^dsara.sbkh@gmail.com

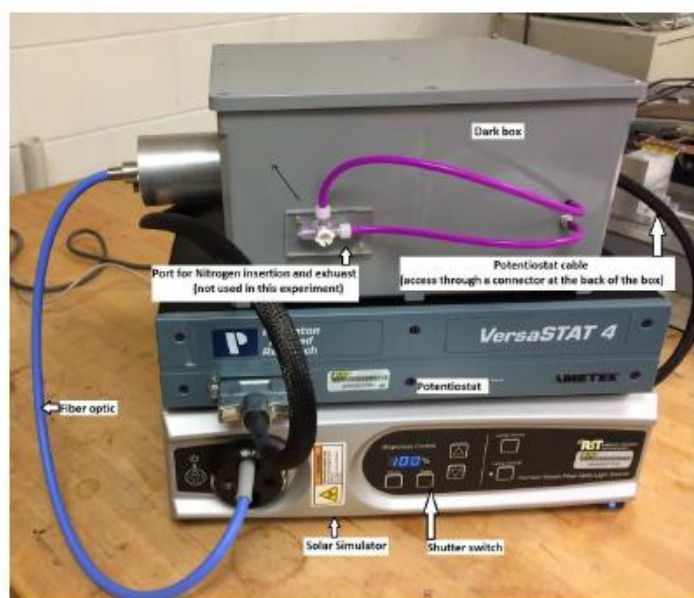


Figure S1. The setup used for testing the photoactive supercapacitors. The sample was placed inside the dark box and the illumination was controlled by turning on and off the shutter switch on the simulator. The output light from the simulator was conducted to the box through the fiber optic cable and was

pointed at the sample inside the box. The potentiostat cable was also connected to the sample through a socket at the back of the dark box.

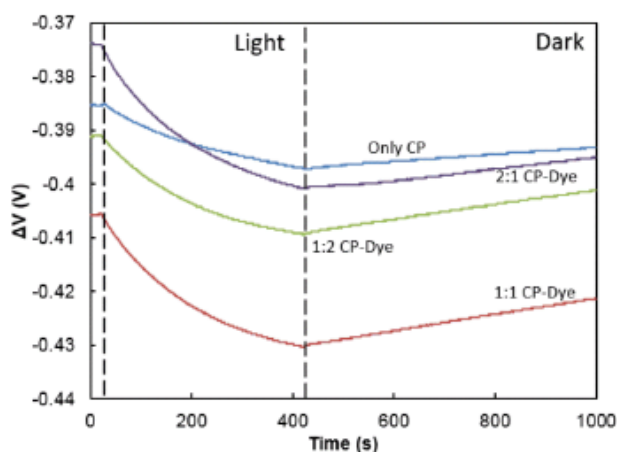


Figure S2. The open circuit voltage in different cells under illumination and after cessation of light.

As shown in Figure S1, the open circuit voltage of different cells showed different voltages in the dark. During the illumination the voltage was changed. The maximum change was observed in the cell with 2:1 CP-dye (porphyrine dye). However, the maximum cell voltage was achieved in the cell with 1:1 CP-dye electrode.

APPENDIX E: MATLAB CODE FOR THE POTENTIOSTAT IN CHAPTER 3

```
%%%%%%%%%%%%%%%%%%%%%%%%%%%%%%%%%%%%%%%%%%%%%%%%%%%%%%%%%%%%%%%%%%%%%%%%%%
%
%   Charging And Discharging of Supercapacitor+ two probes Current voltammetry
%   measurements
%
%       June 2013- Research
%       Author: Tete Tevi
%%%%%%%%%%%%%%%%%%%%%%%%%%%%%%%%%%%%%%%%%%%%%%%%%%%%%%%%%%%%%%%%%%%%%%%%%%

%       Tete Tevi,   June 2012 - Research (Matlab Version: MATLAB R2010a)

function varargout = Potentiostat(varargin)
% POTENTIOSTAT M-file for Potentiostat.fig
%   POTENTIOSTAT, by itself, creates a new POTENTIOSTAT or raises the existing
%   singleton*.
%
%   H = POTENTIOSTAT returns the handle to a new POTENTIOSTAT or the handle to
%   the existing singleton*.
%
%   POTENTIOSTAT('CALLBACK',hObject,eventData,handles,...) calls the local
%   function named CALLBACK in POTENTIOSTAT.M with the given input arguments.
%
%   POTENTIOSTAT('Property','Value',...) creates a new POTENTIOSTAT or raises the
%   existing singleton*. Starting from the left, property value pairs are
%   applied to the GUI before Potentiostat_OpeningFcn gets called. An
%   unrecognized property name or invalid value makes property application
%   stop. All inputs are passed to Potentiostat_OpeningFcn via varargin.
%
%   *See GUI Options on GUIDE's Tools menu. Choose "GUI allows only one
%   instance to run (singleton)".
%
% See also: GUIDE, GUIDATA, GUIHANDLES

% Edit the above text to modify the response to help Potentiostat

% Last Modified by GUIDE v2.5 10-Jul-2012 11:45:44

% Begin initialization code - DO NOT EDIT
gui_Singleton = 1;
gui_State = struct('gui_Name',    mfilename, ...
```

```

        'gui_Singleton', gui_Singleton, ...
        'gui_OpeningFcn', @Potentiostat_OpeningFcn, ...
        'gui_OutputFcn', @Potentiostat_OutputFcn, ...
        'gui_LayoutFcn', { } , ...
        'gui_Callback', { });
if nargin && ischar(varargin{1})
    gui_State.gui_Callback = str2func(varargin{1});
end

if nargout
    {varargout{1:nargout}} = gui_mainfcn(gui_State, varargin{:});
else
    gui_mainfcn(gui_State, varargin{:});
end
% End initialization code - DO NOT EDIT

% --- Executes just before Potentiostat is made visible.
function Potentiostat_OpeningFcn(hObject, eventdata, handles, varargin)
% This function has no output args, see OutputFcn.
% hObject    handle to figure
% eventdata  reserved - to be defined in a future version of MATLAB
% handles    structure with handles and user data (see GUIDATA)
% varargin   command line arguments to Potentiostat (see VARARGIN)

% Choose default command line output for Potentiostat
handles.output = hObject;

% Update handles structure
guidata(hObject, handles);

% UIWAIT makes Potentiostat wait for user response (see UIRESUME)
% uiwait(handles.figure1);

% --- Outputs from this function are returned to the command line.
function varargout = Potentiostat_OutputFcn(hObject, eventdata, handles)
% varargout  cell array for returning output args (see VARARGOUT);
% hObject    handle to figure
% eventdata  reserved - to be defined in a future version of MATLAB
% handles    structure with handles and user data (see GUIDATA)

% Get default command line output from handles structure
varargout{1} = handles.output;

% --- Executes on button press in pushbutton5.
function pushbutton5_Callback(hObject, eventdata, handles)

```

```

clear all;clc;close all;

DIO = digitalio('mcc',0);
lines = addline(DIO,7, 0,'out');putvalue(DIO,0);% Relays : open the input

AO= analogoutput('mcc',0);
chano = addchannel(AO,1);
duration = 1; % 1 second acquisition
set(AO,'SampleRate',8000)
set(AO,'TriggerType','Manual')
ActualRate = get(AO,'SampleRate');
t(1)=0;
putdata(AO,0);
start(AO)
trigger(AO)
stop(AO)
delete(AO)
clear AO
% hObject handle to pushbutton5 (see GCBO)
% eventdata reserved - to be defined in a future version of MATLAB
% handles structure with handles and user data (see GUIDATA)

% --- Executes on button press in pushbutton1.
function pushbutton1_Callback(hObject, eventdata, handles)
clear all;clc;close all;
PORTA = digitalio('mcc',0);
lines = addline(PORTA,7, 0,'out');putvalue(PORTA,0);% Relays : open the input
%% Creating .mat file

prompt = {'Enter file name:'};
dlg_title = 'Matlab File Name';
num_lines = 1;
def = {'YC-YC-TBAP1M-Pot-May25_Al2O3_4nm.mat'};
file_namePOT = inputdlg(prompt,dlg_title,num_lines,def);

%% User interface
time=input('Charging Time (seconds) = '); % charging time
time_OC=input('Open Circuit Time (seconds) = '); % discharging time
cyclePOT=input('Cycles = '); % Charging and discharging cycles
voltage=input('Charging voltages { V1 V2 ... #}(Volts) = ');% Charging voltages
volt=(voltage+4.986)/2;
s=input('Current Range Selector Position 1: {10 mA to 10 uA}, 2: {100 uA to 100 nA} , or 3: {1
uA to 1 nA} = ');% Charging voltages
R={1e+3 1e+5 1e+7};% Virtual Resistance value

for k=1:cyclePOT;

```

```

putvalue(PORTA,1); %% Relays : close input
AO= analogoutput('mcc',0);
chano = addchannel(AO,1);
set(AO,'SampleRate',8000)
set(AO,'TriggerType','Manual')
ActualRate = get(AO,'SampleRate');
t(1)=0;
putdata(AO,volt(k));
start(AO)
trigger(AO)
stop(AO)
%% Acquisition
AI = analoginput('mcc',0);chani = addchannel(AI, {0 1}); % Analog Inputs 0 & 2
set(AI,'SampleRate',8000)
set(AI,'SamplesPerTrigger',8000)
set(AI,'TriggerType','Manual')
start(AI)
trigger(AI)
data = getdata(AI);
dat(1)=data(1,1);dat_I(1)=data(1,2);

%%
for j=1:time_OC+time;
tStart = tic;
stop(AI)
start(AI)
trigger(AI)
data = getdata(AI,1);
dat(j+1)=data(1);dat_I(j+1)=data(2);t(j+1)=t(j)+1;% 1 second acquisition
figure(k)
subplot(2,1,1)
plot(t,dat)
title('Self Discharge-Voltage')
xlabel('Elapsed Time(s)')
ylabel('Potential(V)')
grid on;
subplot(2,1,2)
plot(t,dat_I/R(s))
title('Self Discharge-Current')
xlabel('Elapsed Time(s)')
ylabel('Current(A)')
grid on;
if j==time
putvalue(PORTA,0);
else
end;

```

```

elapsedtime= toc(tStart);
pause(1-elapsedtime);
end

%%

delete(AI)
clear AI
delete(AO)
clear AO

%% Write data to excel file

%title1 = {'Elapsed Time(second)','Potential(Volts)'; 0,0}; title2 = {'Elapsed
Time(second)','Current(Amps)'; 0,0};
% xlswrite(file_namePOT{1}, title1, 2*k-1,'A1');xlswrite(file_namePOT{1}, title2, 2*k,'A1');
% D1(:,1)=t';D1(:,2)=dat';D2(:,1)=t';D2(:,2)=(dat_I/R(s))';
% xlswrite(file_namePOT{1},D1,2*k-1,'A2');xlswrite(file_namePOT{1},D2,2*k,'A2');

%% save to matlab file

D1(:,2*k-1)=t';D1(:,2*k)=dat';D2(:,2*k-1)=t';D2(:,2*k)=(dat_I/R(s))';
save(file_namePOT{1}, 'D1*','D2*')

%%
clear dat; clear dat_I;clear t; % clear D1; clear D2;
end

%%
disp('END OF EXPERIMENT');

% hObject handle to pushbutton1 (see GCBO)
% eventdata reserved - to be defined in a future version of MATLAB
% handles structure with handles and user data (see GUIDATA)

% --- Executes on button press in pushbutton2.
function pushbutton2_Callback(hObject, eventdata, handles)

%%%%%%%%%%%%%%
%
% Current Voltammetry of Supercap %
% June 2012 - Research %
% Author: Tete Tevi %
%%%%%%%%%%%%%%
%%%%%%%%%%%%%%

```

```

% (Matlab Version: MATLAB R2010a)
clear all;clc;close all;
PORTA = digitalio('mcc',0);
lines = addline(PORTA,7, 0,'out');putvalue(PORTA,0);% Relays : open the input
%% Creating .mat file

prompt = {'Enter file name:'};
dlg_title = 'Matlab File Name';
num_lines = 1;
def = {'YC-YC-TBAP1M-CV-May25_Al2O3_4nm.mat'};
file_name= inputdlg(prompt,dlg_title,num_lines,def);

%% User interface
number=input('Number of CVs = ');
Vin=input('Initial Potential (V) = ');
V1=input('Vertex 1(Smallest Vertex) Potential (V) {V1 V2 ... #}= ');
V2=input('Vertex 2 Potential (V) {V1 V2 ... #}= ');
Scan_rate=input('Scan Rate (V/s)= ');
cycle=input('Cycles = ');
s=input('Current Range Selector Position  1:{10 mA to 10 uA}, 2:{100 uA to 100 nA} , or 3:{1
uA to 1 nA} = ');% Charging voltages
R={1e+3 1e+5 1e+7};% Virtual Resistance value

    for n=1:number;
        AO= analogoutput('mcc',0);
        chano = addchannel(AO,1);
        set(AO,'SampleRate',8000)
        set(AO,'TriggerType','Manual')
        ActualRate = get(AO,'SampleRate');
        AI = analoginput('mcc',0);chani = addchannel(AI, {0 1}); % Analog Inputs 0 & 2
        set(AI,'SampleRate',8000)
        set(AI,'SamplesPerTrigger',8000)
        set(AI,'TriggerType','Manual')

        putvalue(PORTA,1); %% Relays : close input
        t(1)=0;j=1;
        V(n)=(Vin+4.999)/2;
        putdata(AO,V(n));
        start(AO)
        trigger(AO)
        stop(AO)
        stop(AI)
        start(AI)
        trigger(AI)
        data = getdata(AI,1);dat(1)=data(1);
    end

```

```

    for k=1:cycle;
    while V(n)<(V2(n)+4.999)/2;
    tStart = tic;
    V(n)=V(n)+Scan_rate;
    stop(AI);
    putdata(AO,V(n));
    start(AO)
    trigger(AO)
    stop(AO)
    % Acquisition
    start(AI)
    trigger(AI)
    data = getdata(AI,1);
    dat(j+1)=data(1);dat_I(j+1)=data(2);t(j+1)=t(j)+1;% 1 second acquisition
    stop(AI)
    figure(n)
    subplot(2,1,1)%
    plot(t,dat)
    title('Current Voltammetry (CV)')
    xlabel('Elapsed Time(s)')
    ylabel('Potential(V)')
    grid on;
    subplot(2,1,2)% figure(2*k)
    plot(dat,dat_I/R(s))
    title('Current Voltammetry (CV)')
    xlabel('Potential(V)')
    ylabel('Current(A)')
    grid on;
    j=j+1;elapsedtime= toc(tStart);
    pause(1-elapsedtime);
    end
    while V(n)>(V1(n)+4.999)/2;
    tStart = tic;
    V(n)=V(n)-Scan_rate;
    stop(AI);
    putdata(AO,V(n));
    start(AO)
    trigger(AO)
    stop(AO)
    % Acquisition
    start(AI)
    trigger(AI)
    data = getdata(AI,1);
    dat(j+1)=data(1);dat_I(j+1)=data(2);t(j+1)=t(j)+1;% 1 second acquisition
    stop(AI)
    figure(n)

```

```

subplot(2,1,1)
plot(t,dat)
title('Current Voltammetry (CV)')
xlabel('Elapsed Time(s)')
ylabel('Potential(V)')
grid on;
subplot(2,1,2)
plot(dat,dat_I/R(s))
title('Current Voltammetry (CV)')
xlabel('Potential(V)')
ylabel('Current(A)')
grid on;
j=j+1;elapsedtime= toc(tStart);
pause(1-elapsedtime);
end

while V(n)<(V2(n)+4.999)/2;
tStart = tic;
V(n)=V(n)+Scan_rate;
stop(AI);
putdata(AO,V(n));
start(AO)
trigger(AO)
stop(AO)
% Acquisition
start(AI)
trigger(AI)
data = getdata(AI,1);
dat(j+1)=data(1);dat_I(j+1)=data(2);t(j+1)=t(j)+1;% 1 second acquisition
stop(AI)
figure(n)
subplot(2,1,1)% figure(2*k-1)
plot(t,dat)
title('Current Voltammetry (CV)')
xlabel('Elapsed Time(s)')
ylabel('Potential(V)')
grid on;
subplot(2,1,2)% figure(2*k)
plot(dat,dat_I/R(s))
title('Current Voltammetry (CV)')
xlabel('Potential(V)')
ylabel('Current(A)')
grid on;
j=j+1;elapsedtime= toc(tStart);
pause(1-elapsedtime);
end

```



```

    end
putvalue(PORTA,0); %% Relays : open input

delete(AI)
clear AI
delete(AO)
clear AO
%% Write data to excel file

% title1 = {'Elapsed Time(second)','Potential(Volts)'; 0,0}; title2 =
{'Potential(Volts)','Current(Amps)'; 0,0};
% xlswrite(file_name{1}, title1, 2*n-1,'A1');xlswrite(file_name{1}, title2, 2*n,'A1');
% D1(:,1)=t';D1(:,2)=dat';D2(:,1)=D1(:,2);D2(:,2)=(dat_I/R(s));
% xlswrite(file_name{1},D1,2*n-1,'A2');xlswrite(file_name{1},D2,2*n,'A2');
%% save to matlab file
%
A{n}(:,2*n-1)=t';A{n}(:,2*n)=dat';B{n}(:,2*n-1)=t';B{n}(:,2*n)=(dat_I/R(s));
save(file_name{1}, 'A*', 'B*')

%%
clear dat; clear dat_I;clear t; %clear D1; clear D2;
%B = repmat(D1,2,1)
end

disp('END OF EXPERIMENT');

%NUMERIC = xlsread('C:\Users\tete\Documents\MATLAB\file_name{1}.xls',1);

% hObject handle to pushbutton2 (see GCBO)
% eventdata reserved - to be defined in a future version of MATLAB
% handles structure with handles and user data (see GUIDATA)

% --- Executes on button press in pushbutton3.
function pushbutton3_Callback(hObject, eventdata, handles)

clear all;clc;close all;
dname = uigetfile('C:\');% Users\tete\Desktop\My Documents\MATLAB
s=load(dname);

A = getfield(s, 'A');
B = getfield(s, 'B');

C=size(A);n=C(:,2);%n=n/2;
Time=B{1}(:,1);

```

```

Voltage=A{1}(:,2)
Current=B{1}(:,2)

figure(1)
subplot(2,1,1)
plot(Time,Voltage);
title('Current Voltammetry (CV)')
xlabel('Elapsed Time(s)')
ylabel('Potential(V)')
grid on;
subplot(2,1,2)
% hold on;
plot(Voltage,Current);
title('Current Voltammetry (CV)')
xlabel('Potential(V)')
ylabel('Current(A)')
grid on;

% %% Creating .xls file
%
% prompt = {'Enter file name:'};
% dlg_title = 'Excel File Name';
% num_lines = 1;
% def = {'YC-YC-TBAP1M-Pot-May25_Al2O3_4nm.xls'};
% file_name = inputdlg(prompt,dlg_title,num_lines,def);
% %% Write data to excel file
%
% title1 = {'Elapsed Time(second)','Potential(Volts)','Current(Amps)'; 0,0,0}; %title2 =
% {'Potential(Volts)','Current(Amps)'; 0,0};
% xlswrite(file_name{1}, title1, Time,'A1');xlswrite(file_name{1}, title1, Voltage,'B1');
% xlswrite(file_name{1}, title1, Voltage,'C1');

%hold on;
% hObject handle to pushbutton3 (see GCBO)
% eventdata reserved - to be defined in a future version of MATLAB
% handles structure with handles and user data (see GUIDATA)

% --- Executes on button press in pushbutton4.
function pushbutton4_Callback(hObject, eventdata, handles)
clear all;clc;close all;

dname = uigetfile('C:\');% Users\tete\Desktop\My Documents\MATLAB
s=load(dname);

D1 = getfield(s, 'D1');

```

```

D2 = getfield(s, 'D2');

C=size(D1);n=C(:,2);n=n/2;

k=1;
while k<=n
hold on
figure(k)
subplot(2,1,1)
plot(D1(:,2*k-1),D1(:,2*k));
title('Self Discharge-Voltage')
xlabel('Elapsed Time(s)')
ylabel('Potential(V)')
grid on;
subplot(2,1,2)
hold on;
plot(D2(:,2*k-1),D2(:,2*k));
title('Self Discharge-Current')
xlabel('Elapsed Time(s)')
ylabel('Current(A)')
grid on;
k=k+1;hold on;
end

% hObject handle to pushbutton4 (see GCBO)
% eventdata reserved - to be defined in a future version of MATLAB
% handles structure with handles and user data (see GUIDATA)

```

APPENDIX F: MATLAB CODE FOR CHAPTER 5

```
%%%%%%%%%%%%%%%%%%%%%%%%%%%%%%%%%%%%%%%%%%%%%%%%%%%%%%%%%%  
%                                                                                               %  
%           Discharging Profile of Supercap knowing thickness                               %  
%           of blocking layer                                                                 %  
%           July 2013 - Research                                                                 %  
%           Author: Tete Tevi                                                                 %  
%%%%%%%%%%%%%%%%%%%%%%%%%%%%%%%%%%%%%%%%%%%%%%%%%%%%%%%%%%
```

```
% Author : Tete Tevi, July 2013 (Matlab Version: MATLAB R2010a)
```

```
% Nota: First copy and paste your self discharge data in two new .txt files and  
% save them in the same folder where this code is saved. Run the code.  
% Nota: This code needs the Ezyfit toolbox to be installed
```

```
%% User interface
```

```
clear all;clc;close all;  
prompt1 = {'Enter "No blocking layer" file name:'};  
dlg_title1 = 'Text File Name';  
num_lines1 = 1;  
def1 = {'NoPPO.txt'};  
file_name1= inputdlg(prompt1,dlg_title1,num_lines1,def1);  
  
close all;  
prompt2 = {'Enter "with blocking layer" file name:'};  
dlg_title2 = 'Text File Name';  
num_lines2 = 1;  
def2 = {'PPO.txt'};  
file_name2= inputdlg(prompt1,dlg_title2,num_lines2,def2);  
% V_ch=input('Charging Voltage (Volts)=');  
cycle=input('Number of Thickness Inputs = '); % discharging cyles  
thick=input('Thicknesses {th1 th2 ... #}(nanometer(s)) = ');% Charging voltages  
display(' ');  
display('-----');  
  
display('Note on PPO on Y-Carbon: Dielectric constant=3.5 ');  
display('--Blocking layer thickness(nm)=1.5');
```

```

display('-- Specific Capacitance before blocking layer(F/g)=12.99');display('--Specific
Capacitance after blocking layer(F/g)=5.7');
display('-----');
display(' ');
thb=input('blocking layer thickness (in nanometers)= ');
diek=input('Dielectrique constant of the blocking layer= ');
% display('Note: PPO dielectric constant=3.5');
C1=input('Specific Capacitance before blocking layer(F/g)= ');
C2=input('Specific Capacitance after blocking layer(F/g)= ');
% C11=input('Capacitance before blocking layer(F)= ');
% C22=input('Capacitance after blocking layer(F)= ');
%% Load data
data1 = load(file_name1{1});datNoPPO =data1;
data2 = load(file_name2{1});datPPO =data2;
V_ch=data1(1,2);

size=size(datNoPPO);
size=size(1); k=1;last_time=size;
for i=1:size;
j=50*(i-1)+1; %% Sampling

    if j > size
    else
    dataNoPPO(k,:)= datNoPPO(j,:);
    dataPPO(k,:)= datPPO(j,:);

    end
k=k+1;
end

%% Curve fitting
xdataNoPPO=dataNoPPO(:,1);
ydataNoPPO=dataNoPPO(:,2);

xdataPPO=dataPPO(:,1);
ydataPPO=dataPPO(:,2);

%%
figure(1)
plot(xdataNoPPO,ydataNoPPO,'*');
% legend('=Experimental Data; V(t)=Fitted Curve');
title(' Curve Fitting - Activation controlled Faradaic-No blocking layer ')
xlabel('t(s)')
ylabel('V(volt)')

```

```

showfit('V(t)=a-b*log(t+c)', 'fitlinewidth',2, 'fitcolor', 'red');
legend('Experimental Data', ' V(t)=Fitted Curve  ')

param=getfield(lastfit, 'm');

a=param(1);b=param(2);c=param(3);

dvdt = diff(ydataNoPPO)./diff(xdataNoPPO); %% take the discrete derivative

k0=-dvdt./ydataNoPPO(1:end-1);%

%plot(ydataNoPPO(1:end-1),k0,'r--')
% t_prime=xdata+c;
% for i=1:size(xdata);
% dv_dt(i)=-b/t_prime(i);
% k0(i)=-dv_dt(i)/ydata(i);
%
%%
figure(2)
plot(ydataNoPPO(1:end-1),k0,'b--');% , '*'
title(' k Versus Voltage - No blocking layer')
xlabel('V(Volt)')
ylabel('k')

showfit('k(V)=a*exp(V/tau)', 'fitlinewidth',2, 'fitcolor', 'red');
legend(' k=(-V)/(\Delta V/\Delta t)', ' Fitted Curve  ')
param=getfield(lastfit, 'm');

aNo=param(1);tauNo=param(2);

RNo=getfield(lastfit, 'r');
EoNo=tauNo*log(1/(aNo));
AlphaNo=(25.693e-3*(1/tauNo));

%% Write Ko(v) to text file
koNv(:,1)=xdataNoPPO(1:end-1);
koNv(:,2)=k0';

fileID = fopen('Ko(v)NoPPO.txt','w');
% fprintf(fileID, '% 6s % 12s\n', 'v', 'Ko(v)');
fprintf(fileID, '% 6.2f % 12.8f\n', koNv);
fclose(fileID);

```

```

%%
figure(11)
plot(xdataPPO,ydataPPO,'*');
%legend('=Experimental Data; V(t)=Fitted Curve');
title(' Curve Fitting - Activation controlled Faradaic- blocking layer ')
xlabel('t(s)')
ylabel('V(volt)')

showfit('V(t)=a-b*log(t+c)','fitlinewidth',2,'fitcolor','red');

legend(' Experimental Data',' Fitted Curve ')
param=getfield(lastfit, 'm');

a=param(1);b=param(2);c=param(3);

dvdt = diff(ydataPPO)./diff(xdataPPO); %% take the discret derivative
k0vp=-dvdt./ydataPPO(1:end-1);
%plot(ydataPPO(1:end-1),k0,'r--')
% t_prime=xdata+c;
% for i=1:size(xdata);
% dv_dt(i)=-b/t_prime(i);
% k0(i)=-dv_dt(i)/ydata(i);
%
%%
figure(12)
plot(ydataPPO(1:end-1),k0vp,'b--');% , '*'
title(' k Versus Voltage - blocking layer')
xlabel('V(Volt)')
ylabel('k')

showfit('k(V)=a*exp(V/tau)','fitlinewidth',2,'fitcolor','red');

legend(' k=(-V)/(\Delta V\Delta t)',' Fitted Curve ')
paramk=getfield(lastfit, 'm');

ap=paramk(1);taup=paramk(2);
Rp=getfield(lastfit, 'r');
Eop=taup*log(1/(ap));
Alphap=(8.314*298.15/(96500*taup));

%% Write Ko(v) to text file
kov(:,1)=xdataPPO(1:end-1);
kov(:,2)=k0';

```

```

fileID = fopen('Ko(v)PPO.txt','w');
% fprintf(fileID,'%6s %12s\n','v','Ko(v)');
fprintf(fileID,'%6.2f %12.8f\n',kov);
fclose(fileID);

%% Beta plotting
% ydataNoPPO(1:end-1),k0-----ydataPPO(1:end-1),k0vp---length(k0)

ybeta=log(k0vp.\(k0*(-10*thb)));

figure(112)
plot(ydataPPO(1:end-1),ybeta,'b--');% , '*'
title(' Beta Versus Voltage ')
xlabel('V(Volt)')
ylabel('Beta')

figure(113)
xbeta2=0:0.05:2;

for i=1:length(xbeta2);
ybeta2(i)=log((ap*exp(xbeta2(i)/taup)/(aNo*exp(xbeta2(i)/tauNo)))/(-10*thb));
end

plot(xbeta2,ybeta2,'b--');% , '*'
title(' Beta Versus Voltage ')
xlabel('V(Volt)')
ylabel('Beta')
showfit('k(V)=a*V+b','fitlinewidth',2,'fitcolor','red');

% AlphaNo
vbeta=aNo*ydataPPO(1:end-1);
ybeta3=(ydataPPO(1:end-1)/taup-log(-dvdtp./vbeta))/(10*thb);

figure(114)
plot(ydataPPO(1:end-1),ybeta3);% , '*'
title(' Beta Versus Voltage ')
xlabel('V(Volt)')
ylabel('Beta')
showfit('k(V)=a*V+b','fitlinewidth',2,'fitcolor','red');
parambeta=getfield(lastfit, 'm');
Coeff_beta=parambeta

%% Beta Estimation through k(P.624 Allen Bard book) Electron transfer by tunneling through
blocking films

```



```

% knowing a specific thickness in nanometer

for l=1:cycle;
mm=(1/tauNo-1/taup)/(thb*1e-9);nn=-log(ap/aNo)/(thb*1e-9);

th=thick(l);
Vol=0:0.001:V_ch;Vol=Vol';
% size=size(Vol);
% size=size(1);

for i=1:length(Vol);
kx(i)=aNo*exp(Vol(i)*(1/tauNo))*exp(-th*1e-9*mm*Vol(i)-th*1e-9*nn);
end
figure(32)
plot(Vol,kx,'b--');% , '*'
%title(' k0 Versus Voltage - for the desired thickness')
xlabel('V(Volt)')
ylabel('ko')

showfit('ko(V)=a*exp(V/tau)','fitlinewidth',2,'fitcolor','red');

paramx=getfield(lastfit, 'm');

Rx=getfield(lastfit, 'r');

ax=paramx(1);taux=paramx(2);
axk(l)=ax;tauxk(l)=taux;Rrk(l)=Rx;Eoxk(l)=tauxk(l)*log(1/(axk(l)));
Alphaxk(l)=(8.314*298.15/(96500*tauxk(l)));
% %% Write Kox(v) to text file
% kox(:,1)=Vol;
% kox(:,2)=kx';
%
%
% fileID = fopen('Kox(v)PPO.txt','w');
% fprintf(fileID,'%6s %12s\n','v','Ko(v)');
% fprintf(fileID,'%6.2f %12.8f\n',kox);
% fclose(fileID);

%% Plotting V versus t : Diff. equation solving

ode1=@(x,y)-axk(l)*y*exp(y/tauxk(l));
% Call Solver With Function Name,
% Independent Variable Range and Initial Value of Dependent Variable
end_of_time=data1(last_time,1);

```

```

{x,y}=ode113(ode1,{0:end_of_time},V_ch); % {x,y}=ode113(ode1,{0:0.1:size},);
% Plotting Segment
xdataxk(:,l)=x;ydataxk(:,l)=y;
figure (41)
plot(x,y,'b--')

xlabel('t(s)')
ylabel('V(volt)')

%title('Solution to dV/dt = -ko*V for desired thickness')
showfit('V(t)=a-b*log(t+c)', 'fitlinewidth',2, 'fitcolor', 'red');
paramvx=getfield(lastfit, 'm');

avx=paramvx(1);bvx=paramvx(2);cvx=paramvx(3);
avxk(l)=avx;bvxk(l)=bvx;cvxk(l)=cvx;

end

%% Plot all the graphs

Markert={' ','-','--','-.-','-*','-+','-o','-^','-d','-v','-s','-<','->','-p','-h'};

siz=length(xdataxk);
k=1;
for i=1:siz;
j=100*(i-1)+1;

    if j > siz
    else
    xdatxk(k,:)= xdataxk(j,:);
    ydatxk(k,:)= ydataxk(j,:);

    end
k=k+1;
end

for l = 1:cycle

    legendInfo{l} = {'thickness = ' num2str(thick(l)) 'nm'};
    mark=Markert{l};
    figure (7)
    plot(xdatxk(:,l),ydatxk(:,l),mark)
    legend(legendInfo)
    xlabel('t(s)')
    ylabel('V(volt)')

```

```

    %title('Self discharge voltage profiles for different thicknesses')
    hold on
end

for l = 1:cycle
    Vol=0:0.025:V_ch;Vol=Vol';

    legendInfo{1} = {'thickness = ' num2str(thick(l)) 'nm'};
    mark=Markert{1};
    figure(33)
    plot(Vol,axk(l)*exp(Vol/tauxk(l)),mark);% , '*'
    legend(legendInfo)
    %title(' k0 Versus Voltage - for the desired thickness')
    xlabel('V(Volt)')
    ylabel('ko(1/s)')
    hold on
end

%% Energy
epsi=8.854187817620e-12;

Cbl=1/(1/C2-1/C1);
% Cbl1=1/(1/C22-1/C11);

for l = 1:cycle
    Vol=(0:0.001:V_ch)';
    siz=length(Vol);
    k=1;
    for i=1:siz;
        j=100*(i-1)+1;

        if j > siz
            else
                Vot(k,:)= Vol(j,:);
                Vot(k,:)= Vol(j,:);

            end
        k=k+1;
    end
    for i=1:length(Vot);
        Vots(i)=Vot(i)*Vot(i);
        Vots=Vots';
    end
end

```

```

legendInfo{1} = {'thickness = ' num2str(thick(1)) 'nm'};
mark=Markert{1};
Cbl1=Cbl*thb/thick(1);
spec_capacitance_bl(1)= 1/(1/Cbl1+1/C1);
% Cbl11=Cbl1*thb/thick(1);
% capacitance_bl(1)= 1/(1/Cbl11+1/C11);
% Leakage_current(1)=(2-ydataxk(1,1))*capacitance_bl(1);
En=(0.5*Vots/((1/C1+1/Cbl1)));
% Enn(:,1)=En;% Find a solution
figure(34)
plot(Vot,En,mark);% , '*'
legend(legendInfo)
%title(' k0 Versus Voltage - for the desired thickness')
xlabel('V(Volt)')
ylabel('E(J/g)')
hold on
end

for l = 1:cycle
size=length(ydatxk);
for i=1:size;
datavk= ydatxk(:,l);
datvk(i)=datavk(i)*datavk(i);

end

legendInfo{1} = {'thickness = ' num2str(thick(1)) 'nm'};
mark=Markert{1};
Cbl1=Cbl*thb/thick(1);
Enr(:,1)=(0.5*(datvk)/(1/C1+1/Cbl1));
delta_E(1)=abs(Enr(1,1)-Enr(size,1));
Error_E(1)=delta_E(1)/Enr(1,1);
figure(35)
plot(ydatxk(:,l),Enr(:,1),mark,'Linewidth',1.25);% , '*'
legend(legendInfo)
%title(' Energy Versus discharge Voltage - for the desired thickness')
xlabel('V(Volt)')
ylabel('E(J/g)')
hold on

figure(36)
plot(xdatxk(:,l),Enr(:,1),mark,'Linewidth',1.25);% , '*'
legend(legendInfo)
%title(' Energy Versus Time - for the desired thickness')

```

```

xlabel('t(s)')
ylabel('E(J/g)')
hold on
end
% axk(l)=ax;tauxk(l)=taux;Rxx(l)=Rx;Eoxk(l)=tauxk(l)*log(1/(axk(l)))

Energy_loss(:,2)= delta_E';Energy_loss(:,1)=thick';
Energy_error(:,2)= Error_E';Energy_error(:,1)=thick';
Energy_begin(:,2)=Enr(1,:);Energy_begin(:,1)=thick';
Energy_end(:,2)=Enr(size,:);Energy_end(:,1)=thick';
%Leakage_current

Energy_begin=Energy_begin'
Energy_end=Energy_end'
voltage_end=ydataaxk(end_of_time,:)

Energy_loss=Energy_loss'
Energy_error=Energy_error'

display('-----End-----')

%%%%%%%%%%%%%%
%
%           Discharging Profile of Supercap knowing thickness
%           of blocking layer (Same initial energy density)
%           July 2013 - Research
%           Author: Tete Tevi
%
%%%%%%%%%%%%%%

% Author : Tete Tevi, July 2013 (Matlab Version: MATLAB R2010a)

% Nota: First copy and paste your self discharge data in two new .txt files and
% save them in the same folder where this code is saved. Run the code.
% This code needs the Ezyfit toolbox to be installed.

%% User interface

clear all;clc;close all;
prompt1 = {'Enter "No blocking layer" file name:'};
dlg_title1 = 'Text File Name';
num_lines1 = 1;
def1 = {'NoPPO.txt'};
file_name1= inputdlg(prompt1,dlg_title1,num_lines1,def1);

```

```

close all;
prompt2 = {'Enter "with blocking layer" file name:'};
dlg_title2 = 'Text File Name';
num_lines2 = 1;
def2 = {'PPO.txt'};
file_name2= inputdlg(prompt1,dlg_title2,num_lines2,def2);
% V_ch=input('Charging Voltage (Volts)=');
cycle=input('Number of Thicknes Inputs = '); % discharging cycles
thick=input('Thicknesses {th1 th2 ... #}(nanometer(s)) = ');% Charging voltages
display(' ');
display('-----');

display('Note on PPO on Y-Carbon: Dielectric constant=3.5 ');
display('--Blocking layer thickness(nm)=1.5');
display('-- Specific Capacitance before blocking layer(F/g)=12.99');display('--Specific
Capacitance after blocking layer(F/g)=5.7');
display('-----');
display(' ');
thb=input('blocking layer thickness (in nanometers)= ');
diek=input('Dielectrique constant of the blocking layer= ');
% display('Note: PPO dielectric constant=3.5');
C1=input('Specific Capacitance before blocking layer(F/g)= ');
C2=input('Specific Capacitance after blocking layer(F/g)= ');
%% Load data
data1 = load(file_name1{1});datNoPPO =data1;
data2 = load(file_name2{1});datPPO =data2;
V_ch=data1(1,2);

size=size(datNoPPO);
size=size(1); k=1;last_time=size;
for i=1:size; % Sampling
j=50*(i-1)+1;

    if j > size
    else
    dataNoPPO(k,:)= datNoPPO(j,:);
    dataPPO(k,:)= datPPO(j,:);

    end
k=k+1;
end

%% Curve fitting
xdataNoPPO=dataNoPPO(:,1);
ydataNoPPO=dataNoPPO(:,2);

```

```

xdataPPO=dataPPO(:,1);
ydataPPO=dataPPO(:,2);

%%
figure(1)
plot(xdataNoPPO,ydataNoPPO,'*');
%legend('=Experimental Data; V(t)=fitted Curve');
title(' Curve Fitting - Activation controlled Faradaic-No blocking layer ')
xlabel('t(s)')
ylabel('V(volt)')

showfit('V(t)=a-b*log(t+c)','fitlinewidth',2,'fitcolor','red');
legend('Experimental Data',' V(t)=fitted Curve ')

param=getfield(lastfit, 'm');

a=param(1);b=param(2);c=param(3);

dvdt = diff(ydataNoPPO)./diff(xdataNoPPO); %% take the discrete derivative

k0=-dvdt./ydataNoPPO(1:end-1);

%plot(ydataNoPPO(1:end-1),k0,'r--')
% t_prime=xdata+c;
% for i=1:size(xdata);
% dv_dt(i)=-b/t_prime(i);
% k0(i)=-dv_dt(i)/ydata(i);
%
%%
figure(2)
plot(ydataNoPPO(1:end-1),k0,'b--');% , '*'
title(' k0 Versus Voltage - No blocking layer')
xlabel('V(Volt)')
ylabel('k0')

showfit('ko(V)=a*exp(V/tau)','fitlinewidth',2,'fitcolor','red');
legend(' Experimental Data',' fitted Curve');
param=getfield(lastfit, 'm');

aNo=param(1);tauNo=param(2);

%% Write Ko(v) to text file

```

```

koNv(:,1)=xdataNoPPO(1:end-1);
koNv(:,2)=k0';

fileID = fopen('Ko(v)NoPPO.txt','w');
%fprintf(fileID,'%6s %12s\n','v','Ko(v)');
fprintf(fileID,'%6.2f %12.8f\n',koNv);
fclose(fileID);

%%
figure(11)
plot(xdataPPO,ydataPPO,'*');
%legend('=Experimental Data; V(t)=fitted Curve');
title(' Curve Fitting - Activation controlled Faradaic- blocking layer ')
xlabel('t(s)')
ylabel('V(volt)')

showfit('V(t)=a-b*log(t+c)','fitlinewidth',2,'fitcolor','red');

legend(' Experimental Data',' fitted Curve ')
param=getfield(lastfit, 'm');

a=param(1);b=param(2);c=param(3);

dvdt = diff(ydataPPO)./diff(xdataPPO); %% take the discret derivative
k0=-dvdt./ydataPPO(1:end-1);
%plot(ydataPPO(1:end-1),k0,'r--')
% t_prime=xdata+c;
% for i=1:size(xdata);
% dv_dt(i)=-b/t_prime(i);
% k0(i)=-dv_dt(i)/ydata(i);
%
%%
figure(12)
plot(ydataPPO(1:end-1),k0,'b--');% , '*'
title(' k0 Versus Voltage - blocking layer')
xlabel('V(Volt)')
ylabel('ko')
showfit('ko(V)=a*exp(V/tau)','fitlinewidth',2,'fitcolor','red');

legend(' Experimental Data',' fitted Curve ')
paramk=getfield(lastfit, 'm');

ap=paramk(1);taup=paramk(2);

```



```

%% Write Ko(v) to text file
kov(:,1)=xdataPPO(1:end-1);
kov(:,2)=k0';

fileID = fopen('Ko(v)PPO.txt','w');
fprintf(fileID,'%6s %12s\n','v','Ko(v)');
fprintf(fileID,'%6.2f %12.8f\n',kov);
fclose(fileID);

for l=1:cycle;
%% Beta Estimation (P.624 Electrochemical methods...Allen J. Bard book) Electron transfer by
tunneling through blocking films
% knowing a specific thickness in nanometer

mm=(1/tauNo-1/taup)/(thb*1e-9);nn=-log(ap/aNo)/(thb*1e-9);

th=thick(l);
Vol=0:0.001:V_ch;Vol=Vol';
% size=size(Vol);
% size=size(1);

for i=1:length(Vol);
kx(i)=aNo*exp(Vol(i)*(1/tauNo))*exp(-th*1e-9*mm*Vol(i)-th*1e-9*nn);
end
figure(32)
plot(Vol,kx,'b--');% , '*'
%title(' k0 Versus Voltage - for the desired thickness')
xlabel('V(Volt)')
ylabel('ko')

showfit('ko(V)=a*exp(V/tau)','fitlinewidth',2,'fitcolor','red');

paramx=getfield(lastfit, 'm');

ax=paramx(1);taux=paramx(2);
axk(1)=ax;tauxk(1)=taux;
% %% Write Kox(v) to text file
% kox(:,1)=Vol;
% kox(:,2)=kx';
%
%
% fileID = fopen('Kox(v)PPO.txt','w');
% fprintf(fileID,'%6s %12s\n','v','Ko(v)');

```

```

% fprintf(fileID,'%6.2f %12.8f\n',kox);
% fclose(fileID);

%% Plotting V versus t

ode1=@(x,y)-axk(l)*y*exp(y/tauxk(l));
% Call the solver with function Name,

end_of_time=data1(last_time,1);
{x,y}=ode45(ode1,{0:end_of_time},V_ch); % {x,y}=ode45(ode1,{0:0.1:size},V_ch);
% Plotting Segment
xdatax(:,l)=x;ydatax(:,l)=y;
figure (41)
plot(x,y,'b--')

xlabel('t(s)')
ylabel('V(volt)')

%title('Solution to dV/dt = -ko*V for desired thickness')
showfit('V(t)=a-b*log(t+c)','fitlinewidth',2,'fitcolor','red');
paramvx=getfield(lastfit, 'm');

avx=paramvx(1);bvx=paramvx(2);cvx=paramvx(3);
avxk(l)=avx;bvxk(l)=bvx;cvxk(l)=cvx;

end

%% Plot all the graphs

Markert={' ','-','--','-.-','-*','-+','-o','-^','-d','-v','-s','-<','->','-p','-h'};

siz=length(xdatax);
k=1;
for i=1:siz; %Sampling
j=100*(i-1)+1;

    if j > siz
    else
    xdatxk(k,:)= xdatax(j,:);
    ydatxk(k,:)= ydatax(j,:);
    end

    end
k=k+1;
end

```

```

for l = 1:cycle

    legendInfo{1} = {'thickness = ' num2str(thick(l)) 'nm'};
    mark=Markert{1};
    figure (7)
    plot(xdatxk(:,l),ydatxk(:,l),mark)
    legend(legendInfo)
    xlabel('t(s)')
    ylabel('V(volt)')
    %title('Self discharge voltage profiles for different thicknesses')
    hold on
end

for l = 1:cycle
    Vol=0:0.025:V_ch;Vol=Vol';

    legendInfo{1} = {'thickness = ' num2str(thick(l)) 'nm'};
    mark=Markert{1};
    figure(33)
    plot(Vol,axk(l)*exp(Vol/tauxk(l)),mark);% , '*'
    legend(legendInfo)
    %title(' k0 Versus Voltage - for the desired thickness')
    xlabel('V(Volt)')
    ylabel('ko(1/s)')
    hold on
end

%% Energy
epsi=8.854187817620e-12;

Cbl=1/(1/C2-1/C1);

for l = 1:cycle
    Vol=(0:0.001:V_ch)';
    siz=length(Vol);
    k=1;
    for i=1:siz;
        j=100*(i-1)+1;

        if j > siz
            else
                Vot(k,:)= Vol(j,:);
                Vot(k,:)= Vol(j,:);

            end
        k=k+1;
    end
end

```

```

end
for i=1:length(Vot);
Vots(i)=Vot(i)*Vot(i);
Vots=Vots';
end

legendInfo{1} = {'thickness = ' num2str(thick(1)) 'nm'};
mark=Markert{1};
Cbll(1)=Cbl*thb/thick(1);
En=(0.5*Vots/(1/C1+1/Cbll(1)))';
% Enn(:,1)=En;% Find a solution
figure(34)
plot(Vot,En,mark);% , '*'
legend(legendInfo)
%title(' k0 Versus Voltage - for the desired thickness')
xlabel('V(Volt)')
ylabel('E(J/g)')
hold on
end

for l = 1:cycle
size=length(ydatxk);
for i=1:size;
datavk= ydatxk(:,i);
datvk(i)=datavk(i)*datavk(i);

end

legendInfo{1} = {'thickness = ' num2str(thick(1)) 'nm'};
mark=Markert{1};
Cbll(1)=Cbl*thb/thick(1);
Enr(:,1)=(0.5*(datvk)/(1/C1+1/Cbll(1)))';
Vcbl(:,1)=V_ch*(1+C1/Cbll(1))^0.5; % Comparison voltage
delta_E(1)=abs(Enr(1,1)-Enr(size,1));
Error_E(1)=delta_E(1)/Enr(1,1);

figure(35)
plot(ydatxk(:,1),Enr(:,1),mark,'Linewidth',1.25);% , '*'
legend(legendInfo)
title(' Energy Versus discharge Voltage - for the desired thickness')
xlabel('V(Volt)')
ylabel('E(J/g)')
hold on

figure(36)
plot(xdatxk(:,1),Enr(:,1),mark,'Linewidth',1.25);% , '*'

```

```

legend(legendInfo)
title(' Energy Versus Time - for the desired thickness')
xlabel('t(s)')
ylabel('E(J/g)')
hold on
end
Energy_loss(:,2)= delta_E';Energy_loss(:,1)=thick';
Energy_error(:,2)= Error_E';Energy_error(:,1)=thick';
Energy_loss
Energy_error

%% Plotting V versus t

for l = 1:cycle
ode1=@(x,y)-axk(l)*y*exp(y/tauxk(l));
%
end_of_time=data1(last_time,1);
{x,y}=ode45(ode1,{0:end_of_time},Vcbl(l)); % {x,y}=ode45(ode1,{0:0.1:size},V_ch);
% Plotting Segment
xdataxkl(:,l)=x;ydataxkl(:,l)=y;
figure (411)
plot(x,y,'b--')

xlabel('t(s)')
ylabel('V(volt)')

%title('Solution to dV/dt = -ko*V for desired thickness')
showfit('V(t)=a-b*log(t+c)', 'fitlinewidth',2, 'fitcolor', 'red');
paramvxl=getfield(lastfit, 'm');

avxl=paramvxl(1);bvxl=paramvxl(2);cvxl=paramvxl(3);
avxkl(l)=avxl;bvxkl(l)=bvxl;cvxkl(l)=cvxl;

end

%% Plot all the graphs

Markert={' ','-','--','-.-','-*','-+','-o','-^','-d','-v','-s','-<','>','-p','-h'};

siz=length(xdataxkl);
k=1;
for i=1:siz;
j=50*(i-1)+1;

if j > siz

```

```

else
    xdatxkl(k,:)= xdatxkl(j,:);
    ydatxkl(k,:)= ydatxkl(j,:);

end
k=k+1;
end

for l = 1:cycle

    legendInfo{1} = {'thickness = ' num2str(thick(l)) 'nm'};
    mark=Markert{1};
    figure (712)
    plot(xdatxkl(:,l),ydatxkl(:,l),mark)
    legend(legendInfo)
    xlabel('t(s)')
    ylabel('V(volt)')
    %title('Self discharge voltage profiles for different thicknesses')
    hold on
end

for l = 1:cycle
size=length(ydatxkl);
for i=1:size;
datavkl= ydatxkl(:,l);
datvkl(i)=datavkl(i)*datavkl(i);

end
    legendInfo{1} = {'thickness = ' num2str(thick(l)) 'nm'};
    mark=Markert{1};
    Cbl(l)=Cbl*thb/thick(l);
    Enrl(:,l)=(0.5*(datvkl)/(1/C1+1/Cbl(l)))';

    deltal_E(l)=abs(Enrl(1,l)-Enrl(size,l));
    Errorl_E(l)=deltal_E(l)/Enrl(1,l);

    figure(351)
    plot(ydatxkl(:,l),Enrl(:,l),mark,'Linewidth',1.25);% ,'*'
    legend(legendInfo)
    title(' Energy Versus discharge Voltage - for the desired thickness')
    xlabel('V(Volt)')
    ylabel('E(J/g)')
    hold on

figure(361)

```

```

plot(xdataxkl(:,1),Enrl(:,1),mark,'Linewidth',1.25);% , '*'
legend(legendInfo)
title(' Energy Versus Time - for the desired thickness')
xlabel('t(s)')
ylabel('E(J/g)')
hold on
end

Energyl_loss(:,2)=deltal_E';Energyl_loss(:,1)=thick';
Energyl_error(:,2)=Errorl_E';Energyl_error(:,1)=thick';
Energyl_begin(:,2)=Enrl(1,:);Energyl_begin(:,1)=thick';
Energyl_end(:,2)=Enrl(size,:);Energyl_end(:,1)=thick';
%Leakage_current
Energyl_begin=Energyl_begin'
Energyl_end=Energyl_end'
voltage_end=ydataxkl(end_of_time,:)

Energyl_loss=Energyl_loss'
Energyl_error=Energyl_error'
display('-----End-----')

```